Master's thesis

NTNU
Norwegian University of Science and Technology
Faculty of Natural Sciences
Department of Physics

Geir Hæreid Hovde

Small Amplitude Approximation of Coherent Light Scattering On Two Dimensional Rough Surfaces

Master's thesis in Applied Physics and Mathematics
Supervisor: Ingve Simonsen
January 2023

NTNU
Norwegian University of
Science and Technology

Geir Hæreid Hovde

Small Amplitude Approximation of Coherent Light Scattering On Two Dimensional Rough Surfaces

Master's thesis in Applied Physics and Mathematics
Supervisor: Ingve Simonsen
January 2023

Norwegian University of Science and Technology
Faculty of Natural Sciences
Department of Physics

NTNU
Norwegian University of
Science and Technology

Abstract

The incoherent component of the Mean Differential Reflection Coefficient (MDRC), Mueller Matrix and depolarization index [1] of two dimensional randomly rough glass and silver surfaces described by a Gaussian Stochastic Process with a Gaussian correlation function were computed using a fourth order Small Amplitude Perturbation approximation. Excitation of Surface Plasmon Polaritons were found to contribute considerably to the scattering from the silver surface and both the enhanced back-scattering peak and a strong increase in in-plane cross-polarization were observed for the incoherent component of the MDRC. The cross-polarized contributions to the intensity in the back-scattering direction were found to depend drastically on the angle of incidence, presenting with a dip for large angles of incidence instead of a peak. The scattering response from the weakly rough surfaces was analysed through inspection of the various contributions to the incoherent expansion of the MDRC, affirming that these phenomena originate from the excitation of Surface Plasmon Polaritons (SPPs), as was shown for a two-dimensional surface using Small Amplitude Perturbation Theory (SAPT) by McGurn et al. for the West & O'Donnel effect spectrum [2]. Back-scattering phenomena akin to the enhanced back-scattering peak were also observed for many of the elements of the incoherent Mueller Matrix of the silver surface. Many of the Mueller Matrix elements did not display the same diminishing trend for larger angles of incidence as the enhanced back-scattering peak in the intensity. As a result of this it was found that the depolarization index has a significant interference phenomenon in the back-scattering direction which presents as a dip or peak depending on the angle of incidence.

Sammendrag

Den inkoherente komponenten av den Gjennomsnittlige Differensielle Refleksjons Koeffisienten (GDRK), Mueller Matrisen og depolarisasjons indeksen [1] for to dimensjonelle tilfeldige ru glass- og sølvoverflater beskrevet av en Gaussisk Stokastisk Prosess med en Gaussisk korrelasjonsfunksjon ble beregnet ved bruk av fjerde orderns liten amplitude perturbasjonsteori. Det ble funnet at eksitasjonen av overflate plasmonpolaritoner hadde omfattende bidrag til spredningen fra sølvoverflaten, og både den forstørrede retro-spekulære spredningstoppen og forsterket krysspolarisert spredning i innfallsplanet ble observert for den inkoherrente komponenten av GDRK. Innfalsvinkelen viste seg å ha en stor innvirkning på de krysspolariserte bidragene til intensiteten i retro-spekulær retning, da man ser en dupp i steden for en topp i retrospekulærretning for store innfalsvinkler. Spredningen fra de svakt ru overflatene ble analysert ved inspeksjon av bidragene til den inkoherente komponenten av GDRK. Dette bekreftet at disse spredningsfenomenene har overflate plasmon polaritoner som opphav, akkurat som tidligere vist av McGurn et al. for West & O'Donnel effektspekteret [2]. Forstørrede retro-spekulære spredningsfenomen i likhet med den forstørrede retro-spekulære spredningstoppen ble observært for noen av elementene i den inkoherente komponenten av Mueller Matrisen for en sølvoverflate. Flere av disse viste ikke den samme synkende trenden med økt innfallsvinkel som er karakteristisk for den forstørrede retro-spekulære spredningstoppen i intensiteten. Som et resultat av dette ble det funnet et interferens fenomen i den retro-spekulære spredningsretningen som utartet seg som en topp eller en dupp avhengig av innfallsvinkel.

Contents

1 Introduction

The study of light scattering has been at the center of scientific and technological breakthroughs and conundrums since the birth of modern physics, and parts of its nature are still subject to active research today. One such field of active research is rough surface scattering, which compared to scattering problem for a smooth planar surface does not lend itself to a complete analytical description. Light scattering from a smooth planar surface is, as one learns in any introductory course to optics, governed by the Fresnel equations discovered by Augustine-Jean Fresnel at the beginning of the 19th century. The world, unfortunately, is not populated by perfectly smooth objects that lend themselves to a simple satisfying description, and while the Fresnel equations are decent approximations of the specular scattering behaviour of a weakly rough surface, they make no attempt to describe the inherent diffusive nature of the scattering response of a randomly rough surface. A better understanding of the scattering behaviour of rough surfaces could have great technological and scientific value, leading to improvements in radar technology and divulging the secrets of subsurface material layers, opening doors to new and exciting discoveries. The work presented within this thesis builds on the authors project thesis from the fall of 2021, as many of the fundamental theoretical concepts are the same.

Describing a surface as rough is rather vague, and all real surfaces are in fact rough, if one only looks closely enough. It is therefore pertinent to classify a rough surface based on its length scale, i.e the scale at which a probe interacting with the surface will be able to observe its roughness. You can imagine that you are walking over terrain, you will only notice bumps that are large enough that you have to alter your stride to compensate for them. An ant walking along the same terrain however, would have quite a different opinion on which structures define the roughness of the surface. Furthermore it is necessary to clarify what is meant when we state that a surface is *randomly* rough.

Two randomly rough surfaces are never identical, even two separate sections of a single randomly rough surface are never identical, yet a suitable description of the surface is necessary in order to tackle the scattering problem. One could measure the surface profile for the randomly rough surface that one seeks to determine the scattering intensity for, but this is both extremely time consuming and only yields information about one particular surface. Instead a common theoretical approach is to utilise the inherent statistical nature of randomly rough surfaces, meaning that one can define the surface profile function as a stochastic process. There are a plethora of different surfaces that allow for such a description, though perturbative methods tend to focus on surfaces described by Gaussian stochastic processes due to their favorable theoretical properties. Using a statistical surface description allows one to compute the diffuse scattering response by averaging over the entire surface, given that the surface is large enough such that all local effects destructively interfere.

The standard starting point in solving the scattering problem for weakly rough surfaces is the Reduced Rayleigh Equation derived by Brown et al. in 1984 [3], which bases itself on the Rayleigh Hypothesis [4], an approximation that assumes the slopes of the rough surface to be suitably small such that the contributions from downwards travelling scattering modes to the reflected electric field can be safely neglected. The Reduced Rayleigh Equation is an integral equation involving either the reflection or transmission amplitudes of the reflected or transmitted light. Solutions to the Reduced Rayleigh equation can be determined by direct numerical simulations or by perturbative approximation schemes. The aim of this thesis is to compute the reflection amplitudes for a variety of weakly rough surfaces using the Small Amplitude Perturbation Theory, which inserts a perturbative expansion of the reflection amplitudes into the Reduced Rayleigh Equation, resulting in equations which can be solved in order to determine the various terms in the expansion. This perturbative expansion is not only subject to the small slope criterion of the Rayleigh Hypothesis, but also restricts the RMS-height to be suitably small compared to the wavelength of the incident light.

In calculating the scattering of weakly rough surfaces we seek to better understand the nature of the coupling between electromagnetic waves and rough surfaces The perturbative expansion is particularly useful in this regard as it allows for the inspection of the contribution from the specific physical scattering processes corresponding to terms in the expansion, yielding further insight into the scattering processes that govern scattering from rough surfaces. By analysing the

scattering response from weakly rough surfaces that have roughness parameters of a suitable scale compared to the wavelength of the incoming light, it is possible to observe interesting phenomena, notably the enhanced back-scattering peak and in-plane cross polarization. The enhanced back-scattering peak was predicted for a one dimensional surface with a Gaussian correlation function through perturbative computations by Celli et al. [5] in 1984, before being observed experimentally in 1987 [6] by O'Donnel and Mendez. This prompted West and O'Donnel to develop surfaces described by an effect-spectrum, now named the West & O'Donnel effect spectrum, which suppressed single-scattering contributions in order to more clearly observe multiple scattering phenomenon [7]. They were successful in observing the enhanced back-scattering peak for highly one-dimensional randomly rough metal surfaces. Leading McGurn et al. to perform an extensive analysis of two-dimensional surfaces described by several types of West & O'Donnel using a fourth order small amplitude perturbation expansion [2], concluding that the enhanced back-scattering peak and in-plane cross-polarization originated from the excitation of Surface Plasmon Polaritons.

This thesis aims to display the difference in scattering response from two dimensional dielectric and metal surfaces with Gaussian correlation functions using Small Amplitude Perturbation Theory, which in effect amounts to analysing the contributions from a type of electromagnetic surface wave known as the Surface Plasmon Polariton [8, p. 18] to the scattering response of weakly rough surfaces. In doing this we seek first to observe the well known enhanced back-scattering peak and enhanced in-plane cross-polarization for the incoherent component of the Mean Differential Reflection Coefficient of a silver surface, confirming agreement with previous analysis of weakly rough surface scattering. Our attentions is then shifted to the incoherent component of the Mueller Matrix, which has been shown to present with enhanced back-scattering contributions for many of its elements in results achieved through Direct Numerical Simulations [9]. We seek to better understand the behaviour of these enhanced back-scattering contributions through analysing the various contributions from the perturbative expansion. Finally we seek to investigate the incoherent depolarization index [1] for dielectric and metal surfaces, notably its dependence on the enhanced back-scattering contributions to the incoherent component of the Mueller Matrix.

2 Theory

This section will introduce the main concepts and relations necessary to evaluate the scattering of electromagnetic waves from a randomly rough surface using a perturbative small wave expansion. To begin the electromagnetic wave equation and its plane wave solution is introduced, both in standard and Helmholtz form, as well as the notation to be used for the remainder of the thesis. Next, a description of the scattering geometry and the framework used to describe the randomly rough surfaces that the thesis will concern itself with will be given. Subsequently the behaviour of the electric field near the surface will be discussed, before the reduced Rayleigh equation for a two media system and the Rayleigh hypothesis are presented, followed by the Mean Differential Reflection Coefficient. The Mueller Matrix and its related framework for polarization will be introduced, as well as the depolarization index. The perturbative expansion of the reflection amplitudes will then be performed, and the fourth order expression for the incoherent component of the Mean Differential Reflection Coefficient and Mueller Matrix will be presented. Finally a brief description of the validity of Small Amplitude Perturbation Theory will be given alongside a validity criteria for the perturbative expansion.

2.1 The Electromagnetic Wave

One of the most profound results from electromagnetics is the discovery that light is an electromagnetic wave described by the electromagnetic wave equation. Given the absence of free charge and free current, and that the media in which the wave is propagating is both linear and homogeneous, the electromagnetic wave equation for a dispersive, isotropic and non-magnetic medium reads [10]

$$\nabla^2 \boldsymbol{E}(\boldsymbol{x}, t) = \mu_0 \varepsilon_0 \varepsilon_r(\omega) \frac{\partial^2 \boldsymbol{E}(\boldsymbol{x}, t)}{\partial t^2}. \tag{1}$$

Here μ_0 is the magnetic permeability in a vacuum, ε_0 is the electric permitivity in a vacuum and ε_r is the dielectric function of the medium. By Assuming an harmonic time-depencence in the electric field and taking the Fourier transform of Eq. (1) with respect to time, this equation can be transformed into the Helmholtz equation

$$\left[\nabla^2 + \varepsilon(\omega)\frac{\omega^2}{c^2}\right] \boldsymbol{E}(\boldsymbol{x}|\omega) = 0. \tag{2}$$

The Helmholtz equatiom allows for plane-wave solutions of the following form

$$\boldsymbol{E}(\boldsymbol{x}|\omega) = \boldsymbol{E}_0 \exp(i\boldsymbol{k} \cdot \boldsymbol{x}). \tag{3}$$

Here the polarization of the light is contained within the vector $\boldsymbol{E}_0$, $\boldsymbol{k}$ is the wave vector, ω is the angular frequency of the wave and c is the speed of light. It is important to note that a plane wave of this form is only a solution to the Helmholtz equation if the two following equations are satisfied

$$\nabla \cdot \boldsymbol{E} = \boldsymbol{k} \cdot \boldsymbol{E}_0 = 0 \tag{4}$$

$$k^2 = \varepsilon(\omega)\frac{\omega^2}{c^2}. \tag{5}$$

The first condition is Gauss' law, which must be satisfied for any solution to Maxwell's equations. The second condition is known as the dispersion relation, and its necessity can be confirmed by insertion of the plane wave solution (3) into the Helmholtz equation (2).

For the purpose of describing surface scattering it is convenient to split the wave vector into two components, one parallel to the surface, and one perpendicular to it, i.e

$$\boldsymbol{k} = \boldsymbol{k}_{\parallel} + \boldsymbol{k}_{\perp}. \tag{6}$$

Inserting this into the dispersion relation yields the following expression for the perpendicular component

$$k_\perp^2 = \varepsilon(\omega)\frac{\omega^2}{c^2} - k_\parallel^2. \tag{7}$$

Taking the square root on both sides and introducing the notation $\alpha_i(k_\parallel|\omega)$, which will be used for the rest of this paper, for the perpendicular component, yields

$$\alpha_i(k_\parallel|\omega) = \sqrt{\varepsilon_i(\omega)\frac{\omega^2}{c^2} - k_\parallel^2}. \tag{8}$$

It is worth noting that $\alpha_i(k_\parallel|\omega)$ may become imaginary for certain $\boldsymbol{k}_\parallel$-vectors, which results in the plane-wave solution having an exponential decay away from the surface. These wave-modes are called *evanescent waves*. Defining our coordinate system such that $\hat{\boldsymbol{x}}_3$ is perpendicular to the surface, the final expression for the wave vector reads

$$\boldsymbol{k} = \boldsymbol{k}_\parallel \pm \alpha(k_\parallel|\omega)\hat{\boldsymbol{x}}_3, \tag{9}$$

where the sign in front of $\alpha(k_\parallel|\omega)$ governs whether the wave is propagating in the positive or negative $\hat{\boldsymbol{x}}_3$-direction.

2.2 Scattering Geometry

In this work the scattering geometry will be described by the incoming wave vector labelled $\boldsymbol{k}$ and the scattered wave vector $\boldsymbol{q}$. A graphical depiction of the scattering geometry can be seen in Fig. 1, where the incident parallel wave vector $\boldsymbol{k}_\parallel$

$$\boldsymbol{k}_\parallel = \sqrt{\varepsilon_1(\omega)}\frac{\omega}{c}\sin\theta_0[\cos\phi_0, \sin\phi_0, 0] \tag{10}$$

and the scattered parallel wave-vector $\boldsymbol{q}_\parallel$

$$\boldsymbol{q}_\parallel = \sqrt{\varepsilon_1(\omega)}\frac{\omega}{c}\sin\theta_s[\cos\phi_s, \sin\phi_s, 0] \tag{11}$$

are depicted, as well as the polar and azimuthal angles of incidence and reflection. The rough surface is defined to lie along the x_1x_2-plane, with deviations in the $\hat{\boldsymbol{x}}_3$-direction, describing the roughness of the surface.

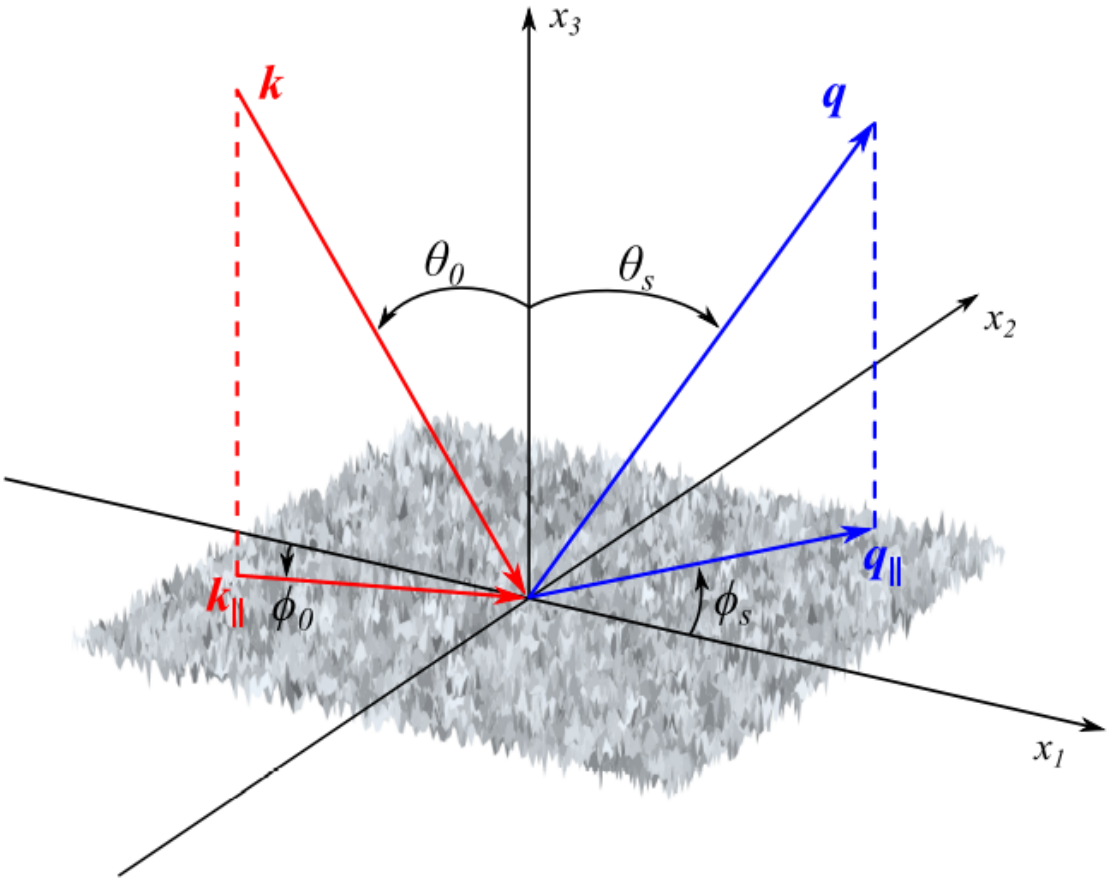

Figure 1: Graphical depiction of the scattering geometry which is investigated in this work. Taken from [11, Fig.1].

In this work it is assumed that the incident field is a monochromatic plane wave (3), inserting the expression for a downwards propagating wave vector (9) yields

$$\boldsymbol{E}_{\text{inc}}(\boldsymbol{x}|\omega) = \boldsymbol{E}_0 \exp(i\boldsymbol{k}_\parallel \boldsymbol{x}_\parallel - i\alpha(k_\parallel|\omega)x_3). \tag{12}$$

The factor $\boldsymbol{E}_0$ describes the polarization of the incoming field

$$\boldsymbol{E}_0(\boldsymbol{k}_\parallel) = \frac{c}{\sqrt{\varepsilon_1}\omega}[\hat{\boldsymbol{k}}_\parallel \alpha_1(k_\parallel|\omega) + \hat{\boldsymbol{x}}_3 k_\parallel]E_{0p} + (\hat{\boldsymbol{x}}_3 \times \hat{\boldsymbol{k}}_\parallel)E_{0s}. \tag{13}$$

The polarization vector satisfies the condition set by Gauss' law, as the reader can readily check. The coefficients $E_{0\alpha}$ are the amplitudes of linearly polarized light, which describes the amount of incoming α-polarized light. The plane drawn out by $\hat{\boldsymbol{k}}_\parallel$ and $\hat{\boldsymbol{x}}_3$ is colloquially known as the *plane of incidence*. The polarization states are named for their orientation in relation to the plane of incidence. The terms p- and s-polarized light originate from the German words *parallel* and *senkrecth*, which translates to *parallel* and *orthogonal* in English. P-polarized light is thereby parallel to the plane of incidence, while s-polarized light is orthogonal.

The scattered wave above and away from the upper boundary of the rough surface can be written as a sum of upwards propagating plane waves given by the following integral

$$\boldsymbol{E}_{sca}(\boldsymbol{x}|\omega) = \int \frac{d^2q_\parallel}{(2\pi)^2} \boldsymbol{\mathcal{E}}_{sc}(\boldsymbol{q}_\parallel) \exp(i\boldsymbol{q}_\parallel \cdot \boldsymbol{x}_\parallel + i\alpha(\boldsymbol{q}_\parallel|\omega)x_3). \tag{14}$$

Here $\mathcal{E}_{\text{sc}}(\boldsymbol{q}_\parallel|\omega)$ contains the polarization of the outgoing waves. Maxwell's equations and the associated boundary conditions at the interface imply a linear relationship between the incoming and outgoing polarization amplitudes given as

$$\boldsymbol{\mathcal{E}}_{sc}(\boldsymbol{q}_{\parallel}) = \boldsymbol{R}(\boldsymbol{q}_{\parallel}|\boldsymbol{k}_{\parallel})\boldsymbol{E_0}(\boldsymbol{k}_{\parallel}). \tag{15}$$

Where the matrix

$$\boldsymbol{R}(\boldsymbol{q}_{\parallel}|\boldsymbol{k}_{\parallel}) = \begin{pmatrix} R_{pp}(\boldsymbol{q}_{\parallel}|\boldsymbol{k}_{\parallel}) & R_{ps}(\boldsymbol{q}_{\parallel}|\boldsymbol{k}_{\parallel}) \\ R_{sp}(\boldsymbol{q}_{\parallel}|\boldsymbol{k}_{\parallel}) & R_{ss}(\boldsymbol{q}_{\parallel}|\boldsymbol{k}_{\parallel}) \end{pmatrix}, \tag{16}$$

contains the reflection amplitudes $R_{\alpha\beta}(\boldsymbol{q}_{\parallel}|\boldsymbol{k}_{\parallel})$ which describe how much incident β-polarized light with wave vector $\boldsymbol{k}_{\parallel}$ is scattered into α-polarized light in the direction of $\boldsymbol{q}_{\parallel}$. In other words, by determining the reflection amplitudes we would be able to completely describe the field scattered from the surface. The total field above the surface is given by

$$\boldsymbol{E}^{+}(\boldsymbol{x}|\omega) = \boldsymbol{E}_{sca}(\boldsymbol{x}|\omega) + \boldsymbol{E}_{inc}(\boldsymbol{x}|\omega). \tag{17}$$

The field propagating downwards through the lower media can be similarly described as

$$\boldsymbol{E}_{tr}(\boldsymbol{x}|\omega) = \int \frac{d^2p_{\parallel}}{(2\pi)^2}\boldsymbol{\mathcal{E}}_{tr}(\boldsymbol{p}_{\parallel})\exp(i\boldsymbol{p}_{\parallel}\cdot\boldsymbol{x}_{\parallel} - i\alpha(\boldsymbol{p}_{\parallel}|\omega)x_3), \tag{18}$$

with transmission amplitudes $T_{\alpha\beta}(\boldsymbol{p}_{\parallel}|\boldsymbol{k}_{\parallel})$ giving the transmitted polarization as

$$\boldsymbol{\mathcal{E}}_{tr}(\boldsymbol{p}_{\parallel}) = \boldsymbol{T}(\boldsymbol{p}_{\parallel}|\boldsymbol{k}_{\parallel})\boldsymbol{E_0}(\boldsymbol{k}_{\parallel}). \tag{19}$$

2.3 Surface Plasmon Polaritons

A type of evanescent wave mode known as the Surface Plasmon Polariton (SPP) is central in the description of rough surface scattering. An SPP is an electromagnetic wave bound to the surface between a dielectric and a metal, characterised by an exponentially decaying factor corresponding to the perpendicular component of the incident wave vector being imaginary. For weakly rough surfaces, such as the ones considered within this thesis, excitation of SPPs is the prinicpal contributor to multiple scattering effects. They are therefore at the origin of many of the characteristic phenomena which are observed in scattering from surfaces that satisfy the Rayleigh Criterion, which will be presented in Sec.2.6. SPPs are governed by the following dispersion relation [8] [p. 18-20]

$$k_{spp}(\omega) = \sqrt{\frac{\varepsilon_{+}(\omega)\varepsilon_{-}(\omega)}{\varepsilon_{+}(\omega)+\varepsilon_{-}(\omega)}}\frac{\omega}{c}, \tag{20}$$

where $\varepsilon_{\pm}(\omega)$ are the dielectric constants in the upper and lower medium. This dispersion relation is valid only when the dielectric functions have opposite signs, as is the case for a dielectric-metal interface. For a more thorough discussion of SPPs the reader is directed to [8][p. 18-20].

2.4 Randomly Rough Surface

Most people have an intuitive feeling for what it means for a surface to be rough. They would probably picture a piece of sandpaper or an asphalt parking lot, but as mentioned in the introduction all the surfaces that we interact with on a daily basis are in fact rough, if only one inspects them closely enough. It can therefore be of great importance to understand how surface roughness affects reflection of light, and to which degree these reflective properties can be controlled.

In nature there exists a plethora of different types of rough surfaces, one of the most useful from a theoretical point of view is to define the surface profile function $x_3 = \zeta(\boldsymbol{x}_{\parallel})$, which describes the height of the surface for every point $\boldsymbol{x}_{\parallel} = x_1\hat{\boldsymbol{x}}_1 + x_2\hat{\boldsymbol{x}}_2$ in the plane perpendicular to $\hat{\boldsymbol{x}}_3$, by a zero-mean stationary Gaussian stochastic process [12] with correlation given by a correlation function depending on the distance between two points on the surface

$$\langle\zeta(\boldsymbol{x}_{\parallel})\zeta(\boldsymbol{x'}_{\parallel})\rangle = \delta^2 W(\boldsymbol{x}_{\parallel} - \boldsymbol{x'}_{\parallel}), \tag{21}$$

where $\langle\zeta(\boldsymbol{x}_{\parallel})^2\rangle = \delta^2$ is the mean-square height of the surface.

The reason that this type of randomly rough surface is so appealing for theoretical applications is that the higher order moments of a Gaussian statistic process is defined by the first and second moment. The usefulness of this property will become evident during calculation of the small amplitude expansion to follow. The zero mean property

$$\langle \zeta(\boldsymbol{x}_\parallel) \rangle = 0, \tag{22}$$

describes the fact that the probability density is symmetrically distributed along the $\hat{\boldsymbol{x}}_3$-axis for a surface defined to be centered around a planar surface in the x_1x_2-plane.

The brackets in Eq. (22) is an average over a large portion of the surface. By assuming the surface to be ergodic we can replace this with an average over surface realizations, which is what these angle brackets will denote for the remainder of this report.

2.4.1 Correlation function

There are numerous correlation functions that correspond to real surfaces. A popular choice for theoretical studies is the Gaussian correlation function defined as

$$W(\boldsymbol{x}_\parallel) = \exp\left(-\frac{x_1^2}{a_1^2} - \frac{x_2^2}{a_2^2}\right). \tag{23}$$

For our purposes it is convenient to also introduce the Fourier transform of the correlation function,

$$g(\boldsymbol{k}_\parallel) = \int_{-\infty}^{\infty} dx_\parallel W(\boldsymbol{x}_\parallel) \exp\left[-i\boldsymbol{k}_\parallel \cdot \boldsymbol{x}_\parallel\right], \tag{24}$$

which for the Gaussian correlation function can be found by straightforward calculations to be

$$g(\boldsymbol{k}_\parallel) = \pi a_1 a_2 \exp\left(-\frac{a_1^2k_1^2 + a_2k_2^2}{4}\right), \tag{25}$$

for $a_1 > 0$ and $a_2 > 0$. Another essential power spectrum in the analysis of diffuse scattering phenomena is the West & O'donnel spectrum defined as

$$g(\boldsymbol{k}_\parallel) = \frac{4\pi}{k_{max}^2 - k_{min}^2}\theta(|\boldsymbol{k}_\parallel| - k_{min})\theta(k_{max} - |\boldsymbol{k}_\parallel|) \tag{26}$$

by West & O'donnel in relation to their experimental research in observation of the enhanced back scattering peak [7]. This power spectrum prohibits single scattering contributions from obscuring the enhanced back scattering peak originating from the double scattering terms, allowing for accurate experimental observations.

Finally we have the following relation

$$\langle \hat{\zeta}(\boldsymbol{k}_\parallel)\hat{\zeta}(\boldsymbol{k'}_\parallel) \rangle = (2\pi)^2\delta^2 g(\boldsymbol{k}_\parallel)\delta(\boldsymbol{k}_\parallel + \boldsymbol{k'}_\parallel) \tag{27}$$

which is calculated in the appendix (114). Eq. (27) will be useful in the computation of the incoherent component of the MDRC and Mueller Matrix to be performed in Sec. 2.11 and 2.13.

2.5 Reduced Rayleigh Equation for a Two Media System

For a two media system with a rough surface at the boundary the fields above the maximum height of the surface and the field below the minimum height are described by equations (17) and (18). However, to determine the reflection amplitudes it is necessary to take into account the boundary conditions at the surface $x_3 = \zeta(\boldsymbol{x}_\parallel)$. The task is then to describe the electric field in the region close to the surface where the general expressions do not hold, since a complete description of the electric field in this region would need to allow for upwards and downwards propagating modes at both sides of the interface.

Assuming that the surface is not too rough and that the local slopes are not too steep, these boundary conditions can be evaluated through employing an approximation known as

the Rayleigh hypothesis [4]. This approximation assumes that the roughness parameters of the surface are sufficiently small such that any deviations from the general expressions can be neglected. Evaluating the boundary conditions with the general expressions for the electric field yields a set of coupled inhomogenous integral equations, which can be uncoupled such that one arrives at a single integral equation known as the Reduced Rayleigh equation for either the reflection or transmission amplitudes. For a detailed derivation the reader is referred to the derivation by Brown et al [3]. The reduced Rayleigh equation in two dimensions containing the reflection amplitudes $\boldsymbol{R}(\boldsymbol{q}_\parallel|\boldsymbol{k}_\parallel)$ (16) reads [11] [eq. 34]

$$\int \frac{d^2 q_\parallel}{(2\pi)^2} \boldsymbol{M}(\boldsymbol{p}_\parallel|\boldsymbol{q}_\parallel)\boldsymbol{R}(\boldsymbol{q}_\parallel|\boldsymbol{k}_\parallel) = -\boldsymbol{N}(\boldsymbol{p}_\parallel|\boldsymbol{k}_\parallel). \tag{28}$$

The matrices $\boldsymbol{M}(\boldsymbol{p}_\parallel|\boldsymbol{q}_\parallel)$ and $\boldsymbol{N}(\boldsymbol{p}_\parallel|\boldsymbol{k}_\parallel)$ are defined as

$$\boldsymbol{M}(\boldsymbol{p}_\parallel|\boldsymbol{q}_\parallel) = I^+(\boldsymbol{p}_\parallel|\boldsymbol{q}_\parallel) \times \begin{pmatrix} p_\parallel q_\parallel + \alpha_2(p_\parallel|\omega)\hat{\boldsymbol{p}}_\parallel \cdot \hat{\boldsymbol{q}}_\parallel \alpha_1(q_\parallel|\omega) & -\frac{\omega}{c}\alpha_2(p_\parallel|\omega)[\hat{\boldsymbol{p}}_\parallel \times \hat{\boldsymbol{q}}_\parallel]_3 \\ \frac{\omega}{c}\alpha_1(q_\parallel|\omega)[\hat{\boldsymbol{p}}_\parallel \times \hat{\boldsymbol{q}}_\parallel]_3 & \frac{\omega^2}{c^2}\hat{\boldsymbol{p}}_\parallel \cdot \hat{\boldsymbol{q}}_\parallel \end{pmatrix} \tag{29}$$

$$\boldsymbol{N}(\boldsymbol{p}_\parallel|\boldsymbol{k}_\parallel) = I^-(\boldsymbol{p}_\parallel|\boldsymbol{k}_\parallel) \times \begin{pmatrix} p_\parallel k_\parallel - \alpha_2(p_\parallel|\omega)\hat{\boldsymbol{p}}_\parallel \cdot \hat{\boldsymbol{k}}_\parallel \alpha_1(k_\parallel|\omega) & -\frac{\omega}{c}\alpha_2(p_\parallel|\omega)[\hat{\boldsymbol{p}}_\parallel \times \hat{\boldsymbol{k}}_\parallel]_3 \\ -\frac{\omega}{c}\alpha_1(k_\parallel|\omega)[\hat{\boldsymbol{p}}_\parallel \times \hat{\boldsymbol{k}}_\parallel]_3 & \frac{\omega^2}{c^2}\hat{\boldsymbol{p}}_\parallel \cdot \hat{\boldsymbol{k}}_\parallel \end{pmatrix}. \tag{30}$$

In writing this equation one has defined

$$I^\pm(\boldsymbol{p}_\parallel|\boldsymbol{q}_\parallel) = \frac{I(\alpha_2(p_\parallel) \mp \alpha_1(q_\parallel)|\boldsymbol{p}_\parallel - \boldsymbol{q}_\parallel)}{\alpha_2(p_\parallel) \mp \alpha_1(q_\parallel)} \tag{31}$$

and finally $I(\gamma|\boldsymbol{Q}_\parallel)$ is given by

$$I(\gamma|\boldsymbol{Q}_\parallel) = \int d^2 x_\parallel \exp\left[-i\gamma\zeta(\boldsymbol{x}_\parallel)\right] \exp\left[-i\boldsymbol{Q}_\parallel \cdot \boldsymbol{x}_\parallel\right]. \tag{32}$$

2.6 Validity of the Rayleigh Criterion

As stated in Sec. 2.5, the Rayleigh Hypothesis neglects the contribution from downwards propagating scattered waves above the surface, and upwards propagated transmitted modes below the surface. Our assumption in applying this approximation is that the surface roughness parameters are such that the slope is sufficiently small, such that these contributions can be ignored. The approximation was originally applied by Lord Rayleigh in his work on scattering from sinusoidal surfaces $\zeta(x_1) = \zeta_0 \sin(\Lambda x_1)$, which others have since derived the following formal validity criterion for [13], given by

$$\zeta_0 \Lambda < 0.448. \tag{33}$$

There exists no such formal validity criterion for a randomly rough surface, but there is a general consensus in the literature [14] that the approximation is valid given the condition

$$\frac{\delta}{a} \ll 1 \tag{34}$$

where δ and a are the rms-height and the correlation length of the surface roughness function.

2.7 Mean Differential Reflection Coefficient

The reflection amplitudes (16), which, as previously stated, completely determine the scattered electric field, are not directly measurable in experiments. We therefore introduce a quantity which is more convenient, both experimentally and, as shall be seen in Sec.2.10, theoretically. This quantity is known as the *mean differential reflection coefficient* (MDRC) [2],

$$\left\langle \frac{\partial R_{\alpha\beta}}{\partial \Omega_s} \right\rangle = \frac{\varepsilon_1}{S} \frac{\omega^2}{(2\pi c)^2} \frac{\cos^2(\theta_s)}{\cos(\theta_0)} \left\langle \left| R_{\alpha\beta}(\boldsymbol{q}_\parallel | \boldsymbol{k}_\parallel) \right|^2 \right\rangle, \tag{35}$$

where S is the total area of the surface considered. The MDRC is defined as the ensemble average of the fraction of incident power of β- polarized light scattered by the surface as α-polarized light into the solid angle element $d\Omega_s(\theta_s, \phi_s)$. The MDRC can be separated into a coherent and incoherent component by rewriting the reflection amplitude as the mean plus the fluctuations from the mean

$$R_{\alpha\beta}(\boldsymbol{q}_\parallel | \boldsymbol{k}_\parallel) = \langle R_{\alpha\beta}(\boldsymbol{q}_\parallel | \boldsymbol{k}_\parallel) \rangle + (R_{\alpha\beta}(\boldsymbol{q}_\parallel | \boldsymbol{k}_\parallel) - \langle R_{\alpha\beta}(\boldsymbol{q}_\parallel | \boldsymbol{k}_\parallel) \rangle). \tag{36}$$

It is then possible to identify a coherent and incoherent component

$$\left\langle \frac{\partial R_{\alpha\beta}}{\partial \Omega_s} \right\rangle = \left\langle \frac{\partial R_{\alpha\beta}}{\partial \Omega_s} \right\rangle_{coh} + \left\langle \frac{\partial R_{\alpha\beta}}{\partial \Omega_s} \right\rangle_{incoh}. \tag{37}$$

These components take on the following forms

$$\left\langle \frac{\partial R_{\alpha\beta}}{\partial \Omega_s} \right\rangle_{coh} = \frac{\varepsilon_1}{S} \frac{\omega^2}{(2\pi c)^2} \frac{\cos^2(\theta_s)}{\cos(\theta_0)} \left| \left\langle R_{\alpha\beta}(\boldsymbol{q}_\parallel | \boldsymbol{k}_\parallel) \right\rangle \right|^2 \tag{38}$$

$$\left\langle \frac{\partial R_{\alpha\beta}}{\partial \Omega_s} \right\rangle_{incoh} = \frac{\varepsilon_1}{S} \frac{\omega^2}{(2\pi c)^2} \frac{\cos^2(\theta_s)}{\cos(\theta_0)} \left[\left\langle \left| R_{\alpha\beta}(\boldsymbol{q}_\parallel | \boldsymbol{k}_\parallel) \right|^2 \right\rangle - \left| \left\langle R_{\alpha\beta}(\boldsymbol{q}_\parallel | \boldsymbol{k}_\parallel) \right\rangle \right|^2 \right]. \tag{39}$$

Both the coherent and incoherent scattering process will contribute to the MDRC, and for surfaces which satisfy the validity criterion of the Rayleigh Hypothesis it is the coherent scattering which will dominate. It is therefore convenient to investigate these quantities separately, even though this is not possible in experiments.

2.8 Mueller Matrix

One can completely describe the polarization response of an optical element, such as a randomly rough surface, by the use of Stokes vectors and Mueller calculus. The stokes vector encompasses the polarization state of the incoming and scattered waves in the stokes parameters as [15]

$$\boldsymbol{S} = \begin{pmatrix} I \\ Q \\ U \\ V \end{pmatrix} = \begin{pmatrix} |E_p|^2 + |E_s|^2 \\ |E_p|^2 - |E_s|^2 \\ E_p E_s^* + E_s E_p^* \\ i E_p E_s^* - E_s E_p^*, \end{pmatrix} \tag{40}$$

where I is the total intensity of the light, Q is the degree of horizontally or vertically polarized light, U is the degree of $45°$ or $-45°$ polarized light, and V is the degree of left- and right-circularly polarized light. The Mueller matrix describes the relation between the incoming and scattered stokes vector by the formula

$$\boldsymbol{S}_s = \boldsymbol{M}(\boldsymbol{q}_\parallel | \boldsymbol{k}_\parallel) \boldsymbol{S}_i. \tag{41}$$

The Mueller matrix can be written exclusively in terms of reflection amplitudes by considering the response from light incident with various polarization configurations [15], resulting in the following expressions for the matrix elements [9].

$$\begin{aligned}
M_{11} &= C[|R_{pp}|^2 + |R_{sp}|^2 + |R_{ps}|^2 + |R_{ss}|^2] \\
M_{12} &= C[|R_{pp}|^2 + |R_{sp}|^2 - |R_{ps}|^2 - |R_{ss}|^2] \\
M_{13} &= C[R_{pp}R_{ps}^* + R_{sp}R_{ss}^* + R_{ps}R_{pp}^* + R_{ss}R_{sp}^*] \\
M_{14} &= iC[R_{pp}R_{ps}^* + R_{sp}R_{ss}^* - R_{ps}R_{pp}^* - R_{ss}R_{sp}^*] \\
M_{21} &= C[|R_{pp}|^2 - |R_{sp}|^2 + |R_{ps}|^2 - |R_{ss}|^2]
\end{aligned}$$

$$
\begin{aligned}
M_{22} &= C[|R_{pp}|^2 - |R_{sp}|^2 - |R_{ps}|^2 + |R_{ss}|^2] \\
M_{23} &= C[R_{pp}R_{ps}^* - R_{sp}R_{ss}^* + R_{ps}R_{pp}^* - R_{ss}R_{sp}^*] \\
M_{24} &= iC[R_{pp}R_{ps}^* - R_{sp}R_{ss}^* - R_{ps}R_{pp}^* + R_{ss}R_{sp}^*] \\
M_{31} &= C[R_{pp}R_{sp}^* + R_{sp}R_{pp}^* + R_{ps}R_{ss}^* + R_{ss}R_{ps}^*] \\
M_{32} &= C[R_{pp}R_{sp}^* + R_{sp}R_{pp}^* - R_{ps}R_{ss}^* - R_{ss}R_{ps}^*] \\
M_{33} &= C[R_{pp}R_{ss}^* + R_{sp}R_{ps}^* + R_{ps}R_{sp}^* + R_{ss}R_{pp}^*] \\
M_{34} &= iC[R_{pp}R_{ss}^* + R_{sp}R_{ps}^* - R_{ps}R_{sp}^* - R_{ss}R_{pp}^*] \\
M_{41} &= -iC[R_{pp}R_{sp}^* - R_{sp}R_{pp}^* + R_{ps}R_{ss}^* - R_{ss}R_{ps}^* \\
M_{42} &= -iC[R_{pp}R_{sp}^* - R_{sp}R_{pp}^* - R_{ps}R_{ss}^* + R_{ss}R_{ps}^* \\
M_{43} &= -iC[R_{pp}R_{ss}^* - R_{sp}R_{ps}^* + R_{ps}R_{sp}^* - R_{ss}R_{pp}^*] \\
M_{44} &= C[R_{pp}R_{ss}^* - R_{sp}R_{ps}^* - R_{ps}R_{sp}^* + R_{ss}R_{pp}^*],
\end{aligned} \tag{42}
$$

where the arguments of the reflection amplitudes have been suppressed $R_{\alpha\beta} = R_{\alpha\beta}(\boldsymbol{q}_\parallel|\boldsymbol{k}_\parallel)$ and the coefficient C is given as

$$
C = \frac{\varepsilon_1}{2S}\left(\frac{\omega}{2\pi c}\right)^2 \frac{\cos^2\theta_s}{\cos\theta_0}. \tag{43}
$$

It is often pertinent to present the Mueller Matrix elements normalized with respect to the first element

$$
\bar{M}_{ij} = M_{ij}/M_{11} \tag{44}
$$

since the first element only contains information about the intensity of the incoming light.

Similarly as for the Mean Differential Reflection Coefficient (35) we are calculating an ensemble averaged Mueller matrix $\langle M\rangle$. The Mueller matrix can be separated into a coherent and incoherent component by following the similar steps as in Sec. 2.7.

$$
\langle R_{\alpha\beta}R_{\sigma\delta}^*\rangle = \langle R_{\alpha\beta}\rangle\langle R_{\sigma\delta}^*\rangle + [\langle R_{\alpha\beta}R_{\sigma\delta}^*\rangle - \langle R_{\alpha\beta}\rangle\langle R_{\sigma\delta}^*\rangle], \tag{45}
$$

giving us a general expression for the coherent and incoherent terms in the Mueller matrix elements

$$
\langle R_{\alpha\beta}R_{\sigma\delta}^*\rangle_{coh} = \langle R_{\alpha\beta}\rangle\langle R_{\sigma\delta}^*\rangle \tag{46}
$$

$$
\langle R_{\alpha\beta}R_{\sigma\delta}^*\rangle_{incoh} = \langle R_{\alpha\beta}R_{\sigma\delta}^*\rangle - \langle R_{\alpha\beta}\rangle\langle R_{\sigma\delta}^*\rangle \tag{47}
$$

2.9 Depolarization Index

The depolarization index D [1] is a scalar condition for a Mueller matrix to describe a non-depolarizing system. In effect this gives a simple condition to describe the degree to which a randomly rough surfaces depolarizes light scattered into a solid angle element $d\Omega_s$. It can take on values in the range $[0, 1]$ where 1 indicates a perfect non-depolarizing system and 0 that the scattered light is completely depolarized. It is defined as

$$
\begin{aligned}
M_{sqs} &= \sum_{i=1}^{4}\sum_{j=1}^{4} M_{ij}^2 \\
D &= \frac{\sqrt{M_{sqs} - M_{11}^2}}{\sqrt{3}M_{11}}.
\end{aligned} \tag{48}
$$

where M_{sqs} has been defined as the sum over all of the Mueller elements squared.

2.10 Small Amplitude Perturbation Theory

Starting from the reduced Rayleigh equation (28)

$$\int \frac{d^2q_\parallel}{(2\pi)^2}\boldsymbol{M}(\boldsymbol{p}_\parallel|\boldsymbol{q}_\parallel)\boldsymbol{R}(\boldsymbol{q}_\parallel|\boldsymbol{k}_\parallel) = -\boldsymbol{N}(\boldsymbol{p}_\parallel|\boldsymbol{k}_\parallel) \tag{49}$$

where the matrix $\boldsymbol{R}(\boldsymbol{q}_\parallel|\boldsymbol{k}_\parallel)$ contains the reflection amplitudes (16)

$$\boldsymbol{R}(\boldsymbol{q}_\parallel|\boldsymbol{k}_\parallel) = \begin{pmatrix} R_{pp}(\boldsymbol{q}_\parallel|\boldsymbol{k}_\parallel) & R_{ps}(\boldsymbol{q}_\parallel|\boldsymbol{k}_\parallel) \\ R_{sp}(\boldsymbol{q}_\parallel|\boldsymbol{k}_\parallel) & R_{ss}(\boldsymbol{q}_\parallel|\boldsymbol{k}_\parallel) \end{pmatrix}. \tag{50}$$

The small amplitude perturbation theory(SAPT) approximates $\boldsymbol{R}(\boldsymbol{q}_\parallel|\boldsymbol{k}_\parallel)$ by the expansion

$$\boldsymbol{R}(\boldsymbol{q}_\parallel|\boldsymbol{k}_\parallel) = \sum_{n=0}^{\infty}\frac{(-i)^n}{n!}\boldsymbol{R}^{(n)}(\boldsymbol{q}_\parallel|\boldsymbol{k}_\parallel), \tag{51}$$

where $\boldsymbol{R}^{(n)}(\boldsymbol{q}_\parallel|\boldsymbol{k}_\parallel)$ is of the n'th order in the Fourier transform of the surface roughness function. These expansion coefficient matrices can then be determined using a recursion relation derived by inserting the expansion into the Reduced Rayleigh equation, which will be shown later in this section. Unfortunately, these coefficient matrices become quite complicate to derive for larger n, and it is therefore necessary to limit the expansion to a small n, usually $n = 3$ or $n = 5$. The series truncation at $n = 4$ is never considered since the fourth order contributions resulting from $\boldsymbol{R}^{(4)}(\boldsymbol{q}_\parallel|\boldsymbol{k}_\parallel)$ cancel in the expression for the incoherent MDRC (39). In spite of this restriction, this method has been found to show a high level of agreement with experiments on surfaces for which the Rayleigh Hypothesis and the perturbative expansion are valid [16].

By truncating the expansion (51) at $n = 3$ and inserting into the expression for the incoherent component of the MDRC (39) we arrive at the following expression for the terms related to the reflection amplitudes $R_{\alpha\beta}(\boldsymbol{q}_\parallel|\boldsymbol{k}_\parallel)$ up to fourth order in the surface profile function

$$\begin{aligned}\langle|R_{\alpha\beta}(\boldsymbol{q}_\parallel|\boldsymbol{k}_\parallel)|^2\rangle - |\langle R_{\alpha\beta}(\boldsymbol{q}_\parallel|\boldsymbol{k}_\parallel)\rangle|^2 = \langle|R^{(1)}_{\alpha\beta}(\boldsymbol{q}_\parallel|\boldsymbol{k}_\parallel)|^2\rangle + \\ +\frac{1}{4}\left[\langle|R^{(2)}_{\alpha\beta}(\boldsymbol{q}_\parallel|\boldsymbol{k}_\parallel)|^2\rangle - |\langle R^{(2)}_{\alpha\beta}(\boldsymbol{q}_\parallel|\boldsymbol{k}_\parallel)\rangle|^2\right] \\ -\frac{1}{3}Re(\langle R^{*(1)}_{\alpha\beta}(\boldsymbol{q}_\parallel|\boldsymbol{k}_\parallel)R^{(3)}_{\alpha\beta}(\boldsymbol{q}_\parallel|\boldsymbol{k}_\parallel)\rangle).\end{aligned} \tag{52}$$

All other terms up to fourth order cancel due to the fact that all odd powers of a Gaussian stochastic variable average to zero [8], i.e

$$\langle\zeta^{(2m+1)}(\boldsymbol{x}_\parallel)\rangle = 0 \tag{53}$$

for any positive integer m. The three remaining terms in the incoherent expansion of the MDRC are colloquially referred to as the One-one, Two-two and Three-one terms, in accordance with the orders of the reflection amplitude from which they originate. The choice of prefactors in the expansion (51) is made obvious when $I(\gamma|\boldsymbol{Q}_\parallel)$ contained in the $\boldsymbol{M}(\boldsymbol{q}_\parallel|\boldsymbol{p}_\parallel)$ (29) and $\boldsymbol{N}(\boldsymbol{p}_\parallel|\boldsymbol{k}_\parallel)$ (30) matrices are rewritten using the series expansion of the exponential function

$$\exp(x) = \sum_{n=0}^{\infty}\frac{x^n}{n!}, \tag{54}$$

this yields

$$I(\gamma|\boldsymbol{Q}_\parallel) = \int d^2x_\parallel \sum_{n=0}^{\infty}\frac{(-i\gamma)^n}{n!}\zeta^n(\boldsymbol{x}_\parallel)\exp\left[-i\boldsymbol{Q}_\parallel\cdot\boldsymbol{x}_\parallel\right] \tag{55}$$

which is equivalent to summing over the Fourier transforms of the different powers of the surface roughness function given as

$$\hat{\zeta}^{(n)}(\boldsymbol{Q}_\parallel) = \int d^2x_\parallel \, \zeta(\boldsymbol{x}_\parallel)^n \exp\left[-i\boldsymbol{Q}_\parallel \cdot \boldsymbol{x}_\parallel\right] \tag{56}$$

which finally yields

$$I(\gamma|\boldsymbol{Q}_\parallel) = \sum_{n=0}^{\infty} \frac{(-i)^n}{n!} \gamma^n \hat{\zeta}^{(n)}(\boldsymbol{Q}_\parallel). \tag{57}$$

Our new expressions for $\boldsymbol{M}(\boldsymbol{p}_\parallel|\boldsymbol{q}_\parallel)$ and $\boldsymbol{N}(\boldsymbol{p}_\parallel|\boldsymbol{k}_\parallel)$ then become

$$\begin{aligned}\boldsymbol{M}(\boldsymbol{p}_\parallel|\boldsymbol{q}_\parallel) = \sum_{n=0}^{\infty} \frac{(-i)^n(\alpha_2(p_\parallel) - \alpha_1(q_\parallel))^{n-1}}{n!} \hat{\zeta}^{(n)}(\boldsymbol{p}_\parallel - \boldsymbol{q}_\parallel) \\ \times \begin{pmatrix} p_\parallel q_\parallel + \alpha_2(p_\parallel)\hat{\boldsymbol{p}}_\parallel \cdot \hat{\boldsymbol{q}}_\parallel \alpha_1(q_\parallel) & -\frac{\omega}{c}\alpha_2(p_\parallel)[\hat{\boldsymbol{p}}_\parallel \times \hat{\boldsymbol{q}}_\parallel]_3 \\ \frac{\omega}{c}\alpha_1(q_\parallel)[\hat{\boldsymbol{p}}_\parallel \times \hat{\boldsymbol{q}}_\parallel]_3 & \frac{\omega^2}{c^2}\hat{\boldsymbol{p}}_\parallel \cdot \hat{\boldsymbol{q}}_\parallel \end{pmatrix}\end{aligned} \tag{58}$$

and

$$\begin{aligned}\boldsymbol{N}(\boldsymbol{p}_\parallel|\boldsymbol{k}_\parallel) = \sum_{n=0}^{\infty} \frac{(-i)^n(\alpha_2(p_\parallel) + \alpha_1(k_\parallel))^{n-1}}{n!} \hat{\zeta}^{(n)}(\boldsymbol{p}_\parallel - \boldsymbol{k}_\parallel) \\ \times \begin{pmatrix} p_\parallel k_\parallel - \alpha_2(p_\parallel)\hat{\boldsymbol{p}}_\parallel \cdot \hat{\boldsymbol{k}}_\parallel \alpha_1(k_\parallel) & -\frac{\omega}{c}\alpha_2(p_\parallel)[\hat{\boldsymbol{p}}_\parallel \times \hat{\boldsymbol{k}}_\parallel]_3 \\ -\frac{\omega}{c}\alpha_1(k_\parallel)[\hat{\boldsymbol{p}}_\parallel \times \hat{\boldsymbol{k}}_\parallel]_3 & \frac{\omega^2}{c^2}\hat{\boldsymbol{p}}_\parallel \cdot \hat{\boldsymbol{k}}_\parallel \end{pmatrix}.\end{aligned} \tag{59}$$

The terms of interest in our expansion are best expressed as

$$\boldsymbol{M}^{(n)}(\boldsymbol{p}_\parallel|\boldsymbol{q}_\parallel) = \frac{(-i)^n \hat{\zeta}^{(n)}(\boldsymbol{p}_\parallel - \boldsymbol{q}_\parallel)}{n!} \boldsymbol{\mathcal{M}}^{(n)}(\boldsymbol{p}_\parallel|\boldsymbol{q}_\parallel) \tag{60}$$

$$\boldsymbol{N}^{(n)}(\boldsymbol{p}_\parallel|\boldsymbol{k}_\parallel) = \frac{(-i)^n \hat{\zeta}^{(n)}(\boldsymbol{p}_\parallel - \boldsymbol{k}_\parallel)}{n!} \boldsymbol{\mathcal{N}}^{(n)}(\boldsymbol{p}_\parallel|\boldsymbol{k}_\parallel). \tag{61}$$

Inserting these expansions into the Reduced Rayleigh equation (28), yields

$$\begin{aligned}\sum_{n=0}^{\infty}\sum_{m=0}^{\infty} \int_{-\infty}^{\infty} \frac{d^2q_\parallel}{(2\pi)^2} \boldsymbol{\mathcal{M}}^{(n)}(\boldsymbol{p}_\parallel|\boldsymbol{q}_\parallel) \frac{(-i)^n}{n!} \hat{\zeta}^{(n)}(\boldsymbol{p}_\parallel - \boldsymbol{q}_\parallel) \frac{\boldsymbol{R}^{(m)}(\boldsymbol{q}_\parallel|\boldsymbol{k}_\parallel)(-i)^m}{m!} \\ = -\sum_{n=0}^{\infty} \boldsymbol{\mathcal{N}}^{(n)}(\boldsymbol{p}_\parallel|\boldsymbol{k}_\parallel) \hat{\zeta}^{(n)}(\boldsymbol{p}_\parallel - \boldsymbol{k}_\parallel) \frac{(-i)^n}{n!}.\end{aligned} \tag{62}$$

Using the fact that $\boldsymbol{M}^{(n)}(\boldsymbol{p}_\parallel|\boldsymbol{q}_\parallel)$, $\boldsymbol{R}^{(m)}(\boldsymbol{q}_\parallel|\boldsymbol{k}_\parallel)$, and $\boldsymbol{N}^{(n)}(\boldsymbol{p}_\parallel|\boldsymbol{k}_\parallel)$ are proportional to $\hat{\zeta}^n(\boldsymbol{Q}_\parallel)$ and the idenity (122), we can equate the terms of the same order in $\hat{\zeta}^{(n)}(\boldsymbol{Q}_\parallel)$. divide by $(i)^n$ on both sides, and rearrange the faculties to obtain the binomial function, finally yielding the following recursion relation for the coefficient matrices $\boldsymbol{R}^{(n)}(\boldsymbol{q}_\parallel|\boldsymbol{k}_\parallel)$

$$\begin{aligned}\sum_{m=0}^{\infty} \binom{n}{m} \int_{-\infty}^{\infty} \frac{d^2q_\parallel}{(2\pi)^2} \boldsymbol{\mathcal{M}}^{(n-m)}(\boldsymbol{p}_\parallel|\boldsymbol{q}_\parallel) \hat{\zeta}^{(n-m)}(\boldsymbol{p}_\parallel - \boldsymbol{q}_\parallel) \boldsymbol{R}^{(m)}(\boldsymbol{q}_\parallel|\boldsymbol{k}_\parallel) \\ = -\boldsymbol{\mathcal{N}}^{(n)}(\boldsymbol{p}_\parallel|\boldsymbol{k}_\parallel) \hat{\zeta}^{(n)}(\boldsymbol{p}_\parallel - \boldsymbol{k}_\parallel).\end{aligned} \tag{63}$$

2.11 Identifying the Expansion Coefficient Matrices

With the recursion relation obtained in the previous section the terms in the coefficient matrix expansion can now be derived. For the zeroth order term the binomial coefficient is zero for all terms except for $m = 0$, resulting in the following equation for the zeroth order contribution

$$\int \frac{d^2q_\parallel}{(2\pi)^2} \boldsymbol{\mathcal{M}}^{(0)}(\boldsymbol{p}_\parallel|\boldsymbol{q}_\parallel)\hat{\zeta}^{(0)}(\boldsymbol{p}_\parallel - \boldsymbol{q}_\parallel)\boldsymbol{R}^{(0)}(\boldsymbol{q}_\parallel|\boldsymbol{k}_\parallel) = -\boldsymbol{\mathcal{N}}^{(0)}(\boldsymbol{p}_\parallel|\boldsymbol{k}_\parallel)\hat{\zeta}^{(0)}(\boldsymbol{p}_\parallel - \boldsymbol{k}_\parallel). \tag{64}$$

Here $\hat{\zeta}^{(n)}(\boldsymbol{Q}_\parallel)$ is the Fourier transform of the n'th-order contribution to the surface roughness, as defined in equation (56). The Fourier transform of $(\zeta(\boldsymbol{x}_\parallel))^0 = 1$ is the Dirac delta function with a factor of $(2\pi)^2$ for normalization in the chosen convention, and the matrices in equation (64) are therefore all proportional to the Dirac delta function of their respective arguments. Performing the integral over $\delta(\boldsymbol{p}_\parallel - \boldsymbol{q}_\parallel)$ yields

$$\boldsymbol{\mathcal{M}}^{(0)}(\boldsymbol{p}_\parallel|\boldsymbol{p}_\parallel)\boldsymbol{R}^{(0)}(\boldsymbol{p}_\parallel|\boldsymbol{k}_\parallel) = -\boldsymbol{\mathcal{N}}^{(0)}(\boldsymbol{p}_\parallel|\boldsymbol{k}_\parallel)\hat{\zeta}^{(0)}(\boldsymbol{p}_\parallel - \boldsymbol{k}_\parallel). \tag{65}$$

The $\boldsymbol{R}^{(0)}(\boldsymbol{q}_\parallel|\boldsymbol{k}_\parallel)$ then becomes

$$\boldsymbol{R}^{(0)}(\boldsymbol{q}_\parallel|\boldsymbol{k}_\parallel) = (2\pi)^2\delta(\boldsymbol{q}_\parallel - \boldsymbol{k}_\parallel)\begin{pmatrix} \frac{\varepsilon_2\alpha_1 - \varepsilon_1\alpha_2}{\varepsilon_2\alpha_1 + \varepsilon_1\alpha_2} & 0 \\ 0 & \frac{\alpha_1 - \alpha_2}{\alpha_2 + \alpha_1} \end{pmatrix} \tag{66}$$

which are the well known Fresnel coefficients for p- and s-polarized light, exactly as expected for a completely flat surface.

2.11.1 First order perturbation

Starting again from equation (63) with $n = 1$, there are now two terms for which the binomial coefficient differs from zero, the equation becomes

$$\begin{aligned} &\begin{pmatrix} 1 \\ 0 \end{pmatrix} \int \frac{d^2q_\parallel}{(2\pi)^2} \boldsymbol{\mathcal{M}}^{(1)}(\boldsymbol{p}_\parallel|\boldsymbol{q}_\parallel)\hat{\zeta}^{(1)}(\boldsymbol{p}_\parallel - \boldsymbol{q}_\parallel)\boldsymbol{R}^{(0)}(\boldsymbol{q}_\parallel|\boldsymbol{k}_\parallel) \\ +&\begin{pmatrix} 1 \\ 1 \end{pmatrix} \int \frac{d^2q_\parallel}{(2\pi)^2} \boldsymbol{\mathcal{M}}^{(0)}(\boldsymbol{p}_\parallel|\boldsymbol{q}_\parallel)\hat{\zeta}^{(0)}(\boldsymbol{p}_\parallel - \boldsymbol{q}_\parallel)\boldsymbol{R}^{(1)}(\boldsymbol{q}_\parallel|\boldsymbol{k}_\parallel) \\ &= -\boldsymbol{\mathcal{N}}^{(1)}(\boldsymbol{p}_\parallel|\boldsymbol{k}_\parallel)\hat{\zeta}^{(1)}(\boldsymbol{p}_\parallel - \boldsymbol{k}_\parallel) \end{aligned} \tag{67}$$

Rearranging and integrating over the δ-functions yields.

$$\begin{aligned} \boldsymbol{\mathcal{M}}^{(0)}(\boldsymbol{p}_\parallel|\boldsymbol{p}_\parallel)\boldsymbol{R}^{(1)}(\boldsymbol{p}_\parallel|\boldsymbol{k}_\parallel) = -\big[&\boldsymbol{\mathcal{M}}^{(1)}(\boldsymbol{p}_\parallel|\boldsymbol{k}_\parallel)\boldsymbol{R}^{(0)}(\boldsymbol{k}_\parallel|\omega) \\ &+ \boldsymbol{\mathcal{N}}^{(1)}(\boldsymbol{p}_\parallel|\boldsymbol{k}_\parallel)\big]\hat{\zeta}^{(1)}(\boldsymbol{p}_\parallel - \boldsymbol{k}_\parallel) \end{aligned} \tag{68}$$

Multiplying from the left by the inverse of $\boldsymbol{\mathcal{M}}^{(0)}(\boldsymbol{p}_\parallel|\boldsymbol{p}_\parallel)$ on both sides

$$\begin{aligned} \boldsymbol{R}^{(1)}(\boldsymbol{p}_\parallel|\boldsymbol{k}_\parallel) = -\boldsymbol{\mathcal{M}}^{(0)}(\boldsymbol{p}_\parallel|\boldsymbol{p}_\parallel)^{-1}\big[&\boldsymbol{\mathcal{N}}^{(1)}(\boldsymbol{p}_\parallel|\boldsymbol{k}_\parallel) \\ &+ \boldsymbol{\mathcal{M}}^{(1)}(\boldsymbol{p}_\parallel|\boldsymbol{k}_\parallel)\boldsymbol{R}^{(0)}(k_\parallel,\omega))\big]\hat{\zeta}^{(1)}(\boldsymbol{p}_\parallel - \boldsymbol{k}_\parallel) \end{aligned} \tag{69}$$

writing the fourier transform of the surface roughness function separately the first order reflection amplitude becomes

$$R^{(1)}_{\alpha\beta}(\boldsymbol{q}_\parallel|\boldsymbol{k}_\parallel) = \mathcal{X}^{(1)}_{\alpha\beta}(\boldsymbol{q}_\parallel|\boldsymbol{k}_\parallel)\hat{\zeta}^{(1)}(\boldsymbol{q}_\parallel - \boldsymbol{k}_\parallel). \tag{70}$$

The elements of $\mathcal{X}^{(1)}_{\alpha\beta}(\boldsymbol{q}_\parallel|\boldsymbol{k}_\parallel)$ are found to be

$$\mathcal{X}^{(1)}_{pp}(\boldsymbol{q}_\parallel|\boldsymbol{k}_\parallel) = -2\alpha_1(k_\parallel)\frac{\varepsilon_2-\varepsilon_1}{\varepsilon_2\alpha_1(q_\parallel)+\epsilon_1\alpha_2(q_\parallel))} \times [q_\parallel k_\parallel \varepsilon_2 - \varepsilon_1\alpha_2(\boldsymbol{q}_\parallel)\hat{\boldsymbol{q}}_\parallel\cdot\hat{\boldsymbol{k}}_\parallel\alpha_2(k_\parallel)] \times \frac{1}{\varepsilon_2\alpha_1(k_\parallel,\omega)+\varepsilon_1\alpha_2(k_\parallel,\omega))} \tag{71}$$

$$\mathcal{X}^{(1)}_{ss}(\boldsymbol{q}_\parallel|\boldsymbol{k}_\parallel) = -2\alpha_1(k_\parallel)\frac{\varepsilon_2-\varepsilon_1}{\alpha_1(q_\parallel)+\alpha_2(q_\parallel)}\frac{\omega^2}{c^2}\,\hat{\boldsymbol{q}}_\parallel\cdot\hat{\boldsymbol{k}}_\parallel\frac{1}{\alpha_1(k_\parallel)+\alpha_2(k_\parallel)} \tag{72}$$

$$\mathcal{X}^{(1)}_{ps}(\boldsymbol{q}_\parallel|\boldsymbol{k}_\parallel) = 2\alpha_1(k_\parallel)\frac{\varepsilon_2-\varepsilon_1}{\varepsilon_2\alpha_1(q_\parallel)+\varepsilon_1\alpha_2(q_\parallel)}\frac{\omega}{c}\,\alpha_2(q_\parallel)[\hat{\boldsymbol{q}}_\parallel\times\hat{\boldsymbol{k}}_\parallel]_3\frac{1}{\alpha_1(k_\parallel)+\alpha_2(k_\parallel)} \tag{73}$$

$$\mathcal{X}^{(1)}_{sp}(\boldsymbol{q}_\parallel|\boldsymbol{k}_\parallel) = 2\alpha_1(k_\parallel)\frac{\varepsilon_2-\varepsilon_1}{\alpha_2(q_\parallel)+\alpha_1(q_\parallel)}\frac{\omega}{c}\,[\hat{\boldsymbol{q}}_\parallel\times\hat{\boldsymbol{k}}_\parallel]_3\alpha_2(k_\parallel)\frac{\varepsilon_1}{\varepsilon_2\alpha_1(k_\parallel)+\varepsilon_1\alpha_2(k_\parallel)}. \tag{74}$$

Finally, averaging over the fourier transforms of the surface roughness function as in Eq. (27), the first term in the expansion of the incoherent MDRC is given as

$$|\mathcal{X}^{(1)}_{\alpha\beta}(\boldsymbol{q}_\parallel|\boldsymbol{k}_\parallel)|^2\langle\hat{\zeta}^{(1)}(\boldsymbol{q}_\parallel-\boldsymbol{k}_\parallel)\hat{\zeta}^{(1)}(\boldsymbol{k}_\parallel-\boldsymbol{q}_\parallel)\rangle = |\mathcal{X}^{(1)}_{\alpha\beta}(\boldsymbol{q}_\parallel|\boldsymbol{k}_\parallel)|^2 S\delta^2 g(\boldsymbol{q}_\parallel-\boldsymbol{k}_\parallel), \tag{75}$$

where the factor $S = L_1L_2$, which is obtained through Eq. (121), is the area of the finite surface considered with side lengths L_1 and L_2.

Each of the terms in the expansion of the incoherent component of the MDRC (39) correspond to a physical rough surface scattering process, which can be determined through inspection of the mathematical form of the equations and physical insight into the nature of perturbative expansions. The terms related to the surface configuration in Eq. 75 are the RMS surface height δ and the effect spectrum $g(\boldsymbol{q}_\parallel-\boldsymbol{k}_\parallel)$ (24). The RMS surface height is independent of the scattering direction, only affecting the magnitude of the scattering contribution. The effect spectrum on the other hand completely governs the effect that the statistical properties of the surface has on the scattering behaviour in a specific scattering direction, it is therefore possible to describe certain aspects of the coupling processes between the incoming light and the rough surface by analysing how the effect spectrum influences the scattering intensity. It is important to note that the effect spectrum is not the sole physical aspect of a surface that influences the scattering behaviour. The material properties of the surface, such as electric permittivity and magnetic permeability, also have an impact, and are included through the $\mathcal{X}_{\alpha\beta}$ term in the reflection amplitude.

Eq. (75) depends on the first order of the effect spectrum evaluated on the difference between the incident and scattered parallel wave vector. This tells us that the scattering contribution is governed by the direct coupling between the incident and scattered wave vector or, as it is more commonly stated, this term is a single scattering contribution.

2.11.2 Second order perturbation

Starting from equation (63) with $n = 2$ we have

$$\begin{aligned}
&\binom{2}{0}\int\frac{d^2q_\parallel}{(2\pi)^2}\boldsymbol{\mathcal{M}}^{(2)}(\boldsymbol{p}_\parallel|\boldsymbol{q}_\parallel)\hat{\zeta}^{(2)}(\boldsymbol{p}_\parallel-\boldsymbol{q}_\parallel)\boldsymbol{R}^{(0)}(\boldsymbol{q}_\parallel|\boldsymbol{k}_\parallel)\\
+&\binom{2}{1}\int\frac{d^2q_\parallel}{(2\pi)^2}\boldsymbol{\mathcal{M}}^{(1)}(\boldsymbol{p}_\parallel|\boldsymbol{q}_\parallel)\hat{\zeta}^{(1)}(\boldsymbol{p}_\parallel-\boldsymbol{q}_\parallel)\boldsymbol{R}^{(1)}(\boldsymbol{q}_\parallel|\boldsymbol{k}_\parallel)\\
+&\binom{2}{2}\int\frac{d^2q_\parallel}{(2\pi)^2}\boldsymbol{\mathcal{M}}^{(0)}(\boldsymbol{p}_\parallel|\boldsymbol{q}_\parallel)\hat{\zeta}^{(0)}(\boldsymbol{p}_\parallel-\boldsymbol{q}_\parallel)\boldsymbol{R}^{(2)}(\boldsymbol{q}_\parallel|\boldsymbol{k}_\parallel)\\
&= -\boldsymbol{\mathcal{N}}^{(2)}(\boldsymbol{p}_\parallel|\boldsymbol{k}_\parallel)\hat{\zeta}^{(2)}(\boldsymbol{p}_\parallel-\boldsymbol{k}_\parallel).
\end{aligned} \tag{76}$$

Integrating over the δ-functions, switching the variables as to have an expression for $\boldsymbol{R}^{(2)}(\boldsymbol{q}_\parallel|\boldsymbol{k}_\parallel)$ and rearranging terms yields the following expression

$$\begin{aligned}\boldsymbol{R}^{(2)}(\boldsymbol{q}_\parallel|\boldsymbol{k}_\parallel) = &-\boldsymbol{\mathcal{M}}^{(0)}(\boldsymbol{q}_\parallel|\boldsymbol{q}_\parallel)^{-1}\boldsymbol{\mathcal{M}}^{(2)}(\boldsymbol{q}_\parallel|\boldsymbol{k}_\parallel)\hat{\zeta}^{(2)}(\boldsymbol{q}_\parallel-\boldsymbol{k}_\parallel)\boldsymbol{R}^{(0)}(\boldsymbol{k}_\parallel|\omega)\\ &-2\boldsymbol{\mathcal{M}}^{(0)}(\boldsymbol{q}_\parallel|\boldsymbol{q}_\parallel)^{-1}\int\frac{d^2p_\parallel}{(2\pi)^2}\boldsymbol{\mathcal{M}}^{(1)}(\boldsymbol{q}_\parallel|\boldsymbol{p}_\parallel)\hat{\zeta}^{(1)}(\boldsymbol{q}_\parallel-\boldsymbol{p}_\parallel)\boldsymbol{R}^{(1)}(\boldsymbol{p}_\parallel|\boldsymbol{k}_\parallel)\\ &-\boldsymbol{\mathcal{M}}^{(0)}(\boldsymbol{q}_\parallel|\boldsymbol{q}_\parallel)^{-1}\boldsymbol{\mathcal{N}}^{(2)}(\boldsymbol{q}_\parallel|\boldsymbol{k}_\parallel)\hat{\zeta}^{(2)}(\boldsymbol{q}_\parallel-\boldsymbol{k}_\parallel).\end{aligned}\tag{77}$$

Defining two new matrices $\boldsymbol{A}(\boldsymbol{q}_\parallel|\boldsymbol{k}_\parallel)$ and $\boldsymbol{B}(\boldsymbol{q}_\parallel|\boldsymbol{p}_\parallel|\boldsymbol{k}_\parallel)$ to make the equations more readable

$$\begin{aligned}\boldsymbol{A}(\boldsymbol{q}_\parallel|\boldsymbol{k}_\parallel) = &-\boldsymbol{\mathcal{M}}^{(0)}(\boldsymbol{q}_\parallel|\boldsymbol{q}_\parallel)^{-1}\boldsymbol{\mathcal{M}}^{(2)}(\boldsymbol{q}_\parallel|\boldsymbol{k}_\parallel)\boldsymbol{R}^{(0)}(\boldsymbol{k}_\parallel|\omega)\\ &-\boldsymbol{\mathcal{M}}^{(0)}(\boldsymbol{q}_\parallel|\boldsymbol{q}_\parallel)^{-1}\boldsymbol{\mathcal{N}}^{(2)}(\boldsymbol{q}_\parallel|\boldsymbol{k}_\parallel)\end{aligned}\tag{78}$$

$$\boldsymbol{B}(\boldsymbol{q}_\parallel|\boldsymbol{p}_\parallel|\boldsymbol{k}_\parallel) = -2\boldsymbol{\mathcal{M}}^{(0)}(\boldsymbol{q}_\parallel|\boldsymbol{q}_\parallel)^{-1}\boldsymbol{\mathcal{M}}^{(1)}(\boldsymbol{q}_\parallel|\boldsymbol{p}_\parallel)\boldsymbol{R}^{(1)}(\boldsymbol{p}_\parallel|\boldsymbol{k}_\parallel).\tag{79}$$

Rewriting $\hat{\zeta}^{(2)}(\boldsymbol{q}_\parallel\boldsymbol{k}_\parallel)$ using Eq. (122) the second order reflection order reflection amplitude becomes

$$\begin{aligned}R^{(2)}(\boldsymbol{q}_\parallel|\boldsymbol{k}_\parallel) = &\boldsymbol{A}(\boldsymbol{q}_\parallel|\boldsymbol{k}_\parallel)\int\frac{d^2p_\parallel}{(2\pi)^2}\hat{\zeta}^{(1)}(\boldsymbol{q}_\parallel-\boldsymbol{p}_\parallel)\hat{\zeta}^{(1)}(\boldsymbol{p}_\parallel-\boldsymbol{k}_\parallel)\\ &+\int\frac{d^2p_\parallel}{(2\pi)^2}\boldsymbol{B}(\boldsymbol{q}_\parallel|\boldsymbol{p}_\parallel|\boldsymbol{k}_\parallel)\hat{\zeta}^{(1)}(\boldsymbol{q}_\parallel-\boldsymbol{p}_\parallel)\hat{\zeta}^{(1)}(\boldsymbol{p}_\parallel-\boldsymbol{k}_\parallel).\end{aligned}\tag{80}$$

Inserting the expression for $R^{(2)}(\boldsymbol{q}_\parallel|\boldsymbol{k}_\parallel)$ into the second order terms in the incoherent component of the MDRC (39) and averaging over the various terms in the Fourier transform of the roughness function, as described in appendix A1: Useful identities, yields the following expression for the second order terms in the expansion (52)

$$\begin{aligned}\langle|R^{(2)}_{\alpha\beta}(\boldsymbol{q}_\parallel|\boldsymbol{k}_\parallel)|^2\rangle - |\langle R^{(2)}_{\alpha\beta}(\boldsymbol{q}_\parallel|\boldsymbol{k}_\parallel)\rangle|^2 = &2|A_{\alpha\beta}(\boldsymbol{q}_\parallel|\boldsymbol{k}_\parallel)|^2\delta^4S\int\frac{d^2p_\parallel}{(2\pi)^2}g(\boldsymbol{q}_\parallel-\boldsymbol{p}_\parallel)g(\boldsymbol{p}_\parallel-\boldsymbol{k}_\parallel)\\ &+\delta^4SA_{\alpha\beta}(\boldsymbol{q}_\parallel|\boldsymbol{k}_\parallel)\int\frac{d^2p_\parallel}{(2\pi)^2}B^*_{\alpha\beta}(\boldsymbol{q}_\parallel|\boldsymbol{p}_\parallel|\boldsymbol{k}_\parallel)\\ &+\delta^4SA_{\alpha\beta}(\boldsymbol{q}_\parallel|\boldsymbol{k}_\parallel)\int\frac{d^2p_\parallel}{(2\pi)^2}B^*_{\alpha\beta}(\boldsymbol{q}_\parallel|\boldsymbol{k}_\parallel+\boldsymbol{q}_\parallel-\boldsymbol{p}_\parallel|\boldsymbol{k}_\parallel)\\ &\times g(\boldsymbol{q}_\parallel-\boldsymbol{p}_\parallel)g(\boldsymbol{p}_\parallel-\boldsymbol{k}_\parallel)\\ &+2\delta^4SA^*_{\alpha\beta}(\boldsymbol{q}_\parallel|\boldsymbol{k}_\parallel)\int\frac{d^2p_\parallel}{(2\pi)^2}B_{\alpha\beta}(\boldsymbol{q}_\parallel|\boldsymbol{p}_\parallel|\boldsymbol{k}_\parallel)\\ &\times g(\boldsymbol{p}_\parallel-\boldsymbol{q}_\parallel)g(\boldsymbol{k}_\parallel-\boldsymbol{p}_\parallel)\\ &+\delta^4S\int\frac{d^2p_\parallel}{(2\pi)^2}B_{\alpha\beta}(\boldsymbol{q}_\parallel|\boldsymbol{p}_\parallel|\boldsymbol{k}_\parallel)B^*_{\alpha\beta}(\boldsymbol{q}_\parallel|\boldsymbol{p}_\parallel|\boldsymbol{k}_\parallel)\\ &\times g(\boldsymbol{q}_\parallel-\boldsymbol{p}_\parallel)g(\boldsymbol{p}_\parallel-\boldsymbol{k}_\parallel)\\ &+\delta^4S\int\frac{d^2p_\parallel}{(2\pi)^2}B_{\alpha\beta}(\boldsymbol{q}_\parallel|\boldsymbol{p}_\parallel|\boldsymbol{k}_\parallel)\\ &\times B^*_{\alpha\beta}(\boldsymbol{q}_\parallel|\boldsymbol{k}_\parallel+\boldsymbol{q}_\parallel-\boldsymbol{p}_\parallel|\boldsymbol{k}_\parallel)g(\boldsymbol{p}_\parallel-\boldsymbol{k}_\parallel)g(\boldsymbol{q}_\parallel-\boldsymbol{p}_\parallel),\end{aligned}\tag{81}$$

where δ is the root mean square height of the surface, and $S = L_1L_2$. Where L_1 and L_2 are the side lengths of the finite surface considered.

In Eq. (75) it was observed that the scattering intensity was proportional to direct coupling between the incident and scattered parallel wave vectors. For the scattering contribution in Eq. (81) it is instead observed that each term has a factor corresponding to an integral over a product of two effect spectra. The first effect spectrum is evaluated for the difference between the incident parallel wave vector $\boldsymbol{k}_\parallel$ and the integration variable $\boldsymbol{p}_\parallel$, while the second is evaluated for the difference between the scattered parallel wave vector $\boldsymbol{q}_\parallel$ and the integration variable. The first term describes how well the incident wave couples to an intermittent wave mode $\boldsymbol{p}_\parallel$, while the second term describes how well the wave mode $\boldsymbol{p}_\parallel$ couples to the scattered wave. In effect, this expresses the contribution to the scattering intensity from an incident wave $\boldsymbol{k}_\parallel$ to an outgoing wave $\boldsymbol{q}_\parallel$, through intermittent scattering via a scattering mode $\boldsymbol{p}_\parallel$. The contribution is thereby made up entirely of *double*-scattering contributions, also known as the lowest order of *multiple*-scattering contribution. The integral is performed over all possible intermittent wave modes, and the complete term thereby describes the scattering intensity from the sum of all contributions with a single intermittent scattering step. The most intuitive way to think of such an intermittent scattering step, is to imagine a geometrical scattering process where the incident light wave bounces of the slope of the rough surface, similar as if it where a massive particle, before bouncing once more of a neighbouring slope in the scattering direction $\boldsymbol{q}_\parallel$. A more apt description is to visualise this scattering contribution through Huygens principle, where all of the points on the surface act as spherical emitters. A portion of each of these spherical waves will again interact with the surface, and it is the contribution from these scattering processes that are considered in the Two-two contribution. This process can of course repeat itself several more times, resulting in higher order multiple scattering contributions, which can be modelled by including higher order terms in the perturbative expansion. It is also important to consider that the intermittent scattering mode is not restricted to be a travelling wave mode. As discussed in Sec. 2.3 dielectric-vacuum interfaces allow for the excitation of surface plasmon polaritons, an exponentially dampened electromagnetic surface wave traveling along the dielectric vacuum interface. These waves can also act as intermittent scattering modes, and are imperative to the description of scattering from weakly rough surfaces.

2.11.3 Third Order perturbation

Starting from equation (63) with $n = 3$ we have

$$\begin{aligned}
&\binom{3}{0}\int \frac{d^2q_\parallel}{(2\pi)^2}\boldsymbol{\mathcal{M}}^{(3)}(\boldsymbol{p}_\parallel|\boldsymbol{q}_\parallel)\hat{\zeta}^{(3)}(\boldsymbol{p}_\parallel-\boldsymbol{q}_\parallel)\boldsymbol{R}^{(0)}(\boldsymbol{q}_\parallel|\boldsymbol{k}_\parallel)\\
+&\binom{3}{1}\int \frac{d^2q_\parallel}{(2\pi)^2}\boldsymbol{\mathcal{M}}^{(2)}(\boldsymbol{p}_\parallel|\boldsymbol{q}_\parallel)\hat{\zeta}^{(2)}(\boldsymbol{p}_\parallel-\boldsymbol{q}_\parallel)\boldsymbol{R}^{(1)}(\boldsymbol{q}_\parallel|\boldsymbol{k}_\parallel)\\
+&\binom{3}{2}\int \frac{d^2q_\parallel}{(2\pi)^2}\boldsymbol{\mathcal{M}}^{(1)}(\boldsymbol{p}_\parallel|\boldsymbol{q}_\parallel)\hat{\zeta}^{(1)}(\boldsymbol{p}_\parallel-\boldsymbol{q}_\parallel)\boldsymbol{R}^{(2)}(\boldsymbol{q}_\parallel|\boldsymbol{k}_\parallel)\\
+&\binom{3}{3}\int \frac{d^2q_\parallel}{(2\pi)^2}\boldsymbol{\mathcal{M}}^{(0)}(\boldsymbol{p}_\parallel|\boldsymbol{q}_\parallel)\hat{\zeta}^{(0)}(\boldsymbol{p}_\parallel-\boldsymbol{q}_\parallel)\boldsymbol{R}^{(3)}(\boldsymbol{q}_\parallel|\boldsymbol{k}_\parallel)\\
&\qquad\qquad = -\boldsymbol{\mathcal{N}}^{(3)}(\boldsymbol{p}_\parallel|\boldsymbol{k}_\parallel)\hat{\zeta}^{(3)}(\boldsymbol{p}_\parallel-\boldsymbol{k}_\parallel).
\end{aligned} \tag{82}$$

Integrating over the δ-functions and rearranging terms yields

$$\begin{aligned}
\boldsymbol{R}^{(3)}(\boldsymbol{p}_\parallel|\boldsymbol{k}_\parallel) = -\boldsymbol{\mathcal{M}}^{(0)}(\boldsymbol{p}_\parallel|\boldsymbol{p}_\parallel)^{-1}\Big[&\boldsymbol{\mathcal{M}}^{(3)}(\boldsymbol{p}_\parallel|\boldsymbol{k}_\parallel)\mathbf{R}^{(0)}(\boldsymbol{k}_\parallel|\omega)\hat{\zeta}^{(3)}(\boldsymbol{p}_\parallel-\boldsymbol{k}_\parallel)\\
&+3\int \frac{d^2q_\parallel}{(2\pi)^2}\boldsymbol{\mathcal{M}}^{(2)}(\boldsymbol{p}_\parallel|\boldsymbol{q}_\parallel)\hat{\zeta}^{(2)}(\boldsymbol{p}_\parallel-\boldsymbol{q}_\parallel)\boldsymbol{R}^{(1)}(\boldsymbol{q}_\parallel|\boldsymbol{k}_\parallel)\\
&+3\int \frac{d^2q_\parallel}{(2\pi)^2}\boldsymbol{\mathcal{M}}^{(1)}(\boldsymbol{p}_\parallel|\boldsymbol{q}_\parallel)\hat{\zeta}^{(1)}(\boldsymbol{p}_\parallel-\boldsymbol{q}_\parallel)\boldsymbol{R}^{(2)}(\boldsymbol{q}_\parallel|\boldsymbol{k}_\parallel)\\
&+\boldsymbol{\mathcal{N}}^{(3)}(\boldsymbol{p}_\parallel|\boldsymbol{k}_\parallel)\hat{\zeta}^{(3)}(\boldsymbol{p}_\parallel-\boldsymbol{k}_\parallel)\Big].
\end{aligned} \tag{83}$$

By inserting the previously derived expressions for the first and second order perturbation the $\langle R^{(1)*}_{\alpha\beta}(\boldsymbol{q}_\parallel|\boldsymbol{k}_\parallel)R^{(3)}_{\alpha\beta}(\boldsymbol{q}_\parallel|\boldsymbol{k}_\parallel)\rangle$ term in the expansion of the incoherent component of the MDRC (39), writing $R^{(1)*}_{\alpha\beta}(\boldsymbol{q}_\parallel|\boldsymbol{k}_\parallel) = \mathcal{X}^{(1)*}_{\alpha\beta}(\boldsymbol{q}_\parallel|\boldsymbol{k}_\parallel)\hat{\zeta}^{(1)}(\boldsymbol{k}_\parallel - \boldsymbol{q}_\parallel)$ we have

$$\begin{aligned}
\langle R^{(1)*}_{\alpha\beta}(\boldsymbol{q}_\parallel|\boldsymbol{k}_\parallel)R^{(3)}_{\alpha\beta}(\boldsymbol{q}_\parallel|\boldsymbol{k}_\parallel)\rangle &= \mathcal{X}^{(1)*}_{\alpha\beta}(\boldsymbol{q}_\parallel|\boldsymbol{k}_\parallel)\mathcal{M}^{(0)}_{\alpha\beta}(\boldsymbol{q}_\parallel|\boldsymbol{q}_\parallel)^{-1} \\
&\times \Big\{ \big[\boldsymbol{\mathcal{M}}^{(3)}(\boldsymbol{q}_\parallel|\boldsymbol{k}_\parallel)\mathbf{R}^{(0)}(\boldsymbol{k}_\parallel|\omega) + \boldsymbol{\mathcal{N}}^{(3)}(\boldsymbol{q}_\parallel|\boldsymbol{k}_\parallel)\big]_{\alpha\beta} \\
&\langle \hat{\zeta}^{(3)}(\boldsymbol{q}_\parallel - \boldsymbol{p}_\parallel)\hat{\zeta}^{(1)}(\boldsymbol{k}_\parallel - \boldsymbol{q}_\parallel)\rangle \\
&+ 3\int \frac{d^2p_\parallel}{(2\pi)^2}\big[\boldsymbol{\mathcal{M}}^{(2)}(\boldsymbol{q}_\parallel|\boldsymbol{p}_\parallel)\boldsymbol{\mathcal{X}}^{(1)}(\boldsymbol{p}_\parallel|\boldsymbol{k}_\parallel)\big]_{\alpha\beta} \\
&\langle \hat{\zeta}^{(2)}(\boldsymbol{q}_\parallel - \boldsymbol{p}_\parallel)\hat{\zeta}^{(1)}(\boldsymbol{k}_\parallel - \boldsymbol{q}_\parallel)\hat{\zeta}^{(1)}(\boldsymbol{p}_\parallel - \boldsymbol{k}_\parallel)\rangle \\
&+ 3\int \frac{d^2p_\parallel}{(2\pi)^2}\big[\boldsymbol{\mathcal{M}}^{(1)}(\boldsymbol{q}_\parallel|\boldsymbol{p}_\parallel)\boldsymbol{A}(\boldsymbol{p}_\parallel|\boldsymbol{k}_\parallel)\big]_{\alpha\beta} \\
&\langle \hat{\zeta}^{(2)}(\boldsymbol{p}_\parallel - \boldsymbol{k}_\parallel)\hat{\zeta}^{(1)}(\boldsymbol{q}_\parallel - \boldsymbol{p}_\parallel)\hat{\zeta}^{(1)}(\boldsymbol{k}_\parallel - \boldsymbol{q}_\parallel)\rangle \\
&+ 3\int \frac{d^2p_\parallel}{(2\pi)^2}\int_{-\infty}^{\infty}\frac{d^2p'}{(2\pi)^2}\big[\boldsymbol{\mathcal{M}}^{(1)}(\boldsymbol{q}_\parallel|\boldsymbol{p}_\parallel)\boldsymbol{B}(\boldsymbol{p}_\parallel|\boldsymbol{p'}_\parallel|\boldsymbol{k}_\parallel)\big]_{\alpha\beta} \\
&\langle \hat{\zeta}^{(1)}(\boldsymbol{q}_\parallel - \boldsymbol{p}_\parallel)\hat{\zeta}^{(1)}(\boldsymbol{k}_\parallel - \boldsymbol{q}_\parallel)\hat{\zeta}^{(1)}(\boldsymbol{p}_\parallel - \boldsymbol{p'}_\parallel)\hat{\zeta}^{(1)}(\boldsymbol{p'}_\parallel - \boldsymbol{k}_\parallel)\rangle\Big\}. \quad (84)
\end{aligned}$$

Using the Fourier identity (122) to rewrite all the terms averaging over the Fourier transforms of the surface profile function, the expression becomes

$$\begin{aligned}
\langle R^{(1)*}_{\alpha\beta}(\boldsymbol{q}_\parallel|\boldsymbol{k}_\parallel)R^{(3)}_{\alpha\beta}(\boldsymbol{q}_\parallel|\boldsymbol{k}_\parallel)\rangle &= \mathcal{X}^{(1)*}_{\alpha\beta}(\boldsymbol{q}_\parallel|\boldsymbol{k}_\parallel)\mathcal{M}^{(0)}_{\alpha\beta}(\boldsymbol{q}_\parallel|\boldsymbol{q}_\parallel)^{-1} \\
&\times \int \frac{d^2p_\parallel}{(2\pi)^2}\int_{-\infty}^{\infty}\frac{d^2p'}{(2\pi)^2} \\
&\Big\{\ 3\big[\boldsymbol{\mathcal{M}}^{(1)}(\boldsymbol{q}_\parallel|\boldsymbol{p}_\parallel)\boldsymbol{B}(\boldsymbol{p}_\parallel|\boldsymbol{p'}_\parallel|\boldsymbol{k}_\parallel)\big]_{\alpha\beta} \\
&+ 3\big[\boldsymbol{\mathcal{M}}^{(1)}(\boldsymbol{q}_\parallel|\boldsymbol{p}_\parallel)\boldsymbol{A}(\boldsymbol{p}_\parallel|\boldsymbol{k}_\parallel)\big]_{\alpha\beta} \\
&+ 3\big[\boldsymbol{\mathcal{M}}^{(2)}(\boldsymbol{q}_\parallel|\boldsymbol{p'}_\parallel)\boldsymbol{\mathcal{X}}^{(1)}(\boldsymbol{p'}_\parallel|\boldsymbol{k}_\parallel)\big]_{\alpha\beta} \\
&+\ \ \big[\boldsymbol{\mathcal{M}}^{(3)}(\boldsymbol{q}_\parallel|\boldsymbol{k}_\parallel)\mathbf{R}^{(0)}(\boldsymbol{k}_\parallel|\omega) + \boldsymbol{\mathcal{N}}^{(3)}(\boldsymbol{q}_\parallel|\boldsymbol{k}_\parallel)\big]_{\alpha\beta}\Big\} \\
&\langle \hat{\zeta}^{(1)}(\boldsymbol{q}_\parallel - \boldsymbol{p}_\parallel)\hat{\zeta}^{(1)}(\boldsymbol{k}_\parallel - \boldsymbol{q}_\parallel)\hat{\zeta}^{(1)}(\boldsymbol{p}_\parallel - \boldsymbol{p'}_\parallel)\hat{\zeta}^{(1)}(\boldsymbol{p'}_\parallel - \boldsymbol{k}_\parallel)\rangle. \quad (85)
\end{aligned}$$

Defining

$$\begin{aligned}
\mathcal{X}^{(3)}_{\alpha\beta}(\boldsymbol{q}_\parallel|\boldsymbol{p}_\parallel|\boldsymbol{p'}_\parallel|\boldsymbol{k}_\parallel) &= 3\big[\boldsymbol{\mathcal{M}}^{(1)}(\boldsymbol{q}_\parallel|\boldsymbol{p}_\parallel)\boldsymbol{B}(\boldsymbol{p}_\parallel|\boldsymbol{p'}_\parallel|\boldsymbol{k}_\parallel)\big]_{\alpha\beta} \\
&+ 3\big[\boldsymbol{\mathcal{M}}^{(1)}(\boldsymbol{q}_\parallel|\boldsymbol{p}_\parallel)\boldsymbol{A}(\boldsymbol{p}_\parallel|\boldsymbol{k}_\parallel)\big]_{\alpha\beta} \\
&+ 3\big[\boldsymbol{\mathcal{M}}^{(2)}(\boldsymbol{q}_\parallel|\boldsymbol{p'}_\parallel)\boldsymbol{\mathcal{X}}^{(1)}(\boldsymbol{p'}_\parallel|\boldsymbol{k}_\parallel)\big]_{\alpha\beta} \\
&+\ \ \big[\boldsymbol{\mathcal{M}}^{(3)}(\boldsymbol{q}_\parallel|\boldsymbol{k}_\parallel)\mathbf{R}^{(0)}(\boldsymbol{k}_\parallel|\omega) + \boldsymbol{\mathcal{N}}^{(3)}(\boldsymbol{q}_\parallel|\boldsymbol{k}_\parallel)\big]_{\alpha\beta}\Big\}, \quad (86)
\end{aligned}$$

and inserting for the average over the surface roughness term (115), we arrive at

$$\begin{aligned}
\langle R^{(1)*}_{\alpha\beta}(\boldsymbol{q}_\parallel|\boldsymbol{k}_\parallel)R^{(3)}_{\alpha\beta}(\boldsymbol{q}_\parallel|\boldsymbol{k}_\parallel)\rangle &= \mathcal{X}^{(1)*}_{\alpha\beta}(\boldsymbol{q}_\parallel|\boldsymbol{k}_\parallel)\mathcal{M}^{(0)}_{\alpha\beta}(\boldsymbol{q}_\parallel|\boldsymbol{q}_\parallel)^{-1} \\
&\times \int \frac{d^2p_\parallel}{(2\pi)^2}\int \frac{d^2p'}{(2\pi)^2}\mathcal{X}^{(3)}_{\alpha\beta}(\boldsymbol{q}_\parallel|\boldsymbol{p}_\parallel|\boldsymbol{p'}_\parallel|\boldsymbol{k}_\parallel)(2\pi)^2\delta^4 S \\
&\times \big[g(\boldsymbol{q}_\parallel - \boldsymbol{p}_\parallel)g(\boldsymbol{p}_\parallel - \boldsymbol{p'}_\parallel)\delta(\boldsymbol{k}_\parallel - \boldsymbol{p}_\parallel) \\
&+\ g(\boldsymbol{q}_\parallel - \boldsymbol{p}_\parallel)g(\boldsymbol{k}_\parallel - \boldsymbol{q}_\parallel)\delta(\boldsymbol{q}_\parallel - \boldsymbol{p'}_\parallel) \\
&+\ g(\boldsymbol{q}_\parallel - \boldsymbol{p}_\parallel)g(\boldsymbol{k}_\parallel - \boldsymbol{q}_\parallel)\delta(\boldsymbol{q}_\parallel - \boldsymbol{p}_\parallel + \boldsymbol{p'}_\parallel - \boldsymbol{k}_\parallel)\big]. \quad (87)
\end{aligned}$$

Integrating over the delta functions yields the final expression for $\left\langle R^{(1)*}_{\alpha\beta}(\boldsymbol{q}_\parallel|\boldsymbol{k}_\parallel)R^{(3)}_{\alpha\beta}(\boldsymbol{q}_\parallel|\boldsymbol{k}_\parallel)\right\rangle$

$$\begin{aligned}\left\langle R^{(1)*}_{\alpha\beta}(\boldsymbol{q}_\parallel|\boldsymbol{k}_\parallel)R^{(3)}_{\alpha\beta}(\boldsymbol{q}_\parallel|\boldsymbol{k}_\parallel)\right\rangle &= \mathcal{X}^{(1)*}_{\alpha\beta}(\boldsymbol{q}_\parallel|\boldsymbol{k}_\parallel)\mathcal{M}^{(0)}_{\alpha\beta}(\boldsymbol{q}_\parallel|\boldsymbol{q}_\parallel)^{-1} \\ &\times \int \frac{d^2p_\parallel}{(2\pi)^2}\delta^4 S \\ &\times \big[\mathcal{X}^{(3)}_{\sigma\delta}(\boldsymbol{q}_\parallel|\boldsymbol{k}_\parallel|\boldsymbol{p}_\parallel|\boldsymbol{k}_\parallel)g(\boldsymbol{q}_\parallel-\boldsymbol{k}_\parallel)g(\boldsymbol{k}_\parallel-\boldsymbol{p}_\parallel) \\ &+ \mathcal{X}^{(3)}_{\sigma\delta}(\boldsymbol{q}_\parallel|\boldsymbol{p}_\parallel|\boldsymbol{q}_\parallel|\boldsymbol{k}_\parallel)g(\boldsymbol{q}_\parallel-\boldsymbol{p}_\parallel)g(\boldsymbol{k}_\parallel-\boldsymbol{q}_\parallel) \\ &+ \mathcal{X}^{(3)}_{\sigma\delta}(\boldsymbol{q}_\parallel|\boldsymbol{p}_\parallel|\boldsymbol{k}_\parallel+\boldsymbol{p}_\parallel-\boldsymbol{q}_\parallel|\boldsymbol{k}_\parallel)g(\boldsymbol{q}_\parallel-\boldsymbol{p}_\parallel)g(\boldsymbol{k}_\parallel-\boldsymbol{q}_\parallel)\big]. \end{aligned} \tag{88}$$

Similarly as for the Two-two contribution in Eq. (81) the Three-One contribution (88) contains an integral over a product of two evaluations of the effect spectrum. One of the effect spectra describes the direct coupling between the incident $\boldsymbol{k}_\parallel$ and scattered $\boldsymbol{q}_\parallel$ wave vector or its reciprocal partner, while the other describes the coupling between either the scattered or incoming wave vector and all possible scattering vectors $\boldsymbol{p}_\parallel$. This results in the Three-one scattering term being an interference term between the scattered direction $\boldsymbol{q}$ and all possible scattering modes. It is intuitive that the term would have a dependence on the behaviour of the direct coupling between the incident and scattered wave modes, since it is composed of the first and third order amplitude. Due to its nature it is often referred to as a single-scattering contribution, even though is in fact an interference term.

2.12 Coherent Expansion and The Reflectivity

It can often be of interest to use SAPT to analyse how the Coherent component of the MDRC behaves for rough surfaces, and through it analyse the behaviour of the reflectivity. This section will therefore introduce these quantities and how they are computed using SAPT. For the rough scattering problem formulated in this thesis the reflectivity takes the following form

$$\mathcal{R}_\beta(\boldsymbol{k}_\parallel,\omega) = \int d\Omega_s \left\langle \frac{\partial R_{\alpha\beta}}{\partial \Omega_s} \right\rangle_{coh} \tag{89}$$

Inserting the perturbative expansion (51) into the coherent component of the MDRC (38) and recalling that all odd moments of a Gaussian stochastic process average to zero (53) the coherent component of the MDRC becomes

$$\left\langle \frac{\partial R_{\alpha\beta}}{\partial \Omega_s} \right\rangle_{coh} = C\left|\langle R^{(0)}_{\alpha\beta}(\boldsymbol{q}_\parallel|\boldsymbol{k}_\parallel) - \frac{1}{2}R^{(2)}_{\alpha\beta}(\boldsymbol{q}_\parallel|\boldsymbol{k}_\parallel) + \frac{1}{24}R^{(4)}_{\alpha\beta}(\boldsymbol{q}_\parallel|\boldsymbol{k}_\parallel)\rangle\right|^2, \tag{90}$$

where C is given by

$$C = \frac{\varepsilon_1}{S}\frac{\omega^2}{(2\pi c)^2}\frac{\cos^2(\theta_s)}{\cos(\theta_0)} \tag{91}$$

Expanding the absolute square and neglecting terms of higher than fourth order in the surface profile function yields

$$\begin{aligned}\left\langle \frac{\partial R_{\alpha\beta}}{\partial \Omega_s} \right\rangle_{coh} &= C\,|\langle R^{(0)}_{\alpha\beta}(\boldsymbol{q}_\parallel|\boldsymbol{k}_\parallel)\rangle|^2 - \frac{1}{2}\langle R^{(0)}_{\alpha\beta}(\boldsymbol{q}_\parallel|\boldsymbol{k}_\parallel)\rangle\langle R^{*(2)}_{\alpha\beta}(\boldsymbol{q}_\parallel|\boldsymbol{k}_\parallel)\rangle \\ &- \frac{1}{2}\langle R^{*(0)}_{\alpha\beta}(\boldsymbol{q}_\parallel|\boldsymbol{k}_\parallel)\rangle\langle R^{(2)}_{\alpha\beta}(\boldsymbol{q}_\parallel|\boldsymbol{k}_\parallel)\rangle + \frac{1}{4}|\langle R^{(2)}_{\alpha\beta}(\boldsymbol{q}_\parallel|\boldsymbol{k}_\parallel)\rangle|^2 \\ &+ \frac{1}{12}Re(R^{(0)}_{\alpha\beta}(\boldsymbol{q}_\parallel|\boldsymbol{k}_\parallel)R^{*(4)}_{\alpha\beta}(\boldsymbol{q}_\parallel|\boldsymbol{k}_\parallel)). \end{aligned} \tag{92}$$

As opposed to the incoherent component of the MDRC the fourth order terms involving $R^{(4)}_{\alpha\beta}(\boldsymbol{q}_\parallel|\boldsymbol{k}_\parallel)$ don't cancel in the coherent component, meaning that it would be necessary to take the expansion one step further in order to compute the coherent component and the reflectivity. The

computation and implementation of the fourth order reflection amplitude in order to compute the reflectivity is a time-consuming and error-prone process, and it is easily avoided by employing conservation of energy.

2.12.1 Conservation of Energy

The MDRC is, as stated in Sec. 2.7, defined as the fraction of incident power of β-polarized light reflected as α-polarized light into a solid angle element $d\Omega_s$. The total power incident on the surface as β-polarized light and scattered as α-polarized light is then given by the integral of the MDRC over all solid angles above the surface. The Mean Differential Transmission Coefficient is defined similarly to the MDRC, but naturally describes the fraction of light transmitted into a solid angle element below the surface. The total power incident as β-polarized light and transmitted as α-polarized light is therefore given by the integral of the MDTC over all solid angles below the surface.

$$\mathcal{U}_{\alpha\beta}^{Sc} = \int d\Omega_s \left\langle \frac{\partial R_{\alpha\beta}}{\partial \Omega_s} \right\rangle \tag{93}$$

$$\mathcal{U}_{\alpha\beta}^{Tr} = \int d\Omega_t \left\langle \frac{\partial T_{\alpha\beta}}{\partial \Omega_t} \right\rangle \tag{94}$$

Lastly it is necessary to sum over the outgoing polarizations. Adding up the contributions from reflection and transmission we arrive at the total fraction of incident power scattered by the system for each of the incoming polarizations

$$\mathcal{U}_\beta = \sum_\alpha^{p,s} \mathcal{U}_{\alpha\beta}^{Sc} + \sum_\alpha^{p,s} \mathcal{U}_{\alpha\beta}^{Tr}. \tag{95}$$

Assuming that our system consists of non-absorbing media, the total fraction of incident power scattered and transmitted by the surface must naturally add up to one for the energy to be conserved. Conservation of energy can thereby be concisely packed into the following criteria

$$\mathcal{U}_\beta = 1, \tag{96}$$

which is what is most commonly used in evaluation of numerical simulations of rough surface scattering [14].

The derivation and computation of the transmission amplitudes can be performed in same manner as for the reflection amplitudes, but it would be time consuming and not necessary for our purposes. Instead Eq. (95) is simplified by limiting the description to a system that consists of an interface between a dielectric and a metal. Unfortunately a real metal is not a perfect conductor at optical wavelengths, and therefore not a non-absorbing media. The general description of a dielectric-metal interface would demand an additional term on the right hand side describing the energy absorbed into the surface. Unfortunately the derivation of such a term is difficult to perform in a rigorous manner, and its description also goes beyond the scope of this thesis.

In order to avoid accounting for the energy being transmitted through and absorbed by the surface, and thereby be able to provide a consistent energy conservation criteria, it is necessary to analyze the scattering from a weakly rough interface between a dielectric and a non-absorbing metal, which can be modelled by setting the imaginary component of the metals dielectric function to zero. The complete energy conservation criteria for scattering from a non-absorbing metal becomes

$$\sum_\alpha^{p,s} \mathcal{U}_{\alpha\beta}^{Sc} = 1 \tag{97}$$

2.12.2 The Reflectivity

Combining the decomposed MDRC (37) with Eq. (93) yields

$$\mathcal{U}_{\alpha\beta}{}^{Sc} = \int d\Omega_s \left[\left\langle \frac{\partial R_{\alpha\beta}}{\partial \Omega_s} \right\rangle_{coh} + \left\langle \frac{\partial R_{\alpha\beta}}{\partial \Omega_s} \right\rangle_{incoh} \right]. \tag{98}$$

Inserting the definition of the reflectivity (89) into Eq. (97) the reflectivity is given by the incoherent component of the MDRC as

$$\mathcal{R}_\beta(\boldsymbol{k}_\parallel, \omega) = 1 - \sum_{\alpha}^{p,s} \int d\Omega_s \left\langle \frac{\partial R_{\alpha\beta}}{\partial \Omega_s} \right\rangle_{incoh}. \tag{99}$$

Yielding an equation for the reflectivity which is independent of the fourth order reflection amplitude.

2.13 Expansion of the Mueller Matrix Elements

Inserting the expansion (51) into the expression for the incoherent Mueller Matrix element (47) yields

$$\begin{aligned} \langle R_{\alpha\beta} R^*_{\sigma\delta} \rangle_{incoh} = \langle R^{(1)}_{\alpha\beta} R^{*(1)}_{\sigma\delta} \rangle + \frac{1}{4} \langle R^{(2)}_{\alpha\beta} R^{*(2)}_{\sigma\delta} \rangle - \frac{1}{4} \langle R^{(2)}_{\alpha\beta} \rangle \langle R^{*(2)}_{\sigma\delta} \rangle \\ - \frac{1}{6} \langle R^{(1)}_{\alpha\beta} R^{*(3)}_{\sigma\delta} \rangle - \frac{1}{6} \langle R^{(3)}_{\alpha\beta} R^{*(1)}_{\sigma\delta} \rangle, \end{aligned} \tag{100}$$

again suppressing the arguments of the reflection amplitudes in an effort to improve readability. All the terms in the sixteen elements of the Mueller Matrix (42) appear either as the absolute square of one of the reflection amplitudes $|R_{\alpha\beta}|^2$ or in one of the following two combinations

$$\langle R_{\alpha\beta} R^*_{\sigma\delta} \rangle + \langle R_{\sigma\delta} R^*_{\alpha\beta} \rangle = 2Re(\langle R_{\alpha\beta} R^*_{\sigma\delta} \rangle) \tag{101a}$$

$$\langle R_{\alpha\beta} R^*_{\sigma\delta} \rangle - \langle R_{\sigma\delta} R^*_{\alpha\beta} \rangle = 2Im(\langle R_{\alpha\beta} R^*_{\sigma\delta} \rangle) i \tag{101b}$$

where the latter is always accompanied by a factor i in front of the complete matrix element, having the consequence that all elements of the Mueller matrix are real. Similarly as for the incoherent MDRC the expansion of the Mueller Matrix can be written in a more theoretically convenient form

$$\begin{aligned} 2Re(\langle R_{\alpha\beta} R^*_{\sigma\delta} \rangle_{incoh}) = 2Re(\langle R^{(1)}_{\alpha\beta} R^{*(1)}_{\sigma\delta} \rangle) + \frac{1}{2} Re(\langle R^{(2)}_{\alpha\beta} R^{*(2)}_{\sigma\delta} \rangle) - \frac{1}{2} Re(\langle R^{(2)}_{\alpha\beta} \rangle \langle R^{*(2)}_{\sigma\delta} \rangle) \\ - \frac{1}{3} Re(\langle R^{(1)}_{\alpha\beta} R^{*(3)}_{\sigma\delta} \rangle) - \frac{1}{3} Re(\langle R^{(3)}_{\alpha\beta} R^{*(1)}_{\sigma\delta} \rangle). \end{aligned} \tag{102}$$

$$\begin{aligned} 2Im(\langle R_{\alpha\beta} R^*_{\sigma\delta} \rangle_{incoh}) = 2Im(\langle R^{(1)}_{\alpha\beta} R^{*(1)}_{\sigma\delta} \rangle) + \frac{1}{2} Im(\langle R^{(2)}_{\alpha\beta} R^{*(2)}_{\sigma\delta} \rangle) - \frac{1}{2} Im(\langle R^{(2)}_{\alpha\beta} \rangle \langle R^{*(2)}_{\sigma\delta} \rangle) \\ - \frac{1}{3} Im(\langle R^{(1)}_{\alpha\beta} R^{*(3)}_{\sigma\delta} \rangle) - \frac{1}{3} Im(\langle R^{(3)}_{\alpha\beta} R^{*(1)}_{\sigma\delta} \rangle). \end{aligned} \tag{103}$$

The terms present in these expansions easily reduces to the expansion of the incoherent MDRC for $\alpha\beta = \sigma\delta$, noting the factor $\frac{1}{2}$ difference in the prefactors. Following the same derivation as for the terms in the expansion of the incoherent MDRC we have

$$\langle R^{(1)}_{\alpha\beta} R^{*(1)}_{\sigma\delta} \rangle = \mathcal{X}^{(1)}_{\alpha\beta}(\boldsymbol{q}_\parallel | \boldsymbol{k}_\parallel) \mathcal{X}^{*(1)}_{\sigma\delta}(\boldsymbol{q}_\parallel | \boldsymbol{k}_\parallel) S \delta^2 g(\boldsymbol{k}_\parallel) \tag{104}$$

$$\begin{aligned}\frac{1}{4}[\langle R^{(2)}_{\alpha\beta}R^{*(2)}_{\sigma\delta}\rangle)-\langle R^{(2)}_{\alpha\beta}\rangle\langle R^{*(2)}_{\sigma\delta}\rangle] &= 2A_{\alpha\beta}(\boldsymbol{q}_\parallel|\boldsymbol{k}_\parallel)A^*_{\sigma\delta}(\boldsymbol{q}_\parallel|\boldsymbol{k}_\parallel)\delta^4 S\int\frac{d^2p_\parallel}{(2\pi)^2}g(\boldsymbol{q}_\parallel-\boldsymbol{p}_\parallel)g(\boldsymbol{p}_\parallel-\boldsymbol{k}_\parallel)\\
&+2\delta^4 SA_{\alpha\beta}(\boldsymbol{q}_\parallel|\boldsymbol{k}_\parallel)\int\frac{d^2p_\parallel}{(2\pi)^2}B^*_{\sigma\delta}(\boldsymbol{q}_\parallel|\boldsymbol{p}_\parallel|\boldsymbol{k}_\parallel)\\
&\times g(\boldsymbol{q}_\parallel-\boldsymbol{p}_\parallel)g(\boldsymbol{p}_\parallel-\boldsymbol{k}_\parallel)\\
&+2\delta^4 SA^*_{\sigma\delta}(\boldsymbol{q}_\parallel|\boldsymbol{k}_\parallel)\int\frac{d^2p_\parallel}{(2\pi)^2}B_{\alpha\beta}(\boldsymbol{q}_\parallel|\boldsymbol{p}_\parallel|\boldsymbol{k}_\parallel)\\
&\times g(\boldsymbol{p}_\parallel-\boldsymbol{q}_\parallel)g(\boldsymbol{k}_\parallel-\boldsymbol{p}_\parallel)\\
&+\delta^4 S\int\frac{d^2p_\parallel}{(2\pi)^2}B_{\alpha\beta}(\boldsymbol{q}_\parallel|\boldsymbol{p}_\parallel|\boldsymbol{k}_\parallel)B^*_{\sigma\delta}(\boldsymbol{q}_\parallel|\boldsymbol{p}_\parallel|\boldsymbol{k}_\parallel)\\
&\times g(\boldsymbol{q}_\parallel-\boldsymbol{p}_\parallel)g(\boldsymbol{p}_\parallel-\boldsymbol{k}_\parallel)\\
&+\delta^4 S\int\frac{d^2p_\parallel}{(2\pi)^2}B_{\alpha\beta}(\boldsymbol{q}_\parallel|\boldsymbol{p}_\parallel|\boldsymbol{k}_\parallel)\\
&\times B^*_{\sigma\delta}(\boldsymbol{q}_\parallel|\boldsymbol{k}_\parallel+\boldsymbol{q}_\parallel-\boldsymbol{p}_\parallel|\boldsymbol{k}_\parallel)g(\boldsymbol{p}_\parallel-\boldsymbol{k}_\parallel)g(\boldsymbol{q}_\parallel-\boldsymbol{p}_\parallel),\end{aligned}\tag{105}$$

$$\begin{aligned}\left\langle R^{(1)*}_{\alpha\beta}(\boldsymbol{q}_\parallel|\boldsymbol{k}_\parallel)R^{(3)}_{\sigma\delta}(\boldsymbol{q}_\parallel|\boldsymbol{k}_\parallel)\right\rangle &= \mathcal{X}^{(1)*}_{\alpha\beta}(\boldsymbol{q}_\parallel|\boldsymbol{k}_\parallel)\mathcal{M}^{(0)}_{\alpha\beta}(\boldsymbol{q}_\parallel|\boldsymbol{q}_\parallel)^{-1}\\
&\times\int\frac{d^2p_\parallel}{(2\pi)^2}\delta^4 S\\
&\times\big[\mathcal{X}^{(3)}_{\alpha\beta}(\boldsymbol{q}_\parallel|\boldsymbol{k}_\parallel|\boldsymbol{p}_\parallel|\boldsymbol{k}_\parallel)g(\boldsymbol{q}_\parallel-\boldsymbol{k}_\parallel)g(\boldsymbol{k}_\parallel-\boldsymbol{p}_\parallel)\\
&+\ \mathcal{X}^{(3)}_{\alpha\beta}(\boldsymbol{q}_\parallel|\boldsymbol{p}_\parallel|\boldsymbol{q}_\parallel|\boldsymbol{k}_\parallel)g(\boldsymbol{q}_\parallel-\boldsymbol{p}_\parallel)g(\boldsymbol{k}_\parallel-\boldsymbol{q}_\parallel)\\
&+\ \mathcal{X}^{(3)}_{\alpha\beta}(\boldsymbol{q}_\parallel|\boldsymbol{p}_\parallel|\boldsymbol{k}_\parallel+\boldsymbol{p}_\parallel-\boldsymbol{q}_\parallel|\boldsymbol{k}_\parallel)g(\boldsymbol{q}_\parallel-\boldsymbol{p}_\parallel)g(\boldsymbol{k}_\parallel-\boldsymbol{q}_\parallel)\big].\end{aligned}\tag{106}$$

2.14 Validity of SAPT

In addition to the Rayleigh Criterion, the accuracy of the small amplitude perturbation expansion also hinges on the assumption that higher order terms can be safely neglected. By inspection of the exponential expansion employed in equation (57) the perturbation parameter in the expansion (51) is $\frac{\delta}{\lambda}$. The expansion presented within this thesis is truncated at $n=3$, and the incoherent MDRC and Mueller Matrix go up to fourth order in the perturbation parameter. Sixth order terms of the form $R^{(3)}_{\alpha\beta}(\boldsymbol{q}_\parallel|\boldsymbol{k}_\parallel)R^{*(3)}_{\alpha'\beta'}(\boldsymbol{q}_\parallel|\boldsymbol{k}_\parallel)$ have been neglected, since its not pertinent to include some sixth order terms, while neglecting others. It is also worth pointing out that any fourth order term that arise from the inclusion of terms up to $n=4$ in the perturbative expansion (51) would have make an equivalent contribution to the two terms present in the incoherent MDRC (39), and would therefore cancel completely. Finally recalling that all odd moments of a Gaussian stochastic process average to zero (53) leaves us with the following criteria for the accuracy of the small amplitude perturbation expansion employed within this thesis.

$$O\Big(\frac{\delta^4}{\lambda^4}\Big)\gg O\Big(\frac{\delta^6}{\lambda^6}\Big),\tag{107}$$

Unfortunately there exists no known formal limit of validity for this criterion, and its direct evaluation would involve the cumbersome and time consuming implementation of higher order terms. There is however a general consensus on SAPT being accurate given that the following criteria is satisfied [8]

$$\frac{\omega}{c}\sqrt{|\varepsilon(\omega)|}\delta=2\pi\sqrt{|\varepsilon(\omega)|}\frac{\delta}{\lambda}\ll 1,\tag{108}$$

given a finite correlation length. Here $\varepsilon(\omega)$ is the dielectric constant of the media of transmission. This criterion states that the expansion parameter must be suitably small so that higher order

terms in the perturbative expansion can be safely neglected, it must obviously be smaller than one since any power series with an expansion parameter larger than one diverges. The criterion leaves us with the problem of estimating how small these parameters have to be in order for the left hand side to classify as being much smaller than one, while still allowing us to discern characteristic phenomena of weak surface scattering. Comparison with DNS or other simulation models can also be used for quantitative estimation of the accuracy for SAPT for a particular surface configuration which satisfies the Rayleigh Criterion. If the results are consistent the various terms in the SAPT expansion can then be used to further analyse the scattering from the given surface.

3 Method

A Fortran program implementing the theoretical concepts described in the previous section was written as the main task of this master thesis. The following section will discuss some of the choices made in the implementation, as well as some of the observations made on the chosen methods.

3.1 Rounding Error and Dimensionless Variables

In working with physical quantities with large variations in magnitude such as that of optical wavelengths $\lambda \propto 10^{-7}m$ and optical frequencies $\omega \propto 10^{15}\frac{rad}{s}$, one has to be acutely aware of the presence of rounding error within the program. A simple measure is to scale the program to a suitable length scale such that the actual numbers treated in the program are of a suitable magnitude as to avoid rounding errors. The dispersion relation in vacuum reads

$$k = \frac{\omega}{c} = \frac{2\pi}{\lambda} \tag{109}$$

where k is the wavenumber, ω is the frequency and λ is the wavelength of incident light. The system can be made dimensionless by multiplying all lengths by $\frac{2\pi}{\lambda}$ and dividing all wave vectors by $\frac{\omega}{c}$. Normally it would be necessary to scale the resulting computation by the relevant units in order to regain the actual result corresponding to the physical system, but this is naturally unnecessary if the physical quantity that is being competed is itself dimensionless, as is the case for the MDRC and the Mueller Matrix. Given that the program is written in such a way that the dimensionless quantities are written as the coefficient of the factor that would restore them to the original units. The programmer then only has to scale the original length unit in any way that they see fit in order to avoid numerical difficulties. This also acts as an excellent test of the implementation, since the dimensionless result should naturally remain unchanged for inputs with magnitudes within a reasonable range. To run the program with dimensionless units, one need simply set the original units such that $\frac{\omega}{c} = 1$.

3.2 Numerical Computations

The fourth order terms in the expansion of the MDRC and the Mueller Matrix include complicated integrals over the entirety of $\mathbb{R}^2$ which are yet to be solved analytically. It is therefore necessary to compute these integrals by use of numerical integration. Since the integral domain is infinitely large, it must be truncated or evaluated using a numerical solver specifically made for integration over infinite domains, such as can be found in the numerical library Quadpack [17].

Truncation is the simplest approach, especially for a quickly diminishing integrands. This is however not ideal, as it leaves the programmer with the task of finding a suitable upper limit, which is neither so large as to take up unecessary computation time nor so small that vital contributions from the integrand is left out.

The aforementioned numerical library Quadpack includes several integration routines aimed at tackling infinite intervals, among them a convenient general purpose routine named QAGI, which maps the infinite interval into $[0, 1]$ before performing the integral using a general purpose routine for integration of a finite interval. Though this routine works excellently for many integrals, it is important to be aware of the fact that some rapidly changing characteristics of the integrand can be lost in the mapping process, making it necessary to evaluate the behaviour of the integrand before blindly using this routine. The integrands related to the fourth order terms of the incoherent MDRC and Mueller matrix present with abrupt peaks in the lower range of integration, before diminishing to zero at a steady pace. In order for these peaks to be properly resolved during integration, it is necessary to divide the integral into two parts, one covering the lower part of the domain where the peaks are present and another covering the infinite integral. There may be other integration libraries which do a better job of dealing with multidimensional integrals of this form, but this has not been investigated, since speeding up the computation was not a priority.

3.3 Evaluation of Accuracy

When analysing the error of results achieved through numerical simulations of a modeled physical system it is essential to verify both the level of accuracy of the model being implemented and the correctness of the numerical program implementing the model. For the scattering problem there are physical properties, such as reciprocity, that have been analytically proven to hold [p. 26][8]. Verifying that these properties are respected by results achieved through numerical simulations is an excellent validation practice for numerical implementations. Numerical simulations using Small Amplitude Perturbation Theory have been carried out by several teams in the past, notably by McGurn et al. on the West & O'Donnel effect spectrum [2]. Achieving accordance with previous implementations which are known to perform well is naturally a good estimator for the correctness of a numerical implementation.

Furthermore, the accuracy of SAPT for a particular surface configuration can be verified through comparison with other numerical simulation techniques, such as Direct Numerical Simulations, which are known to hold for the given configuration. In choosing the surface parameters for the surfaces to be presented in the next section, this has been taken advantage of in lieu of choosing the surfaces parameters solely based on the validity criteria for SAPT (108). In particular the work of Sanchez-gil et al. on the validity of SAPT for a one-dimensional rough surfaces and the work of Nils Petter Jørstad on the analysis of two-dimensional rough surfaces using Direct Numerical Simulations was taken into account.

In addition to this it would have been of great interest to investigate conservation of energy for coherent light incident on a weakly rough Perfect Electric Conductor (PEC). As explained in Sec. 2.12 a PEC allows for no transmitted or absorbed light, meaning that the incoherent and coherent MDRC would have to add up to unity. Unfortunately higher order SAPT methods were found to be unsuitable for treating the Reduced Rayleigh equation for a PEC. Another approach would be to compute the Mean Differential Transmission Coefficient in addition to the MDRC for dielectric surfaces in order to calculate the conservation of energy. However given the limited time available for this thesis, this approach was not attempted.

3.4 Software

The following open source software distributions made the implementation of the program based on the Small Amplitude Perturbation theory much easier. The numerical integration library Quadpack [17], an excellent tool for numerical integration over finite and infinite domains, was used to numerically evaluate the integrals that present in the higher order terms of the perturbative expansion of the MDRC and Mueller Matrix. The library H5Fortran [18], a lightweight polymorphic HDF5 library, greatly simplified the implementation of the HDF5 filetype. Finally, a python package written by Ingve Simonsen and Nils Petter Jørstad dedicated to plotting the incoherent MDRC and Mueller Matrix was a fantastic help in visualising many of the results which are presented in the following section.

4 Results and Discussion

This section will present reflection of coherent light from weakly rough surfaces, calculated using a numerical method based on fourth order Small Amplitude Perturbation Theory. The investigated surfaces are described by a zero mean stationary Gaussian stochastic process with a correlation function describing the correlation between the various points on the surface. The aim is to showcase both the general behaviour of rough surface scattering, as well as the physical processes and phenomena that arise from light coupling with rough surfaces.

Firstly, the correctness of the Small Amplitude Perturbation Theory implementation written in order to numerically compute and integrate the various terms in the incoherent component of the MDRC and Mueller Matrix will be evaluated. This evaluation will consist of a qualitative comparison with previous implementations, notably with the results computed by McGurn et al[2], and comparisons with results achieved by Nils Petter Jørstad using Direct Numerical Simulations [11].

Secondly, the incoherent component of the MDRC will be presented for coherent light in a vacuum incident on two-dimensional randomly rough dielectric and metal surfaces. Both the total incoherent MDRC and the contributions of the separate terms in the incoherent expansion (52) will be presented. Examining these results yields insight into how light couples with weakly rough surfaces and to what degree the coupling depends on the material characteristics of the illuminated surface, i.e how the coupling depends on the excitation of SPPs 2.3. This will naturally include analysis of the enhanced back-scattering peak and heightened in-plane cross-polarization which are characteristic for scattering processes facilitated by SPPs. This thesis will restrict itself to Gaussian and West & O'Donnel correlation functions, as they yield sufficient insight into the phenomena we seek to investigate.

Thirdly, the incoherent component of the Mueller Matrix elements will be assessed for equivalent configurations as those examined for the incoherent component of the MDRC. The incoherent component of the Mueller Matrix completely describes the manner in which the randomly rough surface affects the polarization of the incoming light for all diffuse scattering modes. Similarly as for the incoherent component of the MDRC both the total incoherent component of the Mueller Matrix and the contributions from the various terms in the incoherent expansion (47) will be presented.

Lastly, computations of the depolarization index will be presented and discussed. The behaviour of the depolarization index in the back-scattering direction, which displays an interference phenomenon akin to the well known enhanced back-scattering phenomenon is of particular interest. In order to analyse this interference phenomenon the behaviour of the various elements of the Mueller Matrix in the back-scattering direction is considered.

4.1 Validity of SAPT

Fig. 2 shows the in-plane incoherent MDRC for light incident on a weakly rough surface described by a West & O'Donnel effect spectrum computed using the implementation of Small Amplitude Perturbation Theory written in relation to this thesis. The Surface parameters are equivalent to the parameters employed by McGurn et al. to achieve the results presented in their paper on the enhanced back-scattering peak in surfaces described by various West & O'Donnel effect spectra [2, Fig. 4]. As can be seen from the two figures there is minimal, if any, visible discrepancy between the results computed by the two implementations.

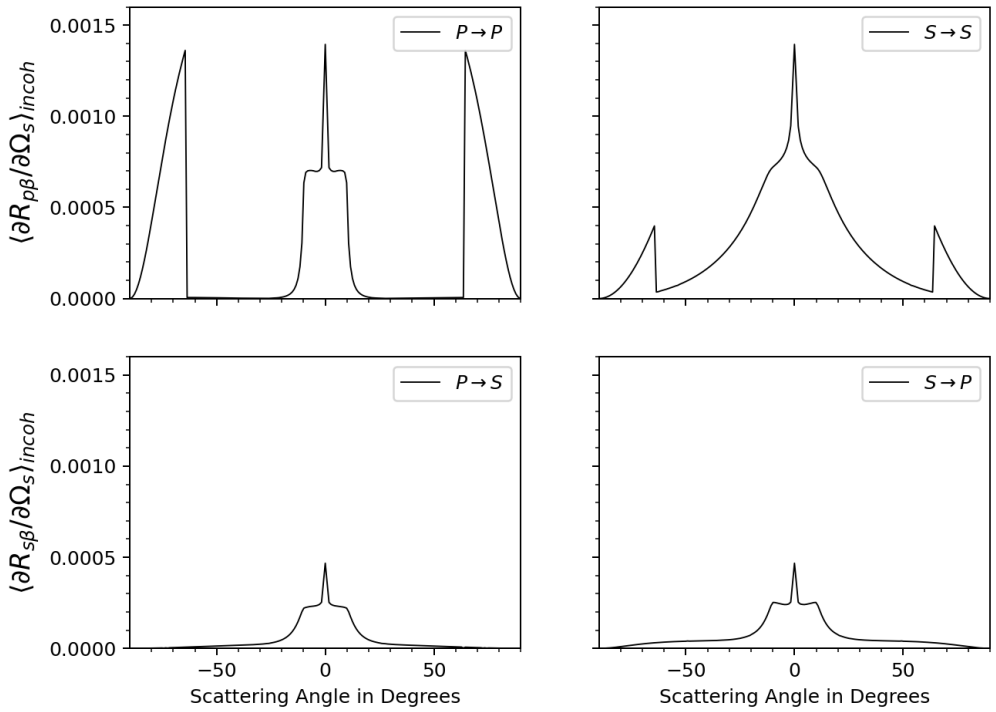

Figure 2: The incoherent in-plane MDRC for light with wavelength $\lambda = 457.9$nm normally incident on a randomly rough surface described by a west & O'Donnel effect spectrum (26) with $k_{min} = 0.9005\frac{\omega}{c}$ and $k_{max} = 1.2478\frac{\omega}{c}$ calculated using a numerical implementation of SAPT written in relation to this thesis. The dielectric constant of silver at this wavelength is $\varepsilon_{silver} = -7.5 + 0.24i$. The incoherent MDRC is resolved over 201 scattering angles.

The aim of this work was to investigate the different scattering properties for weakly rough dielectric and metal surfaces, leaving the necessary task of choosing suitable surface parameters. Sanches-gil et al. found that for computations of the reflectivity up to second order in the perturbation parameter applied to one dimensional glass surfaces with Gaussian correlation functions that satisfy the Rayleigh Criterion there was satisfactory accordance with Direct Numerical Simulations for RMS-heights as large as $\delta = 0.04\lambda$ for light with wavelength $\lambda = 632.8$nm and dielectric constant $\varepsilon_{glass} = 2.25$ [16]. Even though our implementation of SAPT is two-dimensional this is still a good indicator, and since our implementation takes into account contributions up to fourth order this allows us to choose the same surface parameters for the glass surface as employed by N. P. Jørstad for computations of the incoherent component of the MDRC for a weakly rough glass surface using Direct Numerical Simulations [11], making it possible to qualitatively compare results for the glass surface with the results achieved through Direct Numerical Simulations. Figs. 3 show the results achieved by N. P. Jørstad using Direct Numerical Simulations to compute the in-plane incoherent MDRC for a vacuum-glass interface. The surface parameters for this surface are $\delta = 0.05$ with wavelength and dielectric constant equal to the configuration investigated by Sanchez-Gil et al.. Inserting these numerical values into the validity criterion (108) yields $2\pi\sqrt{|\varepsilon(\omega)|}\delta/\lambda = 0.471$. Meaning that the validity criterion is not strongly satisfied for this configuration, however qualitative comparison between these results and the results achieved through our perturbative method shown in Fig. 4 show that there is a large degree of agreement between the two methods for the chosen surface. The MDRC has nearly the exact same shape for both angles of incidence, only showing a notable discrepancy in magnitude, which is to be expected since the involved surface parameters are at the limit of what can be expected to yield good results for a fourth order perturbative expansion. Given the results found by Sanchez-Gil et al. and the level of accordance that was found with the

results acheived using Direct Numerical Simulations, it appears that fourth order SAPT yields very good results, despite the validity criterion not being strongly satisfied.

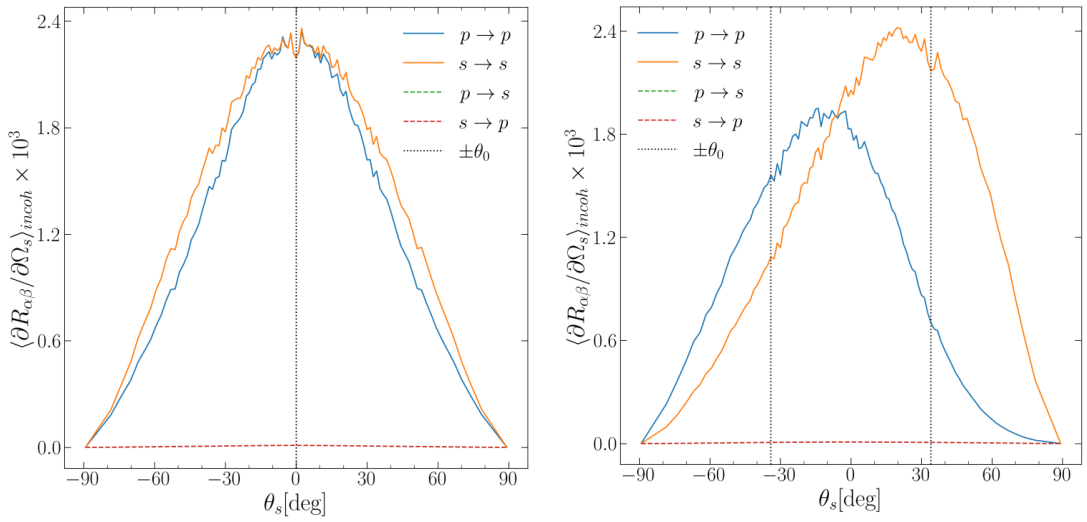

(a): $\theta_0 = 0°$ (b): $\theta_0 = 34.05°$

Figure 3: The incoherent component of the MDRC in the plane of incidence for light with wavelength $\lambda = 632.8$nm incident with normal and non-normal angles of incidence on a weakly rough glass surface described by a Gaussian effect spectrum with RMS-height $\delta = \lambda/20$ and correlation length $a = \lambda/4$ computed using a Direct Numerical Simulation technique by N. P. Jørstad [11, Fig. 3]

The choice of surface parameters for the silver surface was more conservative as multiple scattering effects are known to contribute to a much larger degree for weakly rough metal surfaces compared to dielectrics. In order to more strongly satisfy the validity criterion (108) the wavelength of the incoming light was set to $\lambda = 457.9$nm, as the dielectric function for silver at this wavelength is $\varepsilon = -7.5 + 0.24i$ [2]notably smaller than that for $\lambda = 632.8$nm. The RMS-height of the surface was set to $\delta = \lambda/80$. Inserting these parameters into the expression for the validity criterion yields $2\pi\sqrt{|\varepsilon(\omega)|}\delta/\lambda = 0.215$, which more solidly satisfies the validity criterion than the surface parameters for the glass surface. In addition to this, results for a silver surface with identical surface parameters to the silver surface analysed by Nils Petter Jørstad in [11, Fig. 4] were also computed. Once again the wavelength of incident light was $\lambda = 632.8$nm with a corresponding dielectric function $\varepsilon_{silver} = -16 + 1.088i$ [19]. The surface was described by a Gaussian correlation function and the RMS-height of the surface was $\delta = 0.025$. The perturbative method was found to have a reasonable level of agreement with Direct Numerical Simulations, with nearly no discrepancy in the shape of the in-plane incoherent component of the MDRC, but a larger discrepancy in magnitude than what was observed for the glass surface. For this surface configuration the validity criterion evaluates to $2\pi\sqrt{|\varepsilon(\omega)|}\delta/\lambda = 0.629$. Given the lower level of agreement with Direct Numerical Simulations and that the validity criterion is satisfied to a lower degree, the choice of parameters for the silver surface where chosen to be more conservative than the parameters employed by N. P. Jørstad.

4.2 Mean Differential Reflection Coefficient

The incoherent MDRC for light incident with angles $\theta_0 = 0°$ and $\theta_0 = 34.05°$ on glass and silver surfaces was computed through a numerical integration program based on SAPT. The surfaces were characterised by Gaussian surface statistics with both Gaussian and West & O'Donnel correlation functions. As described in Sec. 2.7 the incoherent MDRC describes the intensity of co- and cross-polarized light scattered into a solid angle element $d\Omega_s(\theta_s, \phi_s)$, allowing the characterisation of the diffuse scattering intensity in any scattering direction $\boldsymbol{q}_s$. The standard approach in quantitative analysis of the incoherent MDRC is to visualise the intensity of scattered light in the region of feasible far-field scattering vectors, either as a complete two-dimensional intensity map, or as cuts through particularly interesting planes, such as the plane of incidence. The former is useful for analysing the general spatial dependency of the diffuse scattering intensity for the co- and cross-polarized scattering modes, while the latter yields insight into more precise phenomena, for instance sudden peaks or dips in the scattering intensity which are easily hidden on a larger intensity map.

4.2.1 Cross sections of the incoherent MDRC

A cross section of the plane of incidence is a natural starting point for analysis of diffuse surface scattering. It allows us to inspect both how the incoherent component of the MDRC behaves for the specular and retro-specular directions, and how the behaviour of the cross-polarization modes vary for in-plane scattering based on the type of surface the light is scattered from. In Fig. 4 the incoherent component of the in-plane MDRC for a weakly rough vacuum-glass surface with a Gaussian correlation function is displayed.

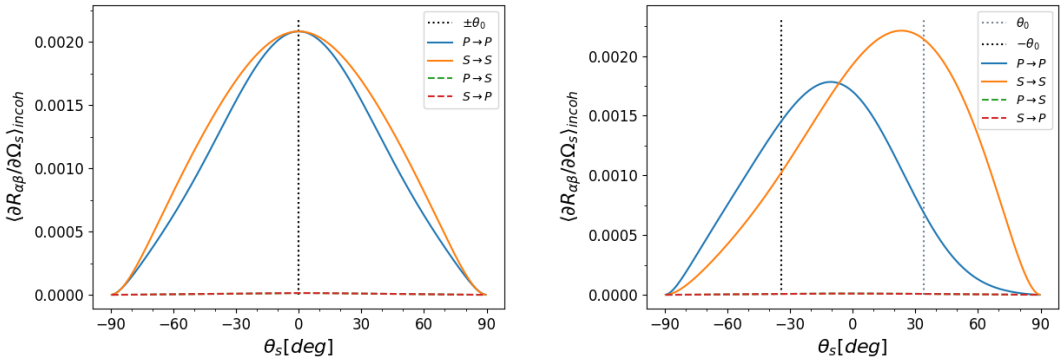

(a): $\theta_0 = 0°$ (b): $\theta_0 = 34.05°$

Figure 4: The incoherent component of the MDRC in the plane of incidence for coherent light of wavelength $\lambda = 632.8$nm incident on a randomly rough surface separating vacuum and glass. The surface was characterized by RMS height $\delta = \lambda/20$ and a gaussian correlation function with correlation lengths $a_1 = a_2 = \lambda/4$. The dielectric function for glass at this wavelength is $\varepsilon_{Glass} = 2.25$. The MDRC was calculated for 201 different scattering angles θ_s

Fig. 4 shows that the incoherent in-plane MDRC for a glass-vacuum interface consists nearly entirely of co-polarized contributions. The cross-polarized terms, though imperceptible in Fig. 4, do in fact contribute. They are two orders of magnitude smaller than the co-polarized contributions, and are shown for normal incidence in Fig. 7. For normal incidence the incoherent component of the MDRC is evenly distributed around the specular direction with $s \to s$ scattering contributing slightly more for larger scattering angles than $p \to p$ scattering. For non normal incidence of $\theta_0 = 34.05°$ the graphs depicting $p \to p$ and $s \to s$ scattering reveal a difference in both magnitude and directional preference for the two co-polarized scattering contributions. The co-polarized s-scattering prefers scattering around the specular direction, while the co-polarized p-scattering prefers scattering around retro-specular direction. Furthermore $s \to s$ scattering presents with a significantly larger magnitude than $p \to p$ scattering.

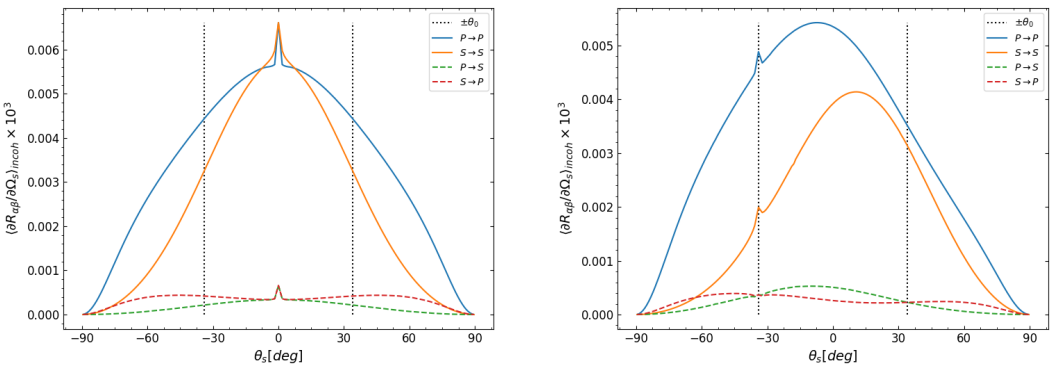

(a): $\theta_0 = 0^\circ$ (b): $\theta_0 = 34.05^\circ$

Figure 5: The incoherent component of the MDRC in the plane of incidence for coherent light of wavelength $\lambda = 457.9$nm incident on a randomly rough surface separating vacuum and silver. The surface was characterized by the RMS height $\delta = \lambda/80$ and a Gaussian correlation function with correlation lengths $a_1 = a_2 = \lambda/4$. The dielectric function for silver at this wavelength is $\varepsilon_{Silver} = -7.5 + 0.24i$. The incoherent component of the MDRC was calculated for 201 different scattering angles θ_s

Fig. 5 depicts the incoherent component of the MDRC in the plane of incidence for a weakly rough vacuum-silver surface with a Gaussian correlation function. For the normally incident light it is observed, similarly as for Fig. 4, that the co-polarized contributions are evenly distributed around the specular direction. However, it is now the $p \to p$ scattering contribution that dominates for larger scattering angles, while $s \to s$ scattering is very diminished for angles larger than 50°. For the non normal incidence a similar preference for the scattering direction as in Fig. 4 is observed, the relationship between the magnitudes however, has been inverted and the dominating scattering contribution is now $p \to p$ scattering. The magnitude of the diffuse scattering intensity of the silver surface is much larger than for the glass surface despite the RMS-height being quartered. This is an expected result since most of the light incident on a glass surface is transmitted through the surface, while only a small portion of the incident intensity is absorbed by the silver surface.

Furthermore Fig. 5 displays two significant physical phenomena that are absent for scattering from glass in Fig. 4, namely a peak in the retro-specular direction and a significant contribution to in-plane cross-polarized scattering. The peak is known as the enhanced back-scattering peak, since it is presents in the retro-specular scattering direction as can be seen from Fig. 5(b). McGurn et al. showed that both of these scattering phenomena are multiple scattering effects caused by the excitation of surface plasmon polaritons [2]. A strong indication of this can be observed from the fact that these scattering effects only contribute for the metal surface, since dielectric surfaces such as glass don't allow for the excitation of SPPs, which is the dominating contributor to multiple scattering in weakly rough surfaces. Fig. 5 indicates a dependence on the angle of incidence in the enhanced back-scattering phenomenon as the peak has a larger magnitude for normal incidence.

To further investigate the behaviour of these multiple scattering phenomena and their consequences for the scattering response from weakly rough surfaces we begin by returning to the West & O'Donnel power spectrum (26) and the findings of McGurn et al.. As explained in Sec. 2.4 this effect spectrum suppresses singular scattering contributions in a region around the origin, facilitating the observation of multiple scattering phenomenon. Fig. 6 shows the contributions from the various terms in the incoherent expansion of the MDRC to the complete fourth order co- and cross-polarized scattering contributions from the surface configuration investigated by McGurn et al.. From this point on the three contributing terms in the incoherent expansion of the MDRC will be referred to, using the naming convention introduced with Eq. (51), as the One-One (75), Two-Two (81) and Three-one (88) terms corresponding to the order of the reflection amplitudes from which they originate.

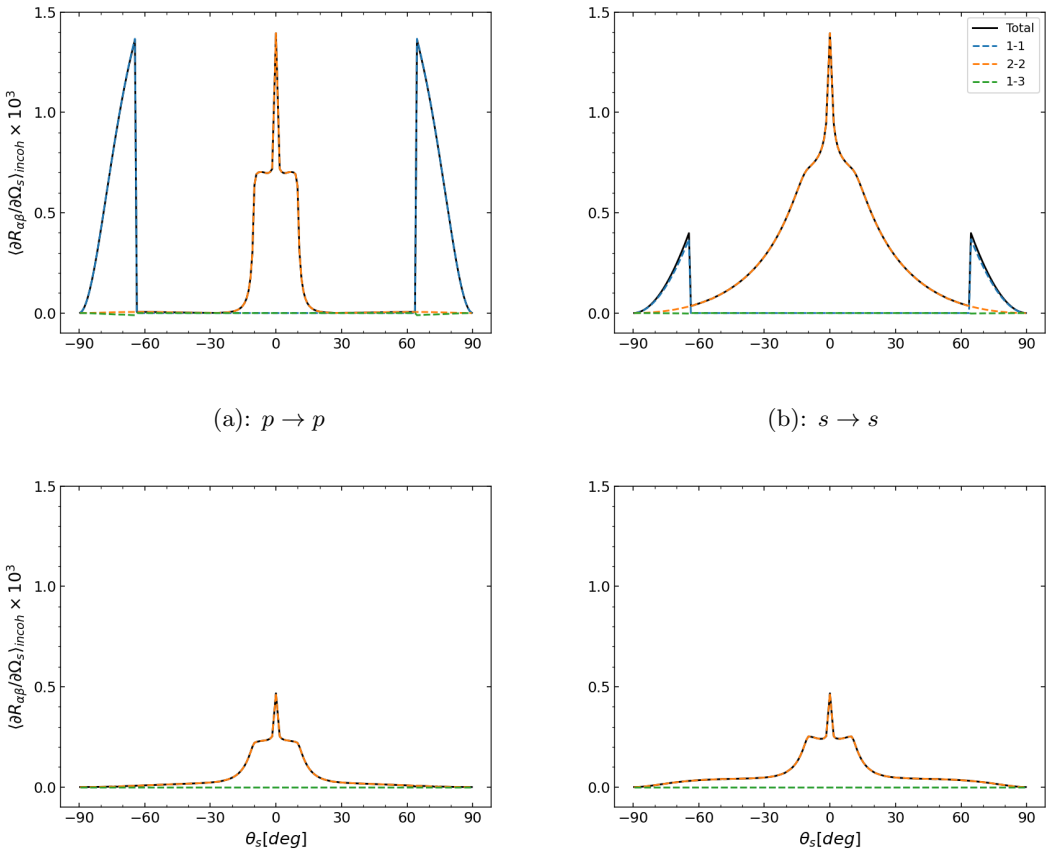

(a): $p \to p$ (b): $s \to s$

(c): $p \to s$ (d): $s \to p$

Figure 6: The in-plane contributions from the various terms in the incoherent expansion of the MDRC to the co- and cross-polarized scattering modes for a surface described by a West & O'Donnel effect spectrum as a function of the scattering angle θ_s. The numerical and surface parameters are identical to Fig. 2

The enhanced back-scattering peak is not suppressed by the West & O'Donnel effect spectrum and is thereby a multiple scattering effect. Furthermore it is observed that there is no contribution from the One-one and Three-one terms in the region where single-scattering is suppressed, showing that the only term contributing to multiple scattering, and thereby the only term contributing to the enhanced back-scattering peak, is the two-two term. This corresponds to the theoretical analysis for each of the contributions presented in Sec. 2.10, since the One-one (75) term describes the single scattering contributions and the Three-one (88) term describes interference with the single scattering contribution. This would naturally lead to them being completely suppressed in a region were single scattering contributions are forbidden.

Fig. 6 also shows that the cross-polarized scattering modes have no contribution from the single-scattering One-one and Three-one terms, even outside the region where single-scattering is forbidden, indicating that this is also a multiple scattering effect originating purely from two-two term.

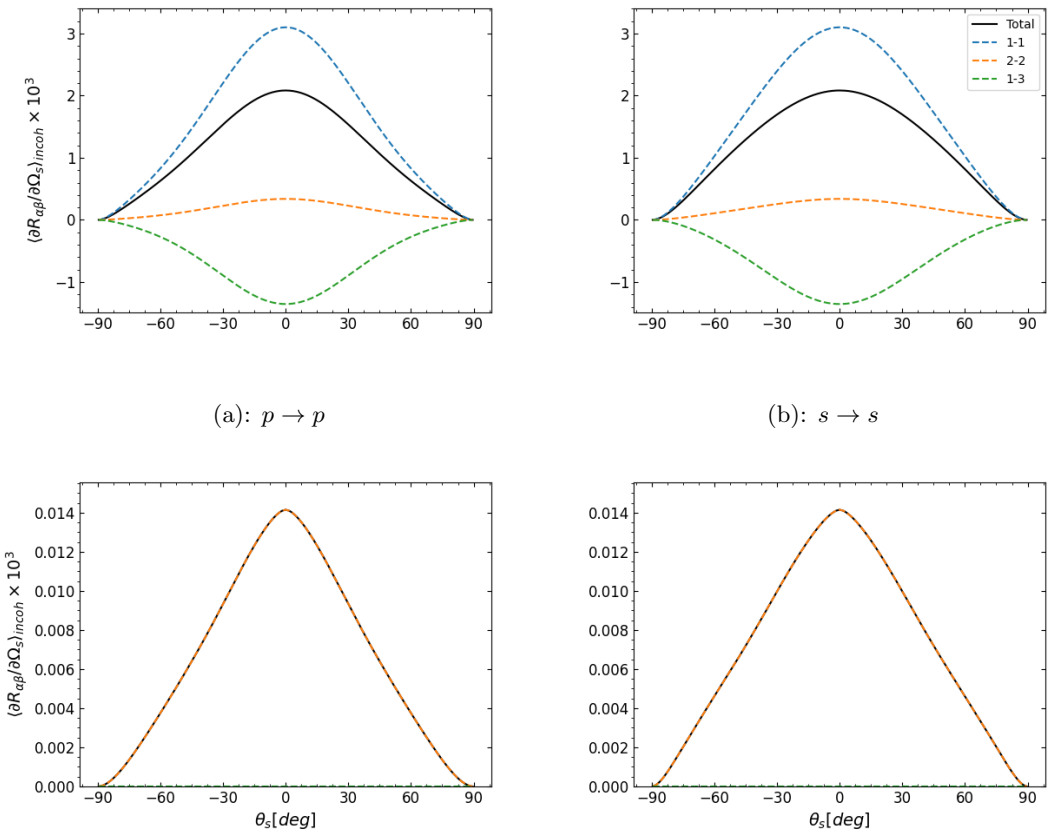

(a): $p \to p$

(b): $s \to s$

(c): $p \to s$

(d): $s \to p$

Figure 7: The in-plane contributions from the three terms in the incoherent expansion of the MDRC to the co- and cross-polarized scattering modes for coherent light with wavelength $\lambda = 632.8$nm incident on a glass surface described by a gaussian effect spectrum as a function of the scattering angle θ_s. The numerical and scattering parameters are identical to Fig. 4. It is important to note the difference in the scale for the co-polarized and cross-polarized components, as the co-polarized is in general two orders of magnitude larger than the cross-polarized terms.

Figs. 7 and 8 show the incoherent MDRC in the plane of incidence for light normally incident on the glass and silver surfaces from Figs. 4 and 5 decomposed into the three terms in the incoherent expansion of the MDRC (39). The surfaces considered are characterised by Gaussian effect spectra, meaning that there is no complete suppression of single-scattering processes, nor of any other scattering processes. Fig. 8 shows, just as for the West O'Donnel power spectrum in Fig. 6, that the enhanced back-scattering and in-plane cross-polarizations are both multiple scattering effects originating from the Two-two contribution.

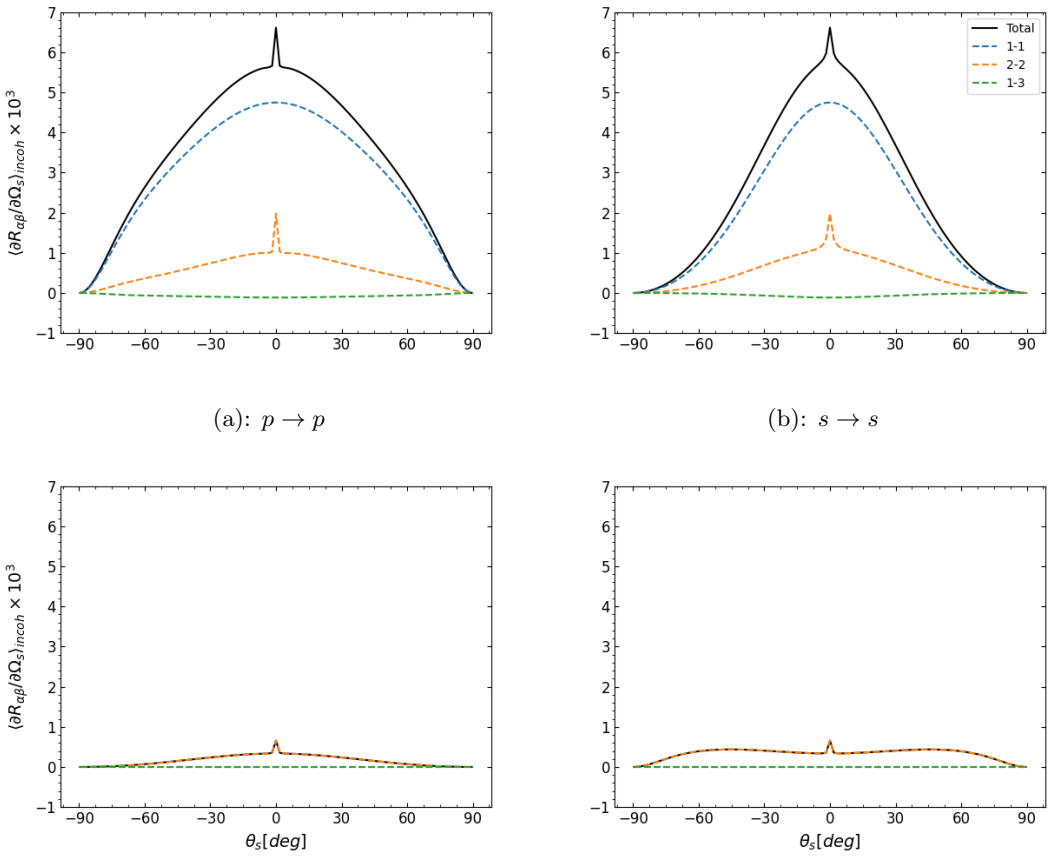

(a): $p \to p$ (b): $s \to s$

(c): $p \to s$ (d): $s \to p$

Figure 8: The in-plane contributions from the three terms in the incoherent expansion of the MDRC to the co- and cross-polarized scattering modes for coherent light with wavelength $\lambda = 457.9$nm incident on a silver surface described by a Gaussian effect spectrum as a function of the scattering angle θ_s. The numerical and scattering parameters are identical to Fig. 5.

In comparing the plots for the silver and glass surfaces in Figs. 7 and 8 it is observed, similarly as for Figs. 4 and 5, that there is no enhanced back-scattering peak in the scattering pattern from the glass surface, and that the cross-polarized scattering contributions are severely diminished. In fact, Fig.7 reveals that the Two-two contribution plays a much less significant role in dielectric surface scattering. Instead the Three-one contribution becomes much more important, in direct contrast with the contributions to the scattering pattern for the silver surface, where the Two-two contribution dominates the Three-one contribution. These two contributions are of the same order in the RMS-height of the surface, the enormous variation in their contribution for the two surface types shows a substantial dependence on the surface material in diffuse scattering.

As stated in Sec. 2.3 the main contributor to multiple surface scattering for weakly rough surfaces is the excitation of SPPs, which is only possible for dielectric-metal interfaces. For a vacuum-glass interface the Two-two term thereby only consists of contributions from geometric scattering , which is severely diminished for surfaces that satisfy the Rayleigh Criterion, leading to the domination of single-scattering contributions. Interestingly, the in-plane cross polarization is not completely extinguished for the vacuum-glass interface, but no enhanced back-scattering peak is observed. This indicates that in-plane cross-polarization is not purely caused by the excitation of SPPs, but rather by any double scattering process. As can be observed in the full angular distribution of the incoherent MDRC in Fig. 13, to be presented in the following section, cross-polarized scattering contributions are not severely diminished for scattering outside of the plane of incidence. This implies that cross-polarized single-scattering dominates for orthogonal out of plane scattering, which can be confirmed by regarding Fig 30 in the appendix. Therefore,

by considering a scattering process where the incident wave first scatters out of the plane of incidence, before scattering from the surface once more in the scattering direction $\boldsymbol{q}_{\parallel}$, will lead to in-plane cross-polarization as a result of double scattering processes that do not involve SPPs.

The question is then, why don't other double-scattering contributions lead to an enhanced back-scattering peak? In double-scattering with SPPs as an intermittent scattering mode the incoming wave excites a surface wave which travels along the surface before being re-emitted in the scattering direction. Due to the random nature of the rough surface any two such intermittent scattering paths will carry a certain phase difference, leading to an incoherence between the contributions from the various scattering paths for a given scattering direction $\boldsymbol{q}_{\parallel}$. Consider now the contributions from scattering through an intermittent SPP and its time-reciprocal partner as depicted in Fig. 9. Since the intermittent scattering path is identical, any phase difference between these two scattering contributions is caused entirely by the difference in distance travelled by the incident and scattered waves, as is also observable in Fig. 9. As a result of this the two scattering contributions will be completely in phase for the back-scattering direction as the phase contributions from the distance travelled by the incident and scattered waves will be identical. This results in the back-scattering peak having double the magnitude of the double scattering contribution from SPPs for adjacent scattering angles, which have contributions that are completely phase-incoherent. The peak would however not have twice the magnitude of the total two-two contribution for adjacent angles, since there are also double scattering contributions from geometrical scattering that do not result in enhanced back-scattering, as observed for scattering from glass surfaces. The contribution from multiple scattering through SPPs dominates for surfaces that satisfy the Rayleigh criterion, and the enhanced back-scattering therefore often has approximately twice the contribution from double-scattering compared to adjacent angles.

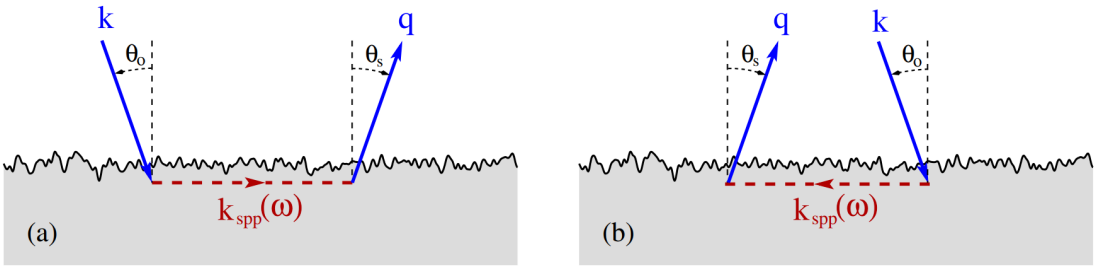

Figure 9: A figure displaying the scattering paths for an SPP and its time-reciprocal partner[8][p.57].

On the other hand, when considering constructive interference between a geometrical scattering mode and its reciprocal partner for weakly rough surface scattering for paths such as the one shown in Fig. 10, it is quickly realized why is is impossible to observe a similar interference effect for geometrical scattering in a system described by the Reduced Rayleigh equation.

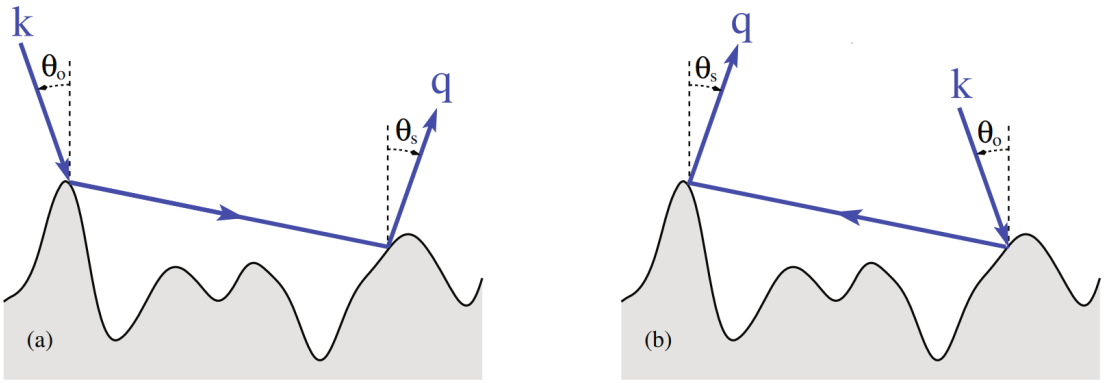

Figure 10: A figure displaying the two reciprocal geometric scattering paths[8][p.57].

The derivation of the Reduced Rayleigh equation relies on the Rayleigh Hypothesis which neglects the contribution of all downwards propagating scattering modes above the surface. As a consequence of this the contribution from one of the paths in a reciprocal pair such as the one in Fig. 10 will be neglected making it impossible to observe any such interference effect.

While both the increase in in-plane cross polarization and the enhanced back-scattering peak originate from multiple scattering contributions with SPPs as an intermittent scattering mode, it is possible to observe from Fig. 8 that the domination of $p \to p$ scattering shown in Fig. 5 is present in all three contributions to the incoherent MDRC. Most importantly this effect is also present in the One-one contribution to which SPPs make no contributions, this indicates a general preference for coupling to outgoing p-polarized light for larger scattering angles that is independent on the excitation of SPPs. In fact it signifies that the preference for p-polarized scattering is independent of the effect-spectrum of the surface, since the contribution from the effect spectrum is independent on the polarization. It is also worth noting that the preference for s-polarized scattering observed for the incoherent MDRC for a glass surface depicted in Fig. 4 is of similar nature to the preference for s-polarized specular reflection from planar surfaces. Indicating a shared preference in polarization for specular and diffuse reflection.

Finally it is of interest to inspect the contributions to the incoherent component of the MDRC for light non-normally incident on a silver surface.

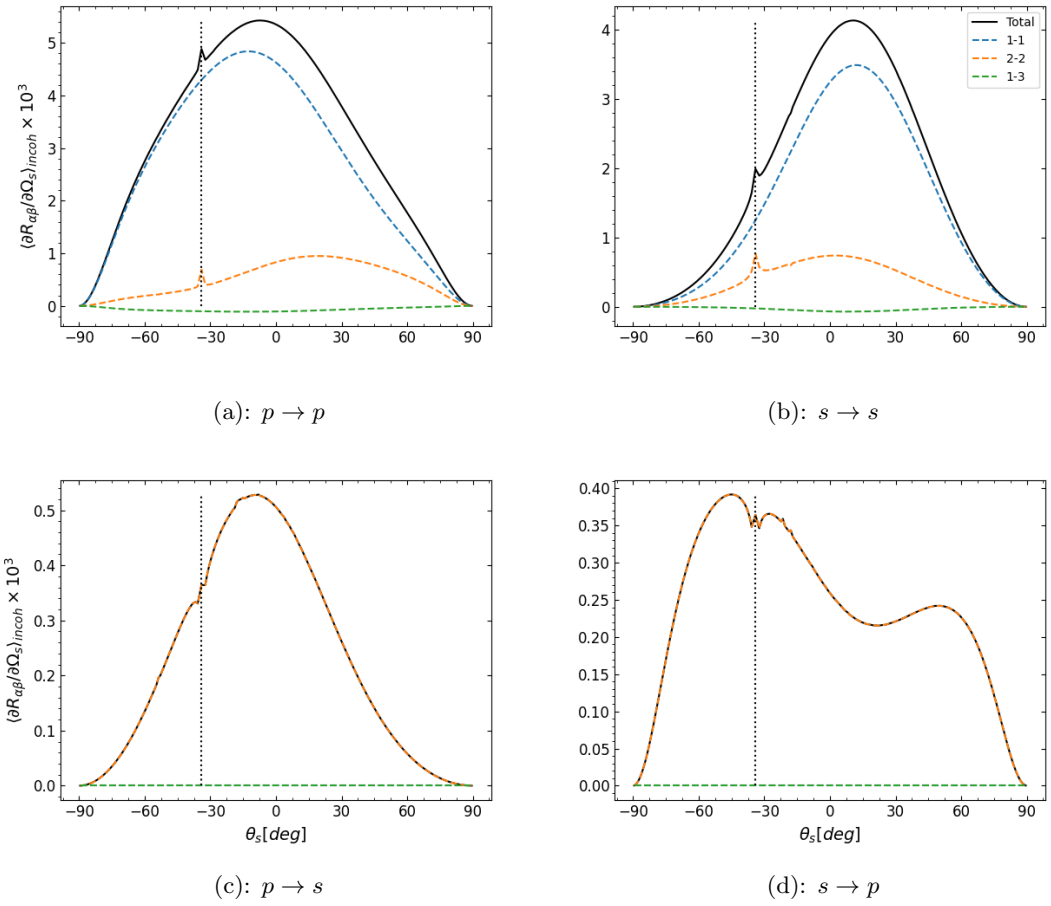

(a): $p \to p$ (b): $s \to s$

(c): $p \to s$ (d): $s \to p$

Figure 11: The in-plane contributions from the three terms in the incoherent expansion of the MDRC to the co- and cross-polarized scattering modes for coherent light with wavelength $\lambda = 457.9$nm incident at an angle of $\theta_0 = 34.05°$ on a silver surface described by a Gaussian effect spectrum as a function of the scattering angle θ_s. The numerical and scattering parameters are identical to Fig. 5.

Fig. 11 shows that the directional preference in the co-polarized scattering contributions in Fig. 5(b) is in fact a single-scattering effect, as the Two-two scattering contribution prefers

the opposite direction of the total scattering intensity. Furthermore one can observe that the reduced magnitude in the enhanced back-scattering peak that was observed in Fig. 5 is caused by the Two-two term contributing to a lesser degree around the back-scattering direction than for normal incidence. Similarly as for normal incidence the cross-polarized scattering modes are made up entirely of multiple scattering effects originating from the two-two contribution. Surprisingly the cross-polarized scattering modes present with a distorted version of the enhanced back-scattering peak in the co-polarized contributions. The present theory suggests that the cross-polarized terms should behave similarly to the co-polarized terms for the back-scattering direction. It appears however, as though a wider destructive phenomenon is competing with the enhanced back-scattering peak for non-normal angles of incidence, resulting in a stunted peak within a slight valley in both the cross-polarized contributions. Fig. 12 depicts the cross-polarized contributions for three different angles of incidence. For $\theta_0 = 25^\circ$ the enhanced back-scattering peak is sharply defined for both of the cross-polarized modes. There appears to be a diminishing effect surrounding both peaks, though it appears to be insignificant compared to the peak. For angles of incidence $\theta_0 = 45^\circ$ and 55° in Fig. 12(c-f) the back-scattering has completely disappeared and is instead replaced by a smooth dip around the back-scattering direction.

It is difficult to determine the exact scattering process at the origin of this phenomenon. One can however be certain that it originates from the excitation of SPPs as no such phenomenon can be observed for scattering from a glass surface, which is clearly visible in Fig. 31 in the appendix which shows the contributions from the three terms in the incoherent expansion of the MDRC for light incident at an angle of $\theta_0 = 34.05^\circ$ on a glass surface.

Unfortunately, further investigations into this phenomenon had to be halted due to time constraints, but the author believes that it could reveal a new aspect of the nature of surface plasmon polaritons.

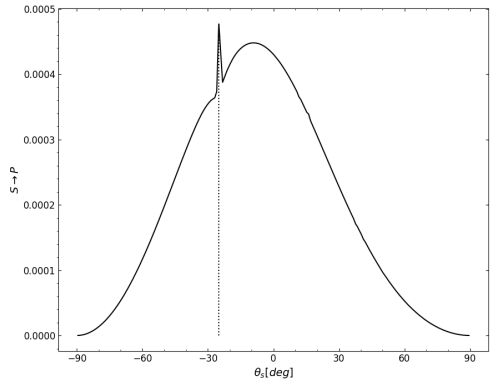

(a): $p \to s$, $\theta_0 = 25°$

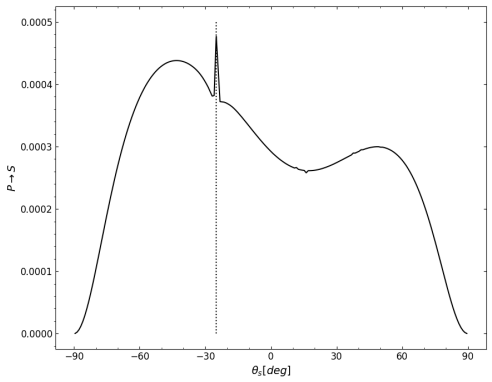

(b): $s \to p$, $\theta_0 = 25°$

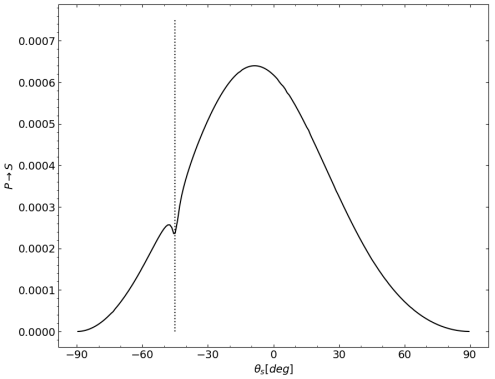

(c): $p \to s$, $\theta_0 = 45°$

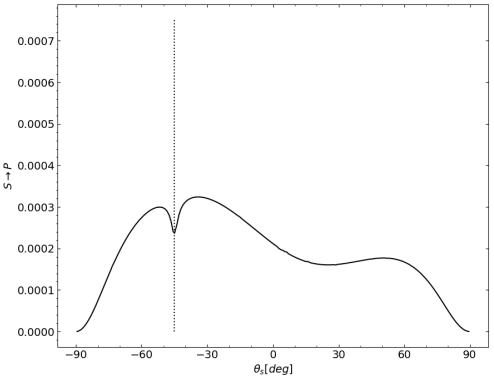

(d): $s \to p$, $\theta_0 = 45°$

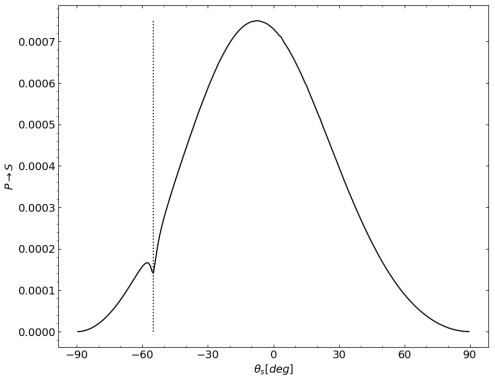

(e): $p \to s$, $\theta_0 = 55°$

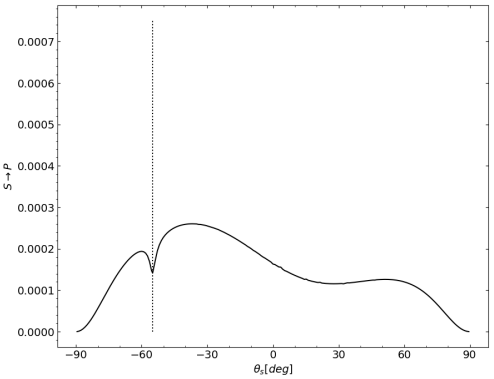

(f): $s \to p$, $\theta_0 = 55°$

Figure 12: The incoherent component of the MDRC for the cross-polarized scattering contributions from coherent light with wavelength $\lambda = 457.9$nm incident on a silver surface characterised by an RMS-height $\delta = \lambda/80$ and a Gaussian correlation function with correlation lengths $a_1 = a_2 = \lambda/4$. The incoherent MDRC was calculated for three different angles of incidence. The dielectric function for glass at this wavelength is $\varepsilon_{silver} = -7.5 + 0.24i$. The MDRC index was calculated for 101 different scattering angles θ_s

4.2.2 The Complete Angular Distribution of the incoherent MDRC

Fig. 13 and 14 show the complete angular distribution for coherent light with wavelength $\lambda = 623.8$nm incident on a randomly rough glass surface with angle of incidence $\theta_0 = 0°$ and $\theta_0 = 34.05°$ respectively. The surface is described by an isotropic Gaussian correlation function. In these figures and subsequent plots of complete angular distributions the axes give the vector components of the in-plane scattering vector $\boldsymbol{q}_\parallel$ in units of ω/c, the full angular distribution is given as a heat map with an associated intensity scale, and the white dot indicates the specular direction. Furthermore, the scattering vector corresponding to the origin has been chosen to have direction along the plane of incidence. Physically this is a simple question of perspective, as any p-polarized light would be considered s-polarized if it was observed from a perspective rotated 90° about the direction of the scattering vector $\boldsymbol{q}_\parallel$. Choosing which scattering orientation to display for the origin is simply a matter of convention. Fig. 13 is composed of nine subfigures labeled from (a-i), displaying the incoherent MDRC for various combinations of incoming and outgoing polarization modes. In Fig. 13 and following plots of the incoherent MDRC $*$ indicates that the polarization of the outgoing light is not recorded, while $\circ$ indicates that the incoming light is unpolarized. The first row consists of Figs. 13(a-c) and depict how the total intensity of light scattered from the surface depends on the polarization of the incoming light. Figs. 13(d-f) and Figs. 13(g-i) make up the second and third row respectively, and describe how the intensity of each of the outgoing polarization modes depends on the polarization of the incoming light.

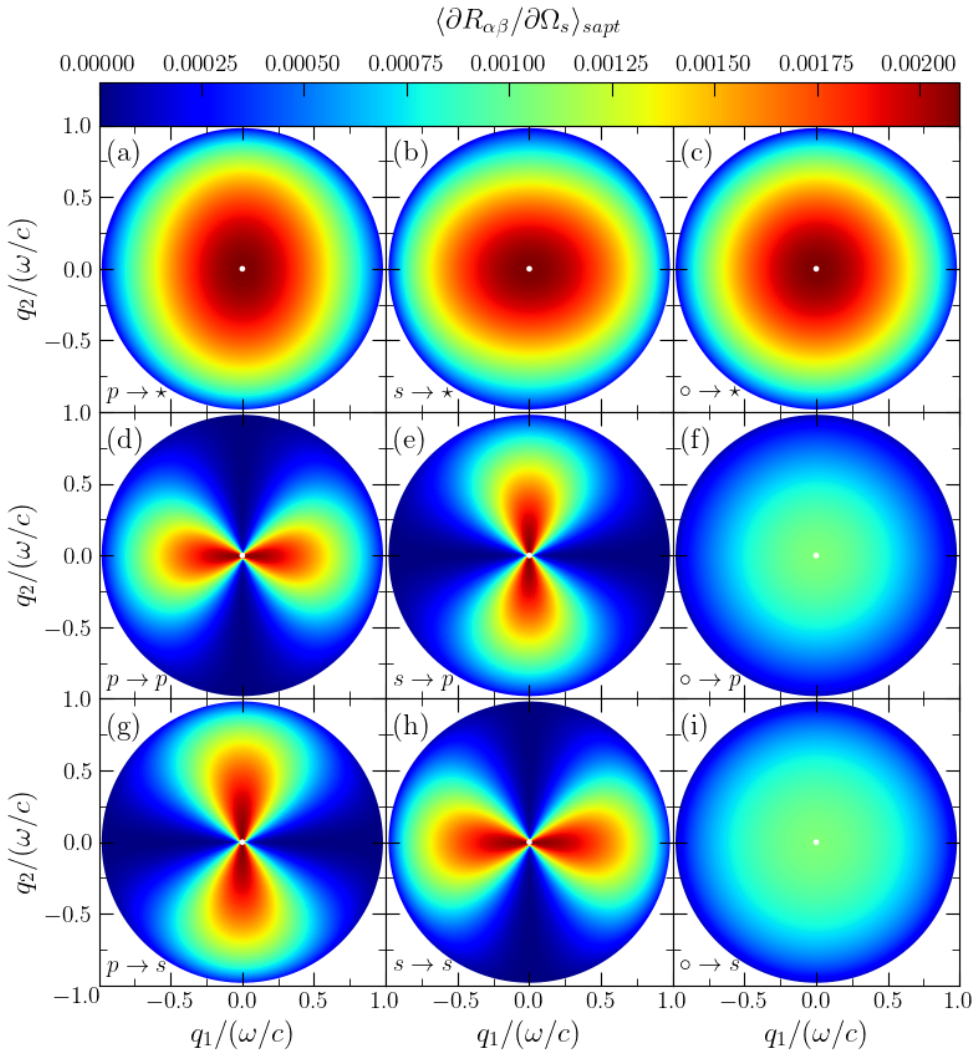

Figure 13: The full angular distribution of the incoherent component of the MDRC for coherent light with wavelength $\lambda = 632.8$nm normally incident on a randomly rough surface separating vacuum and glass. The surface was characterized by the RMS height $\delta = \lambda/20$ and a Gaussian correlation function with correlation lengths $a_1 = a_2 = \lambda/4$. The dielectric function for glass at this wavelength is $\varepsilon_{glass} = 2.25$. The incoherent MDRC is resolved on a grid of 101x101 point and the specular direction is indicated by a white dot.

Figs. 13 (d) and (h) display the same symmetry about the origin in the plane of incidence as observed in the cross-section of the incoherent MDRC in Fig. 4, furthermore Figs. 13 (c), (f) and (i) reveal that this symmetry extends to the outgoing intensity being spherically symmetric for incoming unpolarized light. The cross-polarized contributions in Figs. 13 (e) and (g) are shown to consist almost entirely of out of plane scattering and diminish rapidly as they approach the plane of incidence. The co-polarized scattering contributions display the exact opposite trend and are nearly completely extinguished for orthogonal out of plane scattering. The intensity of the co-polarized scattering contributions are as for Fig.4 nearly indistinguishable, with a slightly wider

scattering pattern for $s \rightarrow s$. The intensity has a similar shape for the cross-polarized terms, the shape of the scattering intensity appears to depend mainly on the outgoing polarization, as the cross-polarized scattering intensities 13 (e) and (g) are the corresponding co-polarized contributions 13 (d) and (h) rotated 90 degrees. This is visible in Figs 13 (f) and (i) where the intensity for the outgoing s-polarized light is brighter for larger scattering angles. This would have to be the case since, as stated at the begin of this subsection, as one is free to choose the plane of incidence This also has the result that the total scattering intensities for incoming p- and s-polarized in Figs. 13 (a) and (b) take on an elliptical shape with major-axis in the plane of incidence for s-polarized light, and major-axis perpendicular to the plane of incidence for p-polarized light.

Fig. 14 shows the incoherent MDRC for the same combinations of incoming and outgoing polarizations as Fig. 13 for light incident at an angle of $\theta_0 = 34.05°$. Figs. 14 (d) and (h) clearly show the directional preferences of the co-polarized scattering contributions from Fig. 4, with scattering predominately centered around the specular direction for the $s \rightarrow s$ contribution and $p \rightarrow p$ scattering predominately centered around the retro-specular direction. A noticeable difference from normally incident light is that the $p \rightarrow p$ scattering contribution is not completely extinguished for 90° out of plane scattering, the $s \rightarrow s$ scattering contribution does not exhibit this behaviour. The cross-polarized scattering contributions 14 (e) and (g) have nearly identical shape, and are completely extinguished in the plane of incidence. They are symmetrical about the plane of incidence as expected from an isotropic surface. Both the cross-polarized scattering contributions show a preference for scattering in positive q_1-direction, though much less notably than for the co-polarized modes. The heightened intensity for s-polarized scattering is also present similarly as for Fig.4, though principally in the co-polarized scattering contribution. Fig. 14 (c) shows that the total scattering intensity has a tendency towards the specular direction, while Figs. 14 (f) and (i) display the same directional preferences as the scattering contributions that they are composed of.

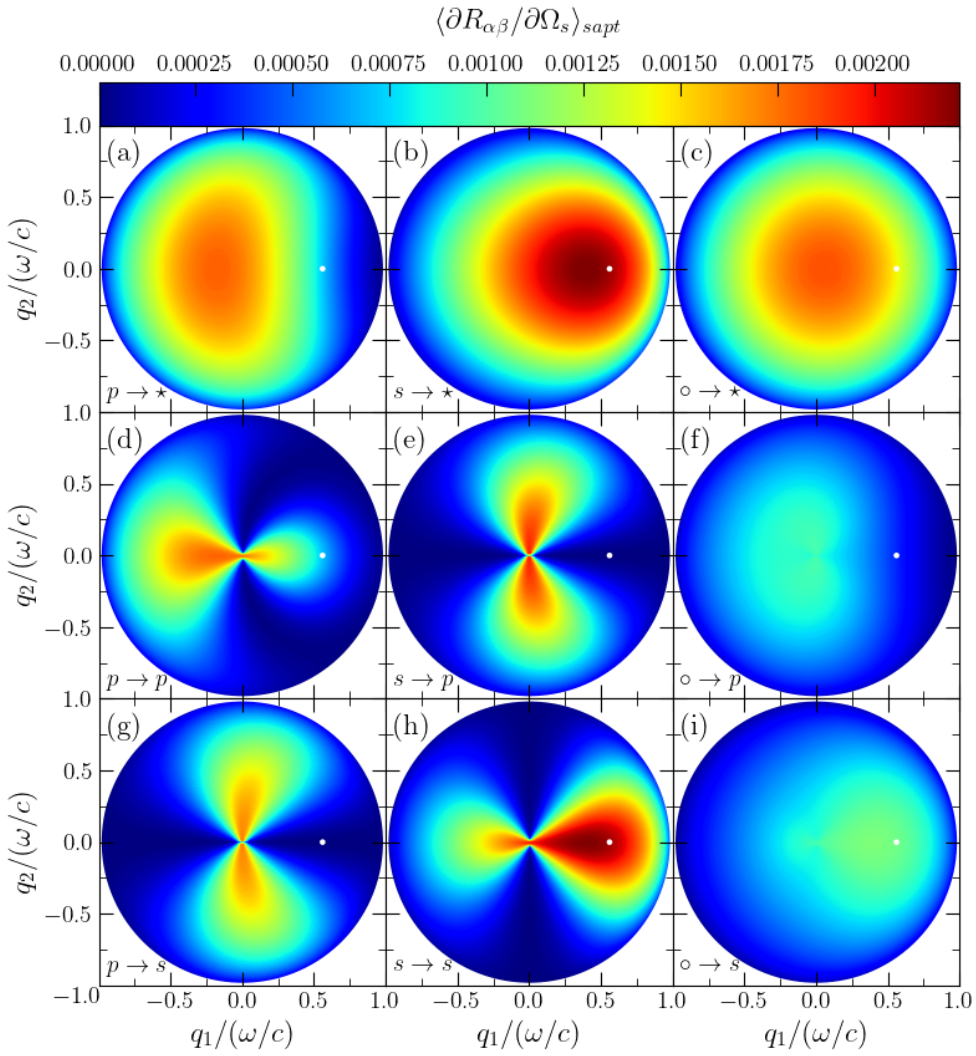

Figure 14: The full angular distribution of the incoherent component of the MDRC $\lambda = 632.8$nm incident on a randomly rough surface separating vacuum and glass with angle of incidence $\theta_0 = 34.05°$. The surface was characterized by the RMS height $\delta = \lambda/20$ and a gaussian correlation function with correlation lengths $a_1 = a_2 = \lambda/4$. The dielectric function for glass at this wavelength is $\varepsilon_{glass} = 2.25$. The incoherent MDRC was calculated for a grid of 101x101 points and the specular direction is indicated by a white dot.

Figures 15 and 16 depict the complete angular distribution for coherent light incident on a randomly rough silver surface with angle of incidence $\theta_0 = 0°$ and $\theta_0 = 34.05°$ respectively. Figs. 15(c),(f) and (i) show the same spherical symmetry that was present in the scattering intensity from normally incident light on a vacuum-glass interface in Fig. 13. Similarly as for the cross-section of the plane of incidence in Fig. 5, it is observed that the cross-polarized modes contribute even for the plane of incidence, and that the co-polarized modes are non-zero for orthogonal out of plane scattering. In fact, Figs.15 (d) and (e) show that the $p \to p$ and $s \to p$ scattering contributions have a significant contribution for nearly all scattering vectors $\boldsymbol{q}_{\parallel}$ that

correspond to a travelling plane wave, diminishing slowly to zero only for the largest possible values of $\boldsymbol{q}_{\parallel}$. This is not the case for the $s \to s$ and $p \to s$ contributions in Figs. 15 (g) and (h), here the intensity approaches zero quite quickly as the magnitude of $\boldsymbol{q}_{\parallel}$ increases. Figs.15 (f) and (i) clearly show that wave-modes scattering as p-polarized light couple more strongly to the surface for larger magnitudes of $\boldsymbol{q}_{\parallel}$, which is opposite of what was observed for the vacuum-glass interface. This is also noticeable in the elliptical shapes of the scattering intensities in Figs.15 (a) and (b), where the scattering pattern resulting from incident p-polarized light now has its major axis along the plane of incidence, and the pattern resulting from incident s-polarized light now has its major axis orthogonal to the surface.

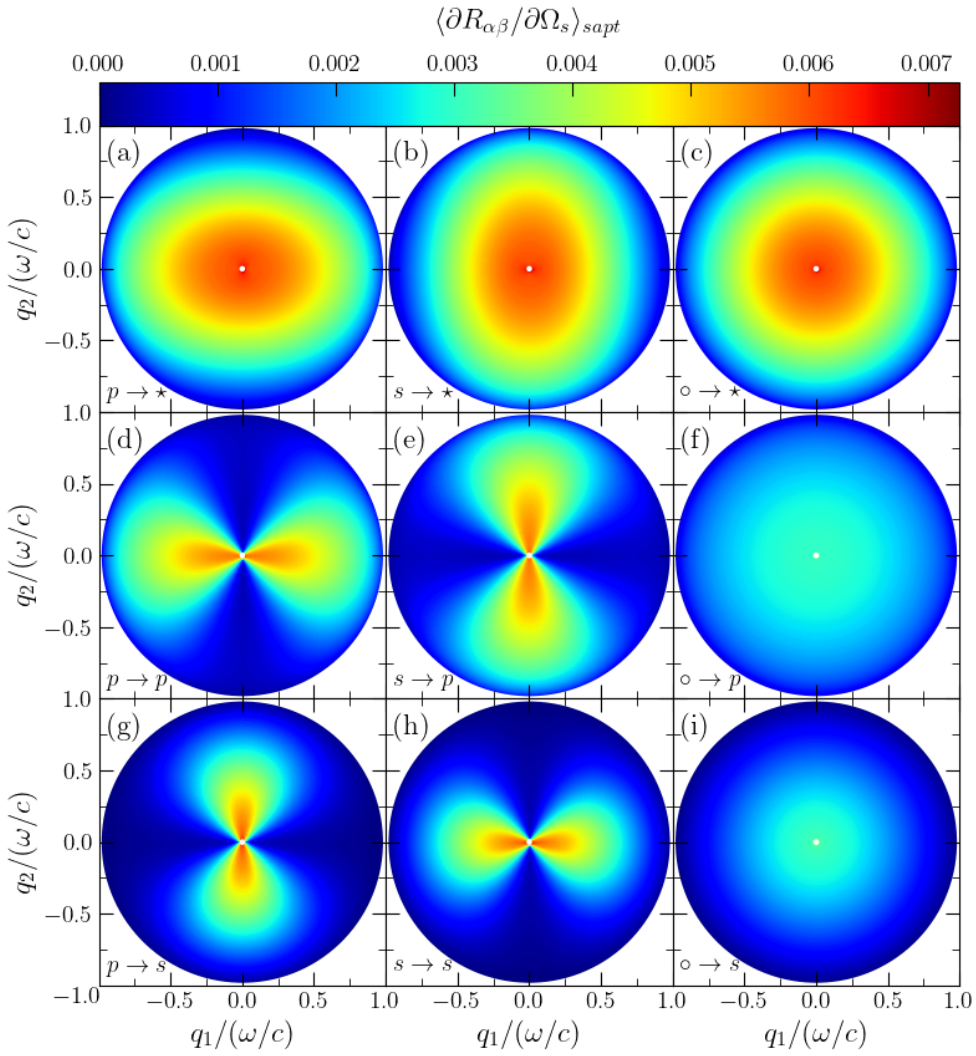

Figure 15: The full angular distribution of the incoherent component of the MDRC for coherent light with wavelength $\lambda = 457.9$nm normally incident on a randomly rough surface separating vacuum and silver. The surface was characterized by the RMS height $\delta = \lambda/80$ and a Gaussian correlation function with correlation lengths $a_1 = a_2 = \lambda/4$. The dielectric function for silver at this wavelength is $\varepsilon_{Silver} = -7.5 + 0.24i$. The resolution is 101x101 points and the specular direction is indicated by a white dot.

In Figs. 16 (d) and (h), similar as for the cross-section in Fig. 5 and the full angular distribution for normal incidence in Fig. 15, the largest co-polarized scattering contribution is from $p \to p$ scattering for all outgoing scattering modes. Figs. 16 (f) and (i) show that, similarly as for normal incidence, the outgoing p-polarized scattering contributions are dominant for large magnitudes of $\boldsymbol{q}_{\parallel}$, though the $p \to s$ contribution is greater than the $s \to p$ contributions for small magnitudes of $\boldsymbol{q}_{\parallel}$. The enhanced back-scattering peak is clearly visible as a bright spot in Figs. 16 (a-d), (f), (h) and (i), affirming that the phenomena only arises for the retro-specular direction.

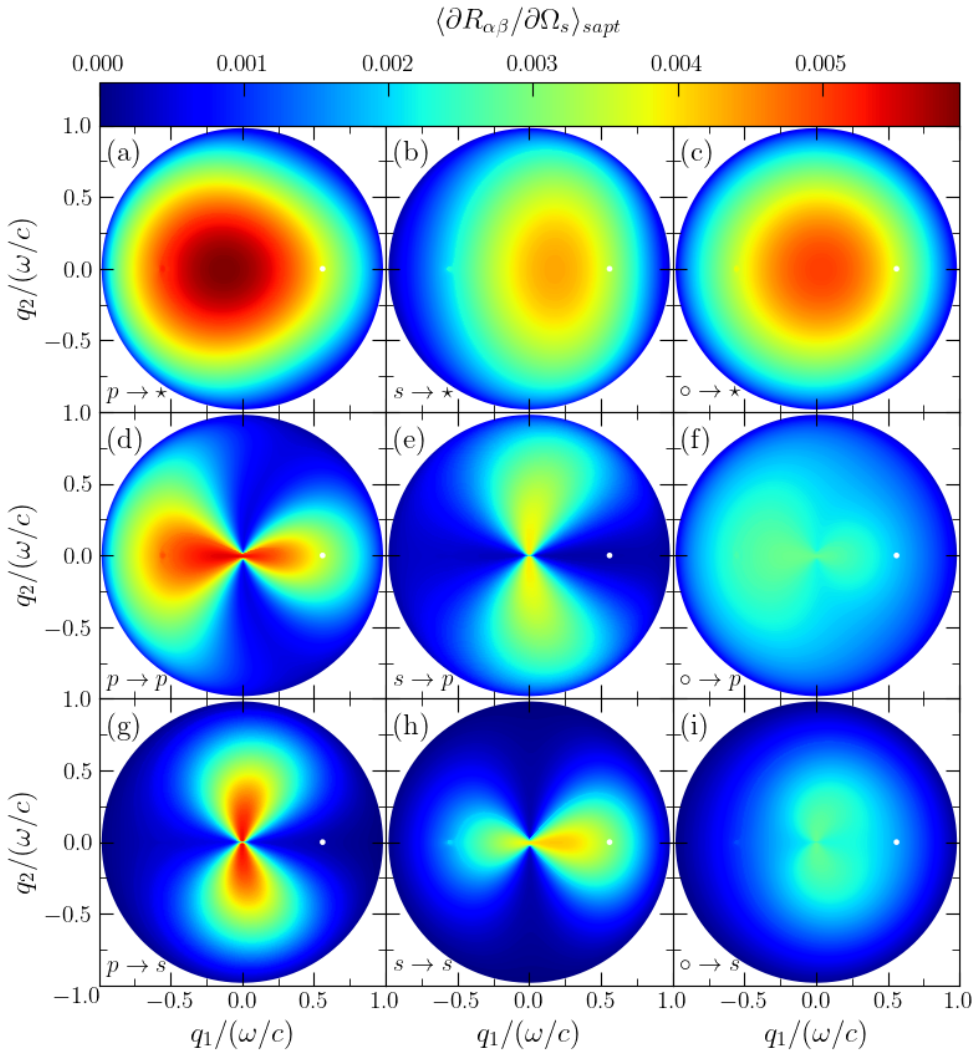

Figure 16: The full angular distribution of the incoherent component of the MDRC for coherent light with wave length $\lambda = 457.9$nm incident on a randomly rough surface separating vacuum and silver with angle of incidence $\theta_0 = 34.05°$. The surface was characterized by the RMS height $\delta = \lambda/80$ and a Gaussian correlation function with correlation lengths $a_1 = a_2 = \lambda/4$. The dielectric function for silver at this wavelength is $\varepsilon_{Silver} = -7.5 + 0.24i$. The incoherent component of the MDRC is resolved on a grid of 101x101 points and the specular direction is indicated by a white dot.

4.3 Mueller Matrix

The incoherent component of the Mueller Matrix allows us, as described in Sec. 2.8, to completely characterise the polarization response of the incoherent scattering contribution from a randomly rough surface for light incident with wave vector $\boldsymbol{k}_{\parallel}$ scattering in direction $\boldsymbol{q}_{\parallel}$. As for the incoherent MDRC it is useful visualize the incoherent component of the Mueller Matrix both as a heatmap over all scattering directions that correspond to a travelling wave mode, and as cuts through planes of particular interest such as the plane of incidence. It can be difficult

to accurately discern the contribution from the different Mueller Matrix elements in the full angular distribution, it is therefore natural to start out with cross-sections of the distribution before moving on to the full angular distribution. Cross-sections also have the advantage that it is easier to visualise and compare the contributions from the One-one, Two-two and Three-one terms in the incoherent expansion of the Mueller Matrix (47).

4.3.1 Cross sections of the Incoherent Mueller Matrix

Figs. 17 and 18 depict the incoherent component of the Muller Matrix and the contributions from the three terms in the incoherent expansion (47) for coherent light incident on a glass surface characterised by a Gaussian correlation function at an angle of $\theta_0 = 0°$ and $\theta_0 = 34.05°$. The total Mueller Matrix elements and the contributions have been normalized with respect to M_{11}. In Fig. 17 one can observe that the upper right and lower left quadrants are zero in the plane of incidence. As a result of this the polarization response is restricted such that the I^s and Q^s only depend on I^i and Q^i, and similarly U^s and V^s only depend on U^i and V^i. Inspecting the first column of Fig. 17 the polarization response from incident unpolarized or linearly polarized light will thereby not result in any circularly- or 45°-polarized light, only a slight decrease in the degree of linearly polarized light for larger scattering angles, corresponding to a preference for linear s-polarized scattering, which was also observed in for the incoherent MDRC in Fig. 4.

Fig. 17(f) shows that the degree of linear polarization of the incident light has almost none, if any impact on the degree of linear polarization of the scattered light, reflecting the fact that in-plane cross-polarization is severely diminished for scattering from weakly rough dielectric surfaces. It is observed that the degree of linear polarization is only modulated by the increased magnitude for the $s \rightarrow s$ scattering contribution as was observed for the incoherent MDRC in the plane of incidence in Fig. 4. This is seen in M_{21} in Fig. 17(e), which varies for larger scattering angles similar to the difference between the magnitude of the co-polarized scattering contributions in Fig. 4. The near-absence of cross-polarized scattering has the consequence that the contributions in Figs. 17(b) and (e) are almost completely identical. In fact, similarly as for the incoherent component of the MDRC in Fig. 7 all the non-zero elements of the Mueller Matrix in the plane of incidence are dominated by single scattering contributions.
Similarly as for unpolarized light incident purely circularly- or 45°-polarized light will result in a slight change in the degree of linearly polarized light through M_{21} in Fig. 17(e). For circularly- and 45°-polarized light a sign change will be observed similar to an ideal mirror, though the influence from the Three-one contribution in the M_{34} and M_{43} elements causes interchange between the V and U terms in the stokes vector, resulting in a deviation from the polarization response of a perfect mirror.

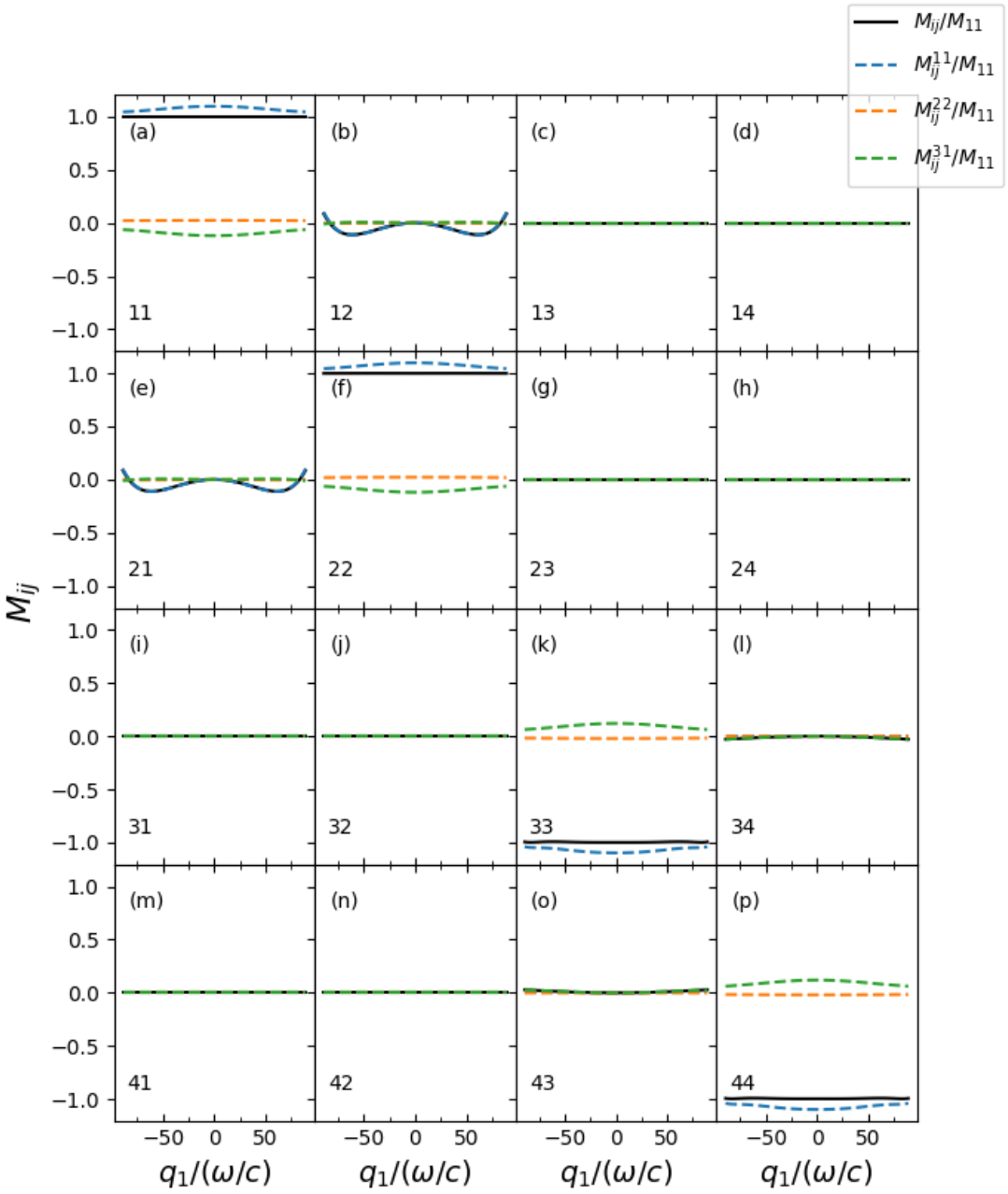

Figure 17: Cross section of the incoherent component of the Mueller Matrix and the various contributions from which it is composed in the plane of incidence for coherent light with wavelength $\lambda = 632.8$nm normally incident on a randomly rough surface separating vacuum and glass. The various contributions have been normalized with respect to M_{11}, M_{ij}^{11} signifying the One-one contribution to element M_{ij} of the Mueller Matrix. The surface was characterized by the RMS height $\delta = \lambda/20$ and a Gaussian correlation function with correlation lengths $a_1 = a_2 = \lambda/4$. The dielectric function for glass at this wavelength is $\varepsilon_{glass} = 2.25$. The Mueller Matrix is resolved for 101 in-plane scattering vectors and the specular direction is indicated by a white dot.

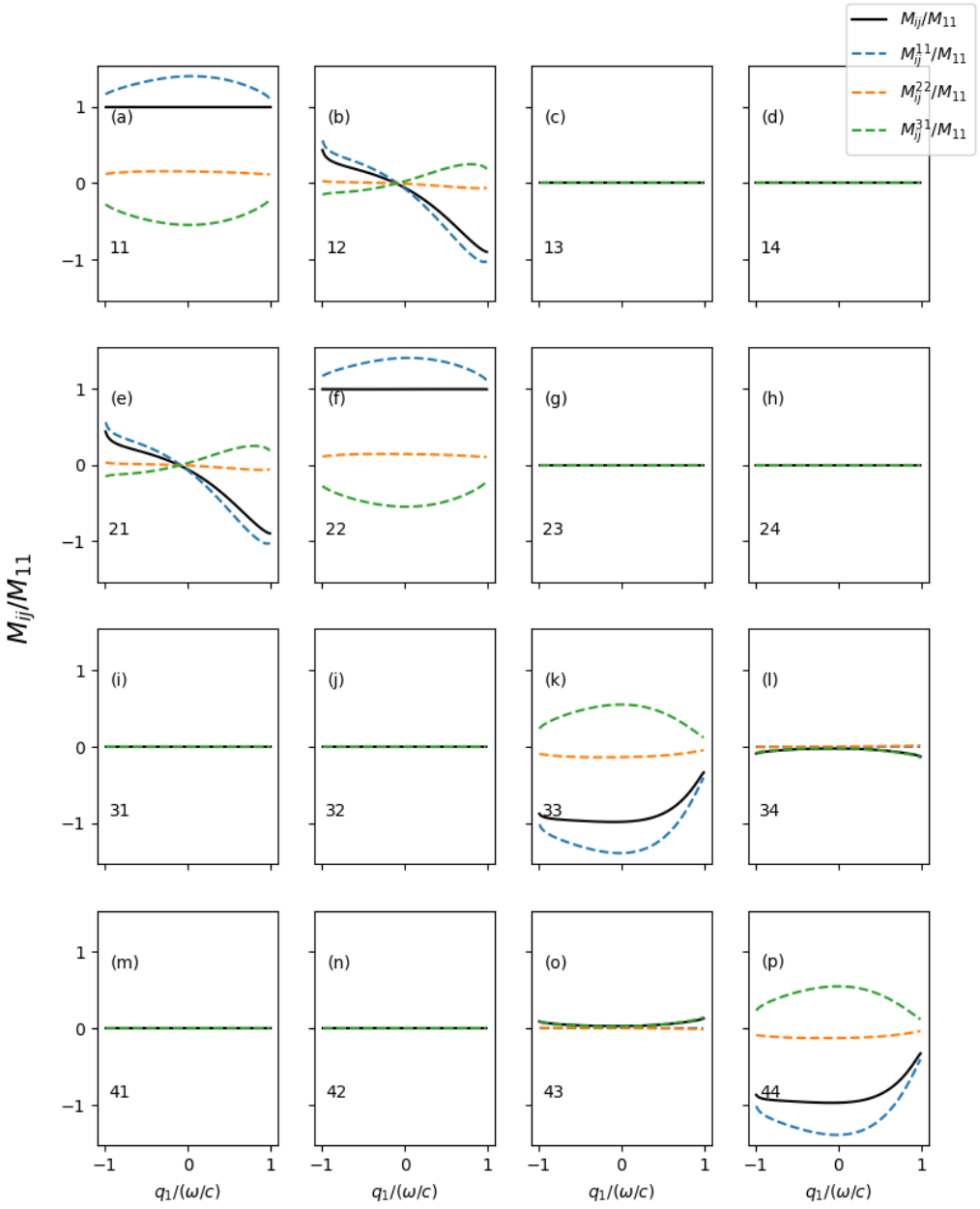

Figure 18: Cross section of the incoherent component of the Mueller Matrix in the plane of incidence for coherent light $\lambda = 632.8$nm incident on a randomly rough surface separating vacuum and glass with angle of incidence $\theta_0 = 34.05°$. The various contributions have been normalized with respect to M_{11}, M_{ij}^{11} signifying the One-one contribution to element M_{ij} of the Mueller Matrix. The surface was characterized by the RMS height $\delta = \lambda/20$ and a Gaussian correlation function with correlation lengths $a_1 = a_2 = \lambda/4$. The dielectric function for glass at this wavelength is $\varepsilon_{glass} = 2.25$. The MDRC is resolved on a grid of 101x101 points and the specular direction is indicated by a white dot.

Fig. 18 displays the incoherent component of the Mueller Matrix in the plane of incidence for light incident on a weakly rough glass surface at an angle of $\theta_0 = 34.05°$. Similarly as

for Fig. 17 it is observed that the upper right and lower left quadrant are equal zero for all scattering vectors in the plane of incidence, meaning that incident unpolarized light will not result in circularly- or 45°-polarized light in the plane of incidence, even for incident angles $\theta_0 > 0$. A significant change can be observed for Figs. 18(b) and (e) in comparison to the same Mueller Matrix elements for normal incidence. It is observed that the change in degree of polarization and intensity now greatly depend on the scattering angle, with the sign being the opposite of q_1 and increasing magnitudes for larger scattering angles. This dependence on the scattering direction reflects the directional preference for the co-polarized scattering modes that was observed in Fig. 4, with s-polarized scattering preferring positive scattering angles and p-polarized preferring negative scattering angles. The Mueller matrix elements in the lower right quadrant have a similar structure to Fig. 17, though there is now a much stronger dependence on the scattering angle, most notably in the diagonal terms.

Figs. 19 and 20 depict a cut through the plane of incidence for the incoherent component of the Muller Matrix and the contributions from the three terms in the incoherent expansion (47) resulting from coherent light incident on a silver surface. The total Mueller Matrix elements and the contributions have been normalized with respect to the total M_{11} element. It is important to note that the peaks present in the single scattering contributions are a consequence of the normalization, not of an enhanced back-scattering effect originating from a single scattering process. Non-normalized plots of the Mueller Matrix will be presented in Sec. 4.4, along with a more in-depth discussion of the contributions from the enhanced back-scattering effect to the Mueller Matrix. Similarly as for Fig. 17 a symmetry about the direction of specular reflection is observed, there are also no contributions from the upper right and lower left quadrants in the plane of incidence. This means that incoming unpolarized or linearly polarized light will not scatter as circularly or 45°-polarized light in the plane of incidence, exactly as was observed for the glass surface. One can however observe a very significant change in the scattering response in the remaining non-zero elements in the upper left and lower right quadrants. The M_{12} and M_{21} elements in Figs. 19(b) and(e) reflect the dominating preference for p-polarized scattering for increasing magnitude of $\boldsymbol{q}_{\parallel}$ that was observed in Fig. 5, while the dampening in the M_{22} term originates from the massive increase in in-plane cross-polarization that is observed for a metal surface compared to a dielectric surface for weakly rough surfaces. The large increase in in-plane cross-polarization also has the effect that the M_{12} and M_{21} terms no longer appear to be identical. For the lower right quadrant a sign change is observed for the off-diagonal elements in Figs. 19 compared to scattering from a glass surface. One can observe that this is also a consequence of the increased contribution to multiple scattering from the Two-two term that is observed for metals, since unlike for the glass surface the Three-one term no longer dominates the M_{34} and M_{43} elements in figs. 19(l) and (o). For the diagonal elements in Figs. 19 a much more significant deviation from the behavior of a perfect mirror is observed, than was observed for the glass surface. The effect is predominately a single scattering effect, with some contribution from the Two-two term around the specular direction for the M_{33} term in Fig. 19(k). The effect being predominately a single scattering effect means that this is a consequence of the preference for p-polarized scattering for larger scattering angles, rather than the excitation of SPPs.

Fig. 20 depicts the incoherent Mueller Matrix in the plane of incidence from light incident at an angle of $\theta_0 = 34.05°$. All elements of the Mueller Matrix and their contributions from the terms in the incoherent expansion have been normalized with respect to the first element M_{11}. It is observed as for normal incidence that the upper right and lower left quadrants have zero contribution in the plane of incidence, indicating that the resultant scattering from incident unpolarized has no component of circularly- or 45°-polarized light. A strong dependence on the scattering direction is observed in the M_{12}, M_{21} and M_{22} elements in Figs. 20(b), (e) and (f). Notably it is observed that the One-one contribution dominates for negative values of q_1 while we see a more significant contribution from the Two-two term for positive values. This indicates a preference for p-polarized single-scattering for negative values of q_1 and a preference for p-polarized double-scattering for positive values of q_2. For large magnitudes of $\boldsymbol{q}_{\parallel}$ both the single- and double scattering contributions show a preference for p-polarized scattering. The lower right quadrant displays similar behavior as for normal incidence. The off-diagonal elements in Figs. 20(l) and (o) are still completely dominated by the Two-two contribution, while the diagonal elements are largely determined by the one-one term, with some contribution from the

multiple scattering terms.

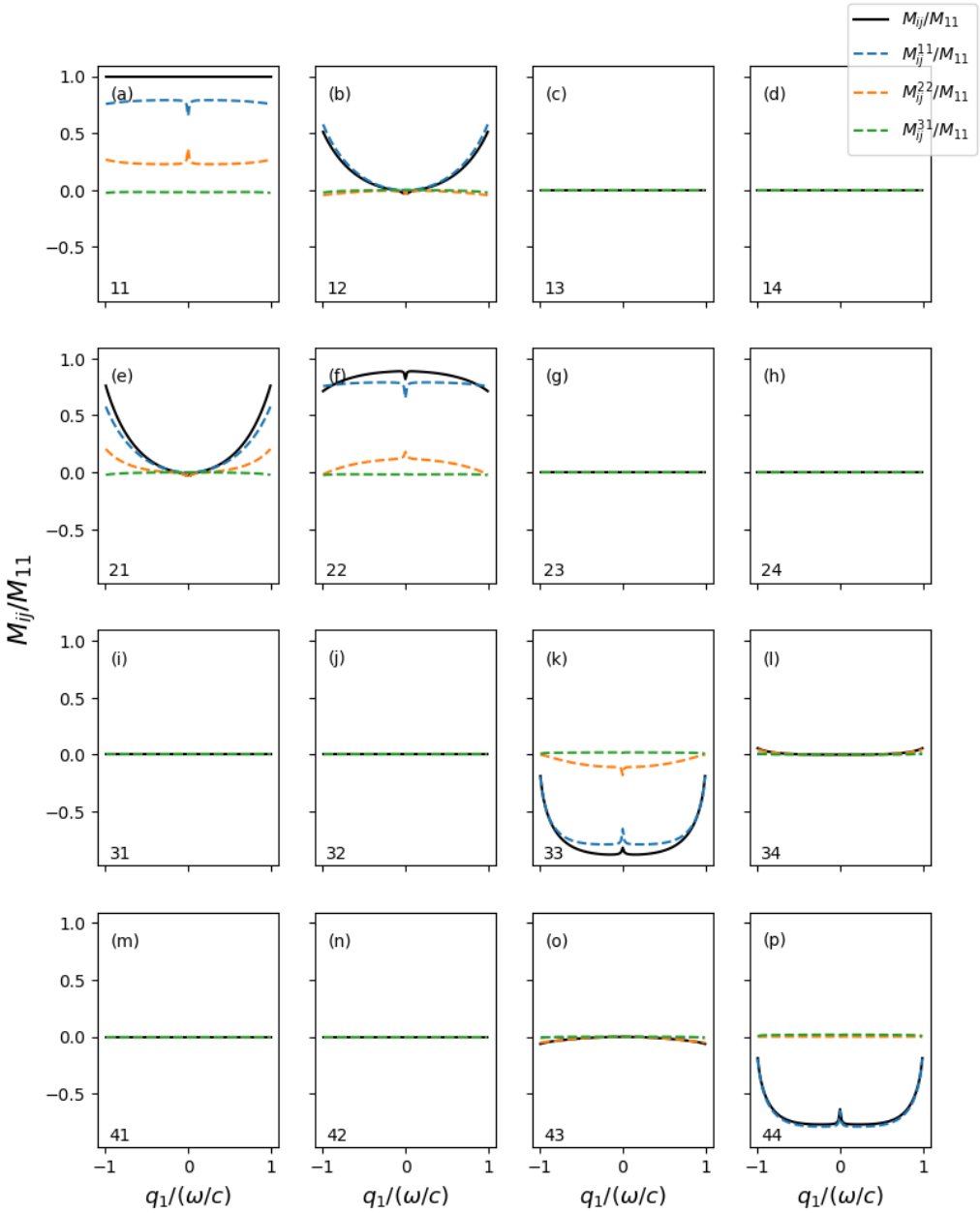

Figure 19: Cross section of the incoherent component of the Mueller Matrix and the various contributions from which it is composed in the plane of incidence for coherent light with wavelength $\lambda = 457.9$nm normally incident on a randomly rough surface separating vacuum and silver. The various contributions have been normalized with respect to M_{11}, M_{ij}^{11} signifying the One-one contribution to element M_{ij} of the Mueller Matrix. The surface was characterized by the RMS height $\delta = \lambda/80$ and a Gaussian correlation function with correlation lengths $a_1 = a_2 = \lambda/4$. The dielectric function for silver at this wavelength is $\varepsilon_{silver} = -7.5 + 0.24i$. The Mueller Matrix is resolved for 101 in-plane scattering vectors and the specular direction is indicated by a white dot.

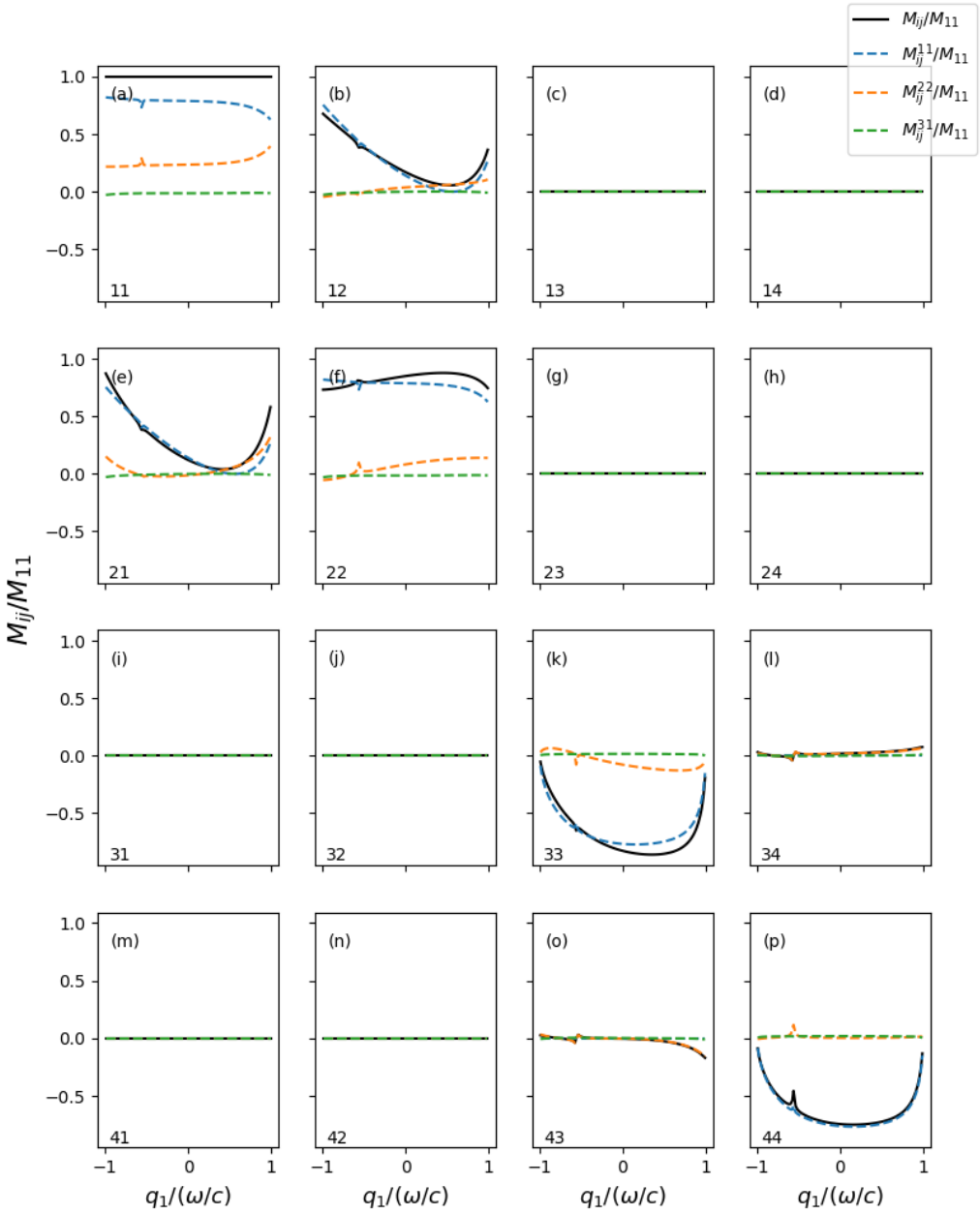

Figure 20: Cross section of the incoherent component of the Mueller Matrix in the plane of incidence for coherent light $\lambda = 457.9$nm incident on a randomly rough surface separating vacuum and glass with angle of incidence $\theta_0 = 34.05°$. The various contributions have been normalized with respect to M_{11}, M_{ij}^{11} signifying the One-one contribution to element M_{ij} of the Mueller Matrix. The surface was characterized by the RMS height $\delta = \lambda/80$ and a Gaussian correlation function with correlation lengths $a_1 = a_2 = \lambda/4$. The dielectric function for silver at this wavelength is $\varepsilon_{silver} = -7.5 + 0.24i$. The Mueller Matrix is resolved for 101 in-plane scattering vectors and the specular direction is indicated by a white dot.

4.3.2 Full Angular Distribution of the incoherent Mueller Matrix

Figs. 21 and 22 display the full angular distribution of the incoherent component of the Mueller Matrix for angle of incidence $\theta_0 = 0°$ and $\theta_0 = 34.05°$. The elements are labeled with a sub-figure index (a-p) in the top left corner and their row- and column index in the bottom left corner. The axes give the vector components of the parallel scattering wave vector $\boldsymbol{q}_{\parallel}$ in units of ω/c and the white dot indicates the specular direction. In order to more accurately discern the various polarizing effects of the surfaces, the elements of the Mueller Matrix have been normalized with respect to the first element, which describes the total incoherent scattering intensity.

Fig. 21 displays the same polarization response for the plane of incidence as in Fig. 17. It is observed that there are non-zero contributions to the upper left and lower right quadrant for scattering directions away from the plane of incidence, though the M_{14}, M_{24}, M_{31} and M_{41} elements in Figs. 21(d), (h), (i) and (m) have no contribution to any scattering modes. Fig. 21 (e) shows that M_{21} is spherically symmetric, meaning that the symmetry about the origin for scattering of unpolarized light as linearly polarized light that was observed in the plane of incidence in Fig. 4(e) extends to a spherical symmetry for the full angular distribution. Interestingly the degree of incident 45°-polarized light influences the intensity of the scattered light through M_{13} in Fig. 13(c), but no similar response can be observed from the intensity to the degree of 45°-polarized light in M_{31} in Fig. 21(i). A change in the intensity caused by the degree of 45°-polarized in the incident light is a result of interference between co-polarized and cross-polarized light with the same outgoing polarization. This can be seen by considering the fact that incoming ±45° polarized light would have p- and s-polarized components being entirely in or out of phase, as a result of this cross-polarized single-scattering of either the p- or s-component would constructively or destructively interfere with a co-polarized contribution. Since there are no single-scattering contributions to cross-polarization in the plane of incidence it is logical that no contribution to the M_{13} element was observed in Fig. 17(c). However, from observing the full angular distribution of the incoherent component of the MDRC in Fig. 13 one would expect a more significant contribution from this interference phenomenon, since there is substantial overlap between the co- and cross-polarized contributions for both outgoing polarizations. This can be explained by considering the M_{23} element in Fig. 21 (g) and the expressions for the two Mueller Matrix elements (42). The two Mueller Matrix elements are composed of the same two terms, only differing in the sign in front of the $2Re(R^*_{sp}R_{ss})$ term involving outgoing s-polarized scattering. From this one can garner that the $2Re(R^*_{sp}R_{ss})$ and $2Re(R^*_{ps}R_{pp})$ terms which contribute to the M_{13} element have the same shape as observed in the M_{23} element, but have opposite sign and slightly differing magnitudes. As expected from the observed preference for outgoing s-polarized scattering observed for the incoherent component of the MDRC 13. Similarly the lack of contributions to the M_{31} term in Fig 13(i) can be explained in a similar manner, the corresponding term now being M_{32} in Fig. 13(j). The major difference is that it is now combinations of co- and cross-polarized scattering modes with the same incident polarization which are considered, the preference for s-polarized scattering thereby yields an equal contribution to both terms and they cancel out completely.

For 90° out of plane scattering a very similar polarization response to that in the plane of incidence is observed, as there is no contribution from the elements in the upper right and lower left quadrant. Interestingly a sign change is observed for the elements in Figs.21(b), (f), (k) and (o). For the M_{22} element in Fig. 21(f) this follows from 90° out of plane scattering consisting nearly entirely of cross-polarized scattering contributions, having the consequence that any disproportion between the amount of s- and p-polarized light would be flipped. Similarly the change in sign for the M_{12} element in Fig. 21 describes the fact that incoming p-polarized light results in a larger scattered intensity for 90° out of plane scattering, since cross-polarized scattering dominates, and there is a preference for scattering of s-polarized light as the magnitude of the scattering vector increases, as was seen in Fig. 13(i). The M_{33} element in Fig. 21(k) reveals that the change of sign in the degree of 45°-polarized light that was observed in the plane of incidence, is canceled out by the change in polarization. The M_{34} contribution is spherically symmetric, while M_{43} appears to be a 90° rotation of M_{12}. In addition to this it is observed that $M_{44} = -M_{11}$ for all scattering modes, indicating that the last two entries in the stokes vector have a similar but inverted interplay to that observed for the first two entries.

The complete angular distribution of the Mueller Matrix for light incident at an angle $\theta_0 =$

34.05° on a glass surface. Similarly as for the cross-section of the plane of incidence in Fig. 18 a rather radical change from the case of normal incidence can be observed. The central elements in Figs. 22(f), (g), (j) and (k) present as distorted images of their corresponding entries for normal incidence, most notably for the diagonal elements. A strong dependence on the scattering direction is observed in Figs. 22 (b) and (e), similarly as for the interplay between the incident and outgoing intensity and degree of polarization in the cross-section in Fig. 18. A most significant difference between normal and non-normal incidence can be observed in Figs. 22(h) and (i) which show that the polarization response has contributions from both the M_{31} and M_{24} elements away from the plane of incidence. Non-zero contributions to the M_{31} has the consequence that incident unpolarized light now scatters both as linearly- and 45°-polarized light. The drastic change compared to normal incidence can be attributed to the radical difference between the co-polarized scattering contributions for non-normal incidence, meaning that the contributing terms in the M_{13} and M_{31} elements now differ greatly for most scattering directions. Furthermore the contributions to both the M_{24} and M_{42} elements reveal that there is now interchange between the degree of linear- and circular polarization. There is still no observed interchange between the intensity and the degree of circularly polarized light, though one can notice a similar structure in the M_{44} element in Fig. 22 as was observed for the plane of incidence.

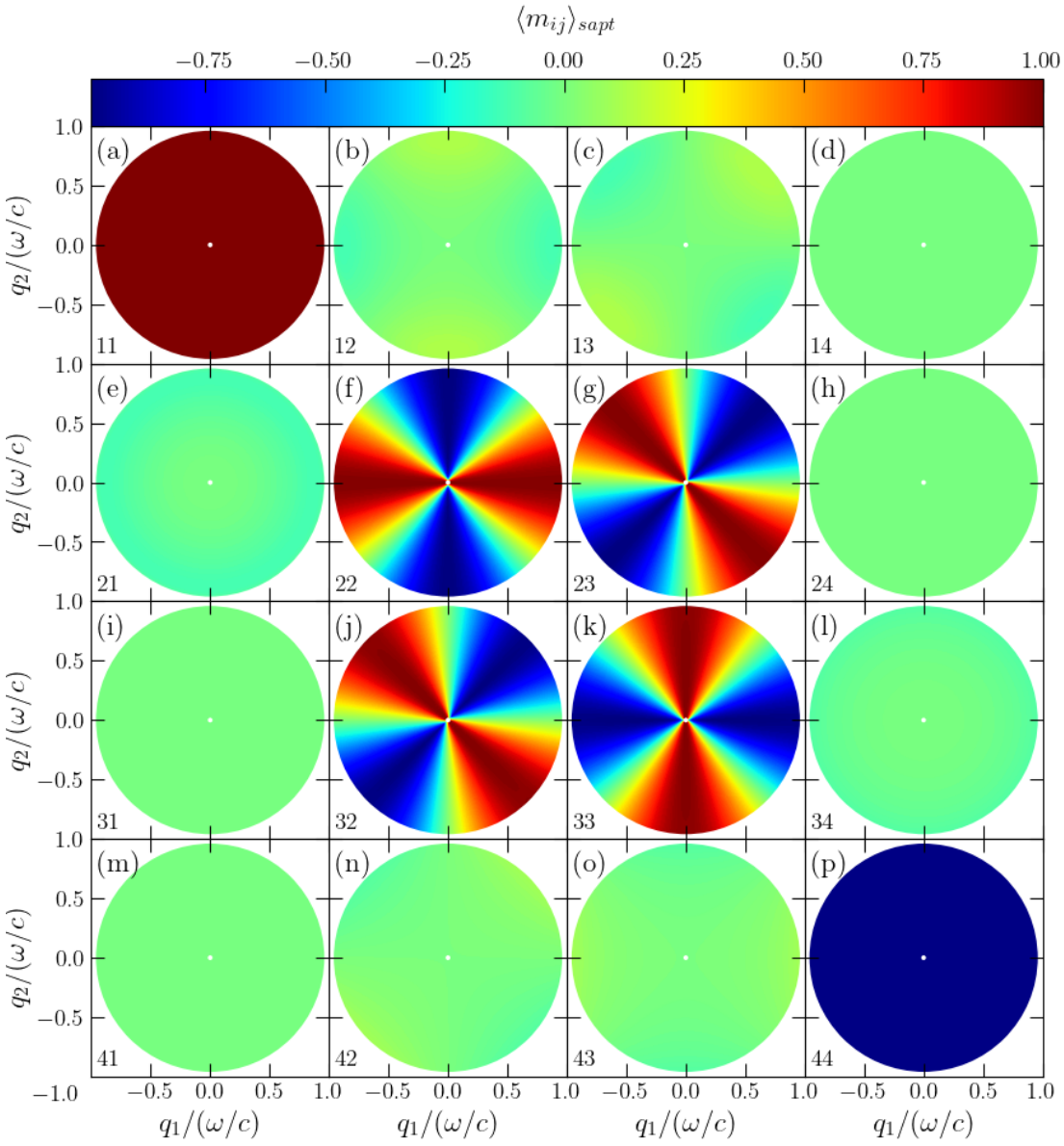

Figure 21: The full angular distribution of the incoherent component of the Mueller Matrix for coherent light $\lambda = 632.8$nm normally incident on a randomly rough surface separating vacuum and glass. The surface was characterized by the RMS height $\delta = \lambda/20$ and a Gaussian correlation function with correlation lengths $a_1 = a_2 = \lambda/4$. The dielectric function for glass at this wavelength is $\varepsilon_{glass} = 2.25$. The MDRC is resolved on a grid of 101x101 points and the specular direction is indicated by a white dot.

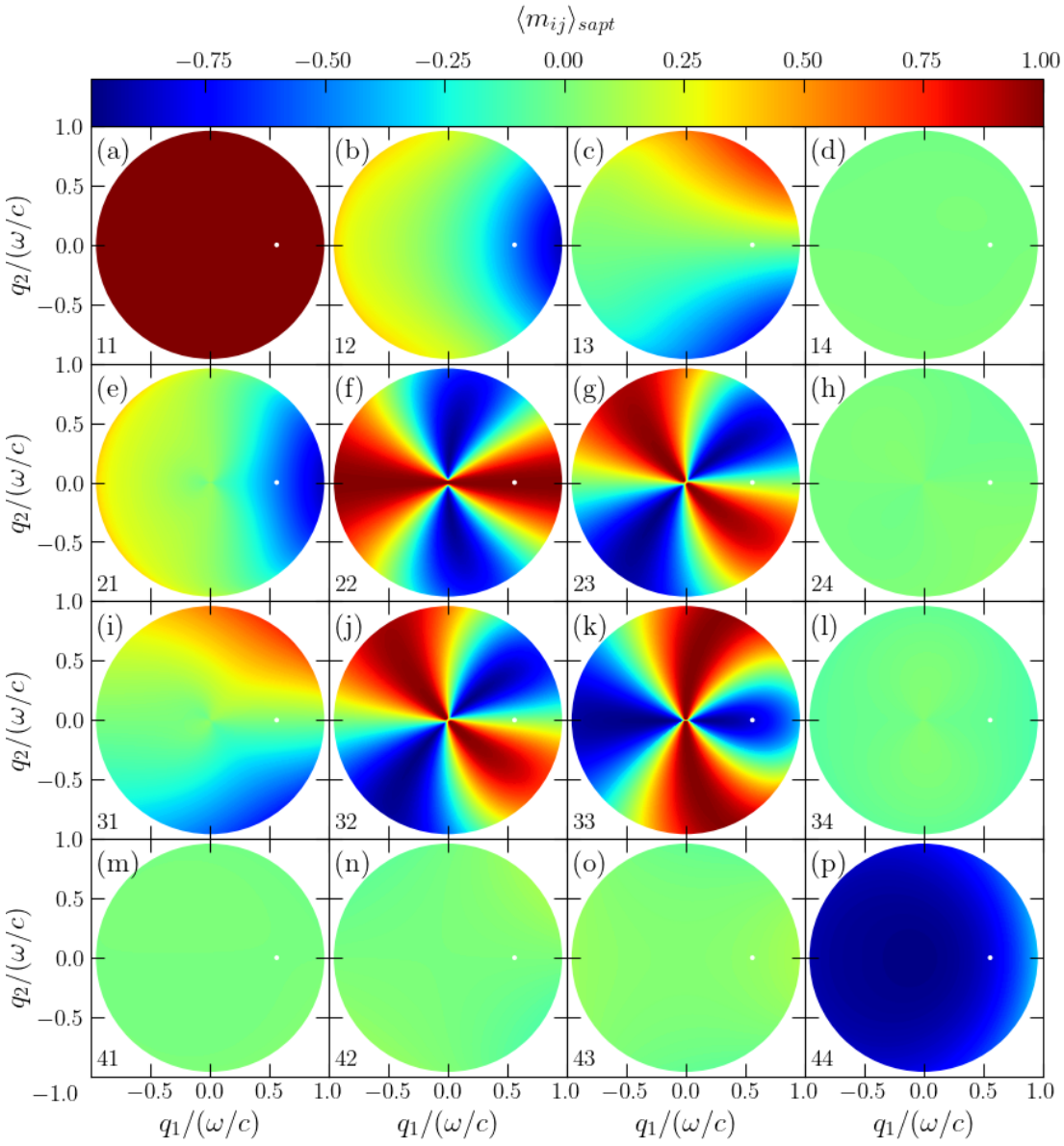

Figure 22: The full angular distribution of the incoherent component of the Mueller Matrix for coherent light $\lambda = 632.8$nm incident on a randomly rough surface separating vacuum and glass with angle of incidence $\theta_0 = 34.05°$. The surface was characterized by the RMS height $\delta = \lambda/20$ and a Gaussian correlation function with correlation lengths $a_1 = a_2 = \lambda/4$. The dielectric function for glass at this wavelength is $\varepsilon_{glass} = 2.25$. The MDRC is resolved on a grid of 101x101 points and the specular direction is indicated by a white dot.

Figs. 23 and 24 depict the full angular distribution of the Mueller Matrix for light incident on a silver surface with angle of incidence $\theta_0 = 0°$ and $\theta_0 = 34.05°$. Here, as in previous plots of the Mueller Matrix all the elements have been normalized with respect to first elements M_{11}, which

only contains information about the total intensity scattered from the surface. For normally incident light in Fig. 23 it is observed, that similarly as for the glass surface in Fig. 21, that there are contributions from the upper right and lower left quadrants, but that the M_{14}, M_{24}, M_{31} and M_{41} have zero contribution for all scattering modes. The central elements in Figs. 23(f), (g), (j) and (k) are not as sharply defined as for the corresponding elements for the glass surface in Fig. 21. This reflects the increased contribution from cross-polarized scattering modes for the silver surface and the substantial preference for p-polarized scattering for large values of $|\boldsymbol{q}_{\parallel}|$. Fig. 23(e) shows that similarly as for the glass surface that the M_{21} element is spherically symmetric, and thereby so is the contribution from unpolarized light to the degree of linearly polarized light. The M_{21} element also presents with a heightened intensity compared to the glass surface, this is especially noticeable for larger $|\boldsymbol{q}_{\parallel}|$, and is a consequence of the preference for p-polarized scattering observed in Fig. 13(f). This discrepancy between the preference for the two outgoing polarization modes, can also be seen to have an effect for large values of $\boldsymbol{q}_{\parallel}$ in the M_{12} in Figs. 23(b) which has heightened intensity and flipped signs compared to the glass surface. This is exactly as expected since the glass surface shows a slight preference for s-polarized scattering for larger scattering angles, while the silver surface shows a significant preference for p-polarized scattering. The M_{13} element in Fig. 15(c) has a similar pattern as for the glass surface with a heightened intensity, the pattern is also inverted since outgoing p-polarized scattering dominates for large scattering angles instead of s-polarized scattering. For the M_{42} and M_{43} elements in Figs. 23 (n) and (o) the same change in sign is observed as for M_{12} and M_{13} but the magnitude for these elements are significantly dampened compared to the glass surface, as is M_{34} in fig. 23 (l). Finally it is observed that the shape of the M_{44} observed in Fig. 19 reflects a spherically symmetric shape about the plane of incidence.

In Fig. 24 which depicts the incoherent Mueller Matrix resulting from light incident at an angle of $\theta_0 = 34.05°$. The central elements in Figs. 23(f), (g), (j) and (k) present with similar shapes as for the glass surface, though just as for normal incidence these elements are not as sharply defined as for the glass surface. In addition to this the M_{33} element has a much less pronounced deviation from normal incidence and the M_{23} and M_{32} elements are no longer nearly identical. As was observed for normal incidence the M_{21} element in Fig. 24(e) presents with a significantly heightened magnitude compared to the glass surface, though the effect that the significant preference for p-polarized scattering has on the M_{21} element that was observed for the in-plane Mueller Matrix in Fig. 20(e) results in a drastic change from the glass surface. For the M_{12} element in Fig. 24(b) it is observe that there are two regions in the upper and lower right for which incoming s-polarized light has a stronger contribution to total scattering intensity than p-polarized light. By inspecting the complete angular distribution of the incoherent MDRC in Fig. 14 it is observed that this is caused by the $s \rightarrow p$ contribution being the only scattering contribution to have any significant contribution in these regions. Comparably as for normal incidence the M_{13} element in Fig. 24(c) is similar to its glass counterpart mirrored about the q_2-axis, in addition both the M_{13} and M_{31} elements are severely diminished compared to the glass surface. This can be explained by the lack of overlap between the co- and cross-polarized scattering modes in the incoherent component of the MDRC in Fig. 15 compared to the glass surface. In the lower right quadrant it is observed that there are nearly no contributions to the off-diagonal elements, while the M_{44} element displays a preference for the negative q_1 direction in contrast to the glass surface in contrast to the preference for the positive q_1 direction observed for the glass surface. Finally a back-scattering phenomenon can be observed for some of the elements of the Mueller Matrix, most noticeably in the M_{44} element.

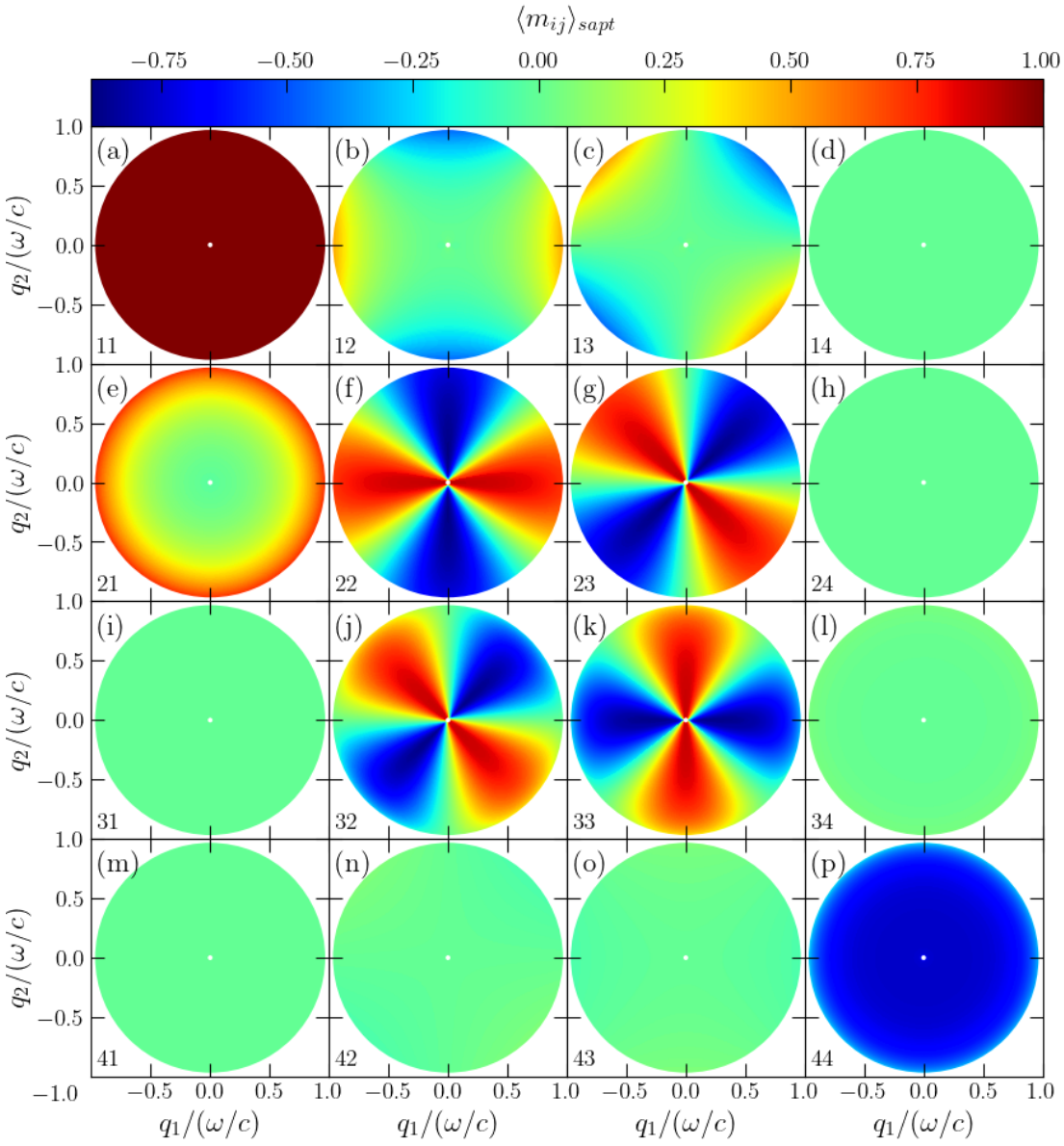

Figure 23: The full angular distribution of the incoherent component of the Mueller Matrix normalized with respect to the M_{11} element for coherent light $\lambda = 457.9$nm normally incident on a randomly rough surface separating vacuum and silver. The surface was characterized by the RMS height $\delta = \lambda/80$ and a Gaussian correlation function with correlation lengths $a_1 = a_2 = \lambda/4$. The dielectric function for silver at this wavelength is $\varepsilon_{silver} = -7.5 + 0.24i$. The Mueller Matrix is resolved on a grid of 101x101 points and the specular direction is indicated by a white dot.

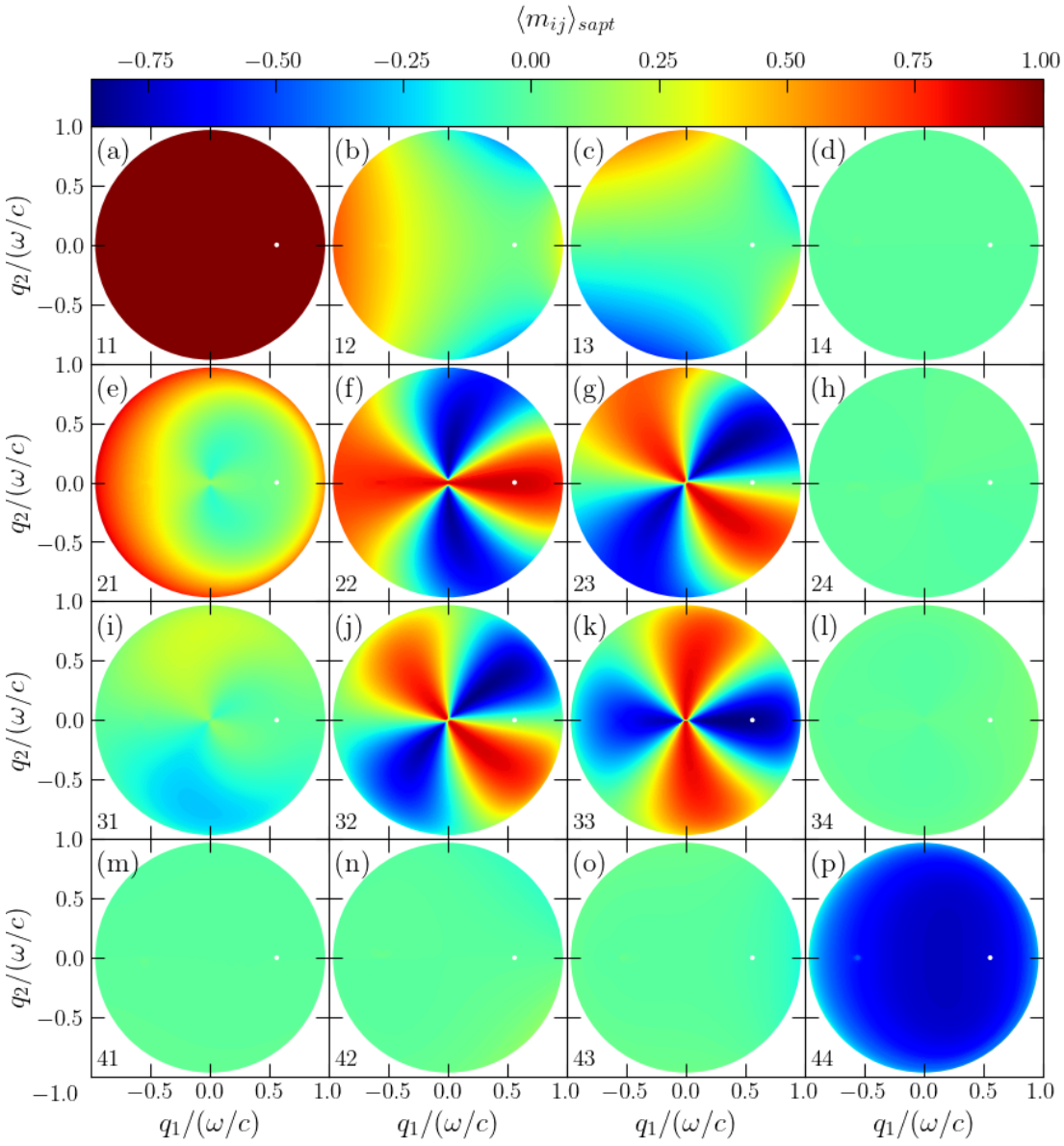

Figure 24: The full angular distribution of the incoherent component of the Mueller Matrix normalized with respect to the M_{11} element for coherent light $\lambda = 457.9$nm incident on a randomly rough surface separating vacuum and silver with angle of incidence $\theta_0 = 34.05°$. The surface was characterized by the RMS height $\delta = \lambda/80$ and a Gaussian correlation function with correlation lengths $a_1 = a_2 = \lambda/4$. The dielectric function for silver at this wavelength is $\varepsilon_{silver} = -7.5 + 0.24i$. The Mueller Matrix is resolved on a grid of 101x101 points and the specular direction is indicated by a white dot.

4.4 Depolarization

Finally the topic of discussion turns to the depolarization index which, as presented in Sec. 2.9, is a scalar condition for a Mueller matrix to describe a non-depolarizing system. Fig. 25 presents the depolarization index for the incoherent scattering component of coherent light normally and non-normally incident on a glass surface. Since the depolarization index is not linear in the Mueller Matrix elements, as can be seen in Eq (48), it is more informative to inspect how the depolarization index changes as more higher order terms are taken into account, rather than calculating the depolarization index while only considering one term in the incoherent expansion of the Mueller Matrix (47) at a time. For Fig. 25 and all following plots of the depolarization index the dashed blue line indicates the depolarization index computed from only the One-one contribution to the incoherent Mueller Matrix, the orange dashed line indicates that both the One-one and Two-two terms have been taken into account, and the solid black line depicts the depolarization calculated from all terms in the incoherent expansion. The surface parameters for the glass surface were chosen as to more strongly satisfy the validity criterion for the Small Amplitude Expansion (108), as results calculated with DNS for the depolarization index of a glass surface were not readily available for comparison.

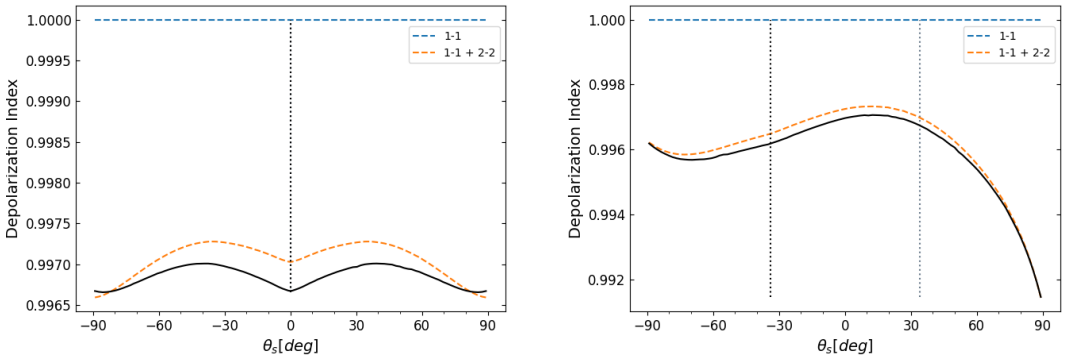

(a): $\theta_0 = 0°$ (b): $\theta_0 = 34.05°$

Figure 25: The depolarization index for coherent light with wavelength $\lambda = 632.8$nm normally incident on a glass surface characterised by an RMS-height $\delta = \lambda/40$ and a Gaussian correlation function with correlation lengths $a_1 = a_2 = \lambda/4$. The dielectric function for glass at this wavelength is $\varepsilon_{glass} = 2.25$. The depolarization index was calculated for 101 different scattering angles θ_s

For normal incidence in Fig. 25(a) it is observed that the depolarization index is symmetric around the plane of incidence, with a minimum at the origin and one each at $\theta_s \approx \pm 80°$. It is observed that the glass surface system is nearly a non-depolarizing system, and that all the depolarizing effects originate from the multiple scattering terms. Interestingly almost all of the depolarizing nature of the system originate from the Two-two term, with only a slight decrease in the depolarization index when also considering the Three-one term, even though the Three-one term makes a much more significant contribution to the Mueller Matrix of a glass surface as seen in Figs. 17 and 18. Similarly for non-normal incidence in Fig. 25(b) there is scarcely any deviation from a non-polarizing system. The depolarization index falls slightly lower than for normal incidence, dipping quite low for large positive scattering angles .

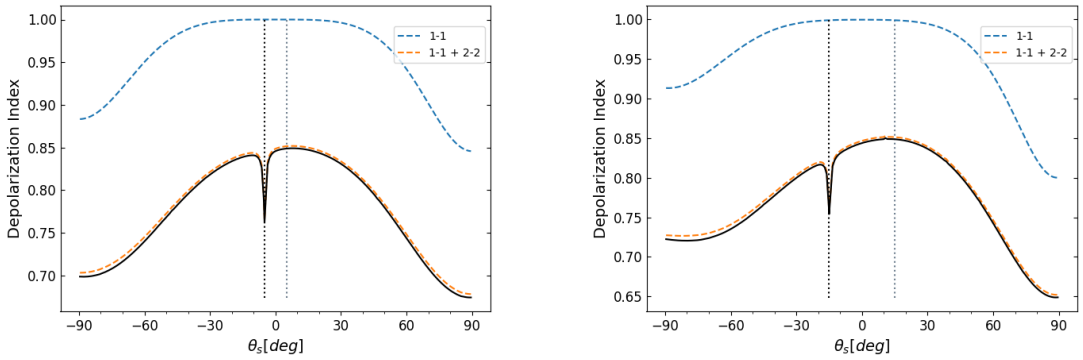

(a): $\theta_0 = 5°$

(b): $\theta_0 = 15°$

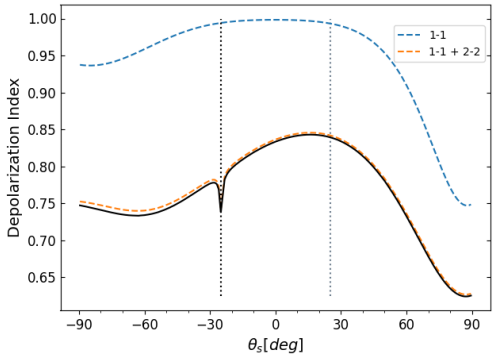

(c): $\theta_0 = 25°$

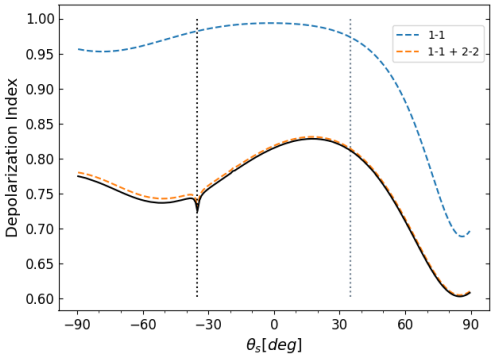

(d): $\theta_0 = 35°$

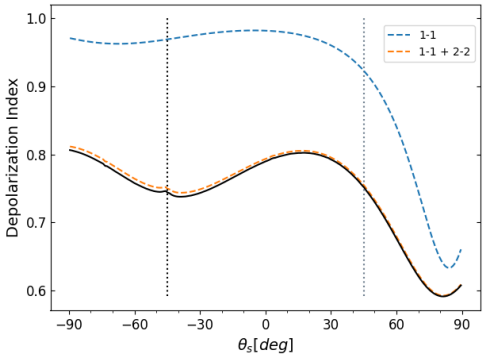

(e): $\theta_0 = 45°$

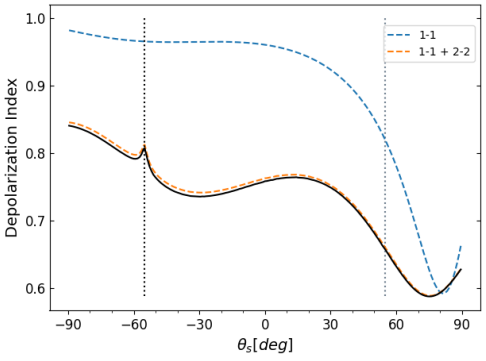

(f): $\theta_0 = 55°$

Figure 26: The depolarization index for coherent light with wavelength $\lambda = 457.9$nm incident on a silver surface characterised by an RMS-height $\delta = \lambda/80$ and a Gaussian correlation function with correlation lengths $a_1 = a_2 = \lambda/4$. The depolarization index was calculated for six different angles of incidence. The dielectric function for glass at this wavelength is $\varepsilon_{silver} = -7.5 + 0.24i$. The depolarization index was calculated for 101 different scattering angles θ_s

Fig. 26 depicts the depolarization index for coherent light scattering of a weakly rough silver surface for six different angles of incidence. Given that decrease in the depolarization index for glass surfaces are caused predominately by multiple scattering effects originating from the Two-two contribution, one would expect a much more significant drop in the depolarization index for a silver surface. This is exactly what is observed in Fig. 26, but interestingly, it is no longer purely caused by multiple scattering contributions. Even when only single scattering contributions are considered, a significant decrease in the depolarization index is observed for large scattering angles. A lowered depolarization index is thereby not inherently a result of

multiple scattering as would be assumed from the results for a glass surface. Furthermore an interference phenomenon akin to the enhanced back-scattering peak is observed for the retro-specular direction. This interference phenomenon presents as a dip for angles of incidence smaller than $\theta_0 \approx 40°$, increasing in magnitude as the angle of incidence approaches zero. As the angle of incidence increases beyond $\theta_0 \approx 40°$ the dip is inverted, presenting instead as a peak in the retro-specular direction. The origin of this behaviour can be determined by investigating the non-normalized in plane component of the incoherent Mueller Matrix. Starting with Fig. 27 which depicts the incoherent component of the Mueller Matrix in the plane of incidence for light incident at an angle of $\theta_0 = 5°$. As expected enhanced back-scattering peaks are observed for some of the Muller Elements (42) that are composed of the intensity contributions from the co- and cross-polarized scattering modes, but interestingly there are also enhanced peaks in the back-scattering contributions to some of the Mueller Matrix elements which are composed entirely of cross terms, such as M_{33}. In Fig. 27, the three major enhanced back-scattering contributions can be found in the M_{11}, M_{22} and M_{33} elements. In addition to the fact that the enhanced back-scattering phenomenon only appears for the silver surface it is observed that, similarly as for the contributions to the incoherent in-plane MDRC for a silver surface in Fig. 8, the enhanced back-scattering peak originates from the Two-two term. Thereby one can conclude that the observed enhanced back-scattering in the various Mueller Elements originates from the same interference phenomenon as for the scattering intensities, namely an interference effect between two reciprocal scattering paths with an SPP as an intermediary.

In Fig. 27 the peak in the M_{11} element has a significantly larger magnitude than the ones presenting in M_{22} and M_{33}. In Fig. 28 which depicts the incoherent Mueller Matrix for $\theta_0 = 35°$ it is observed that similarly as was seen for the incoherent MDRC in Fig. 5 the enhanced back-scattering peak is dampened for larger scattering angles, this effect is also noticeable in the M_{22} and M_{33} elements. Interestingly for a larger angle of incidence the M_{34}, M_{43} and M_{44} elements now present with notable enhanced back-scattering contributions. Most importantly the M_{44} element presents with a relative dip in the back-scattering direction. For $\theta_0 = 55°$ the back-scattering peak in M_{11} is completely unobservable and the peaks in the M_{22} and M_{33} terms are more diminished. The dip in the M_{44} term is of similar magnitude as for $\theta_0 = 35°$.

By inspection of the mathematical expression for the depolarization index (48) one can observe that there are two factors that contribute to the enhanced back-scattering phenomenon in the depolarization index. Firstly, a peak in the retro-specular direction in the M_{11} element will result in a larger denominator for the retro-specular direction in Eq. (48), yielding a dip in the depolarization index. Secondly, enhanced back-scattering peaks or dips in the Mueller Matrix elements that enter into the numerator will counteract or contribute to this dip. In light of this and the Mueller Matrix elements for various angles of incidence in Figs. 27, 28 and 29, the dependence on angle of incidence observed for the back-scattering phenomenon in Fig.26 can be found to originate from the enhanced back-scattering peak in the M_{11} diminishing for larger angles of incidence. For angle of incidence $\theta_0 = 55°$ in Fig. 29 the M_{11} presents with no enhanced back-scattering peak, meaning that the contributions to the enhanced back-scattering phenomenon originate from the Mueller matrix elements in the numerator, resulting in a peak for the retro-specular direction.

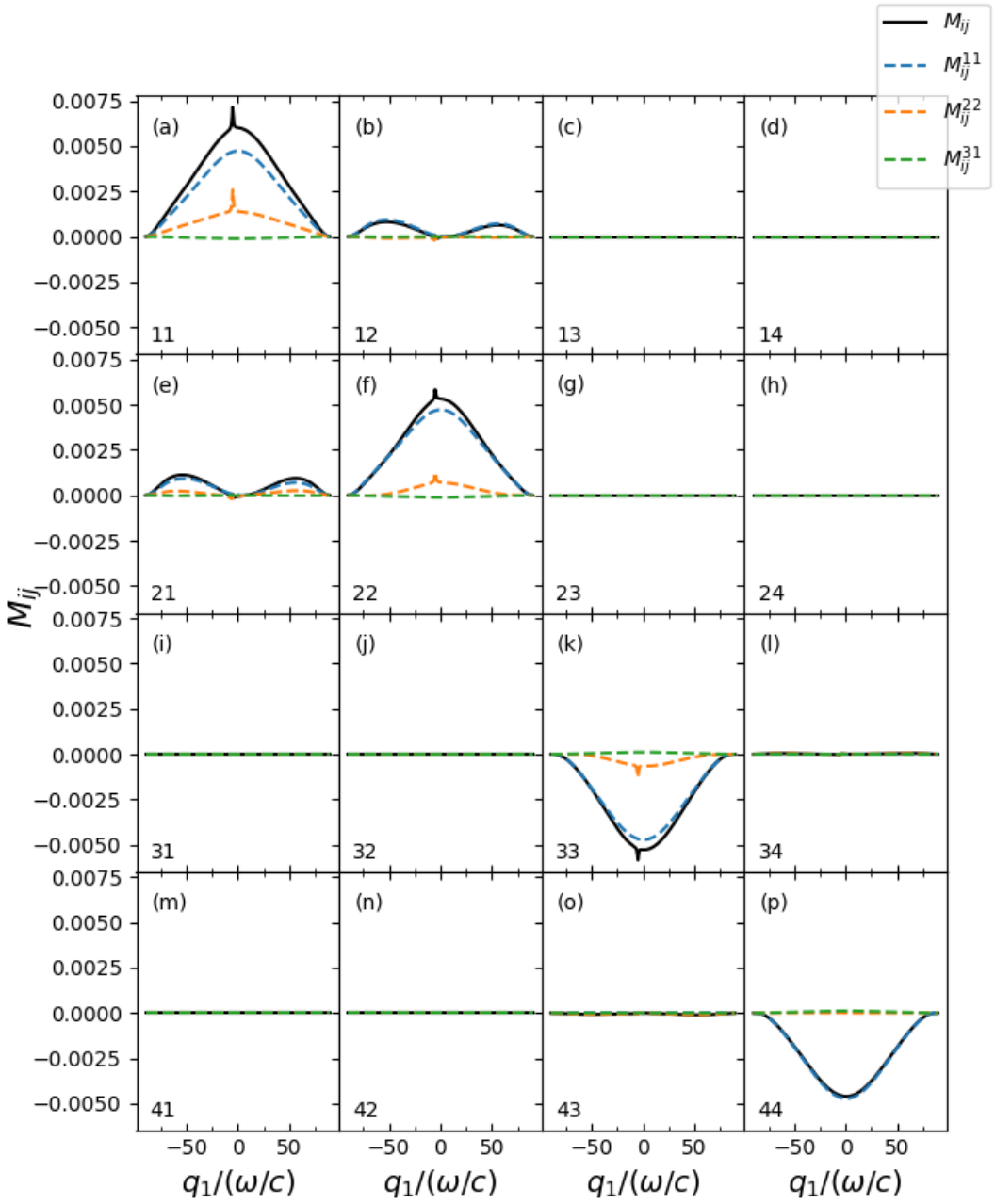

Figure 27: Cross section of the incoherent component of the Mueller Matrix in the plane of incidence for coherent light $\lambda = 457.9$nm incident on a randomly rough surface separating vacuum and glass with angle of incidence $\theta_0 = 5^\circ$. The surface was characterized by the RMS height $\delta = \lambda/80$ and a Gaussian correlation function with correlation lengths $a_1 = a_2 = \lambda/4$. The dielectric function for silver at this wavelength is $\varepsilon_{silver} = -7.5 + 0.24i$. The Mueller Matrix is resolved for 101 scattering angles

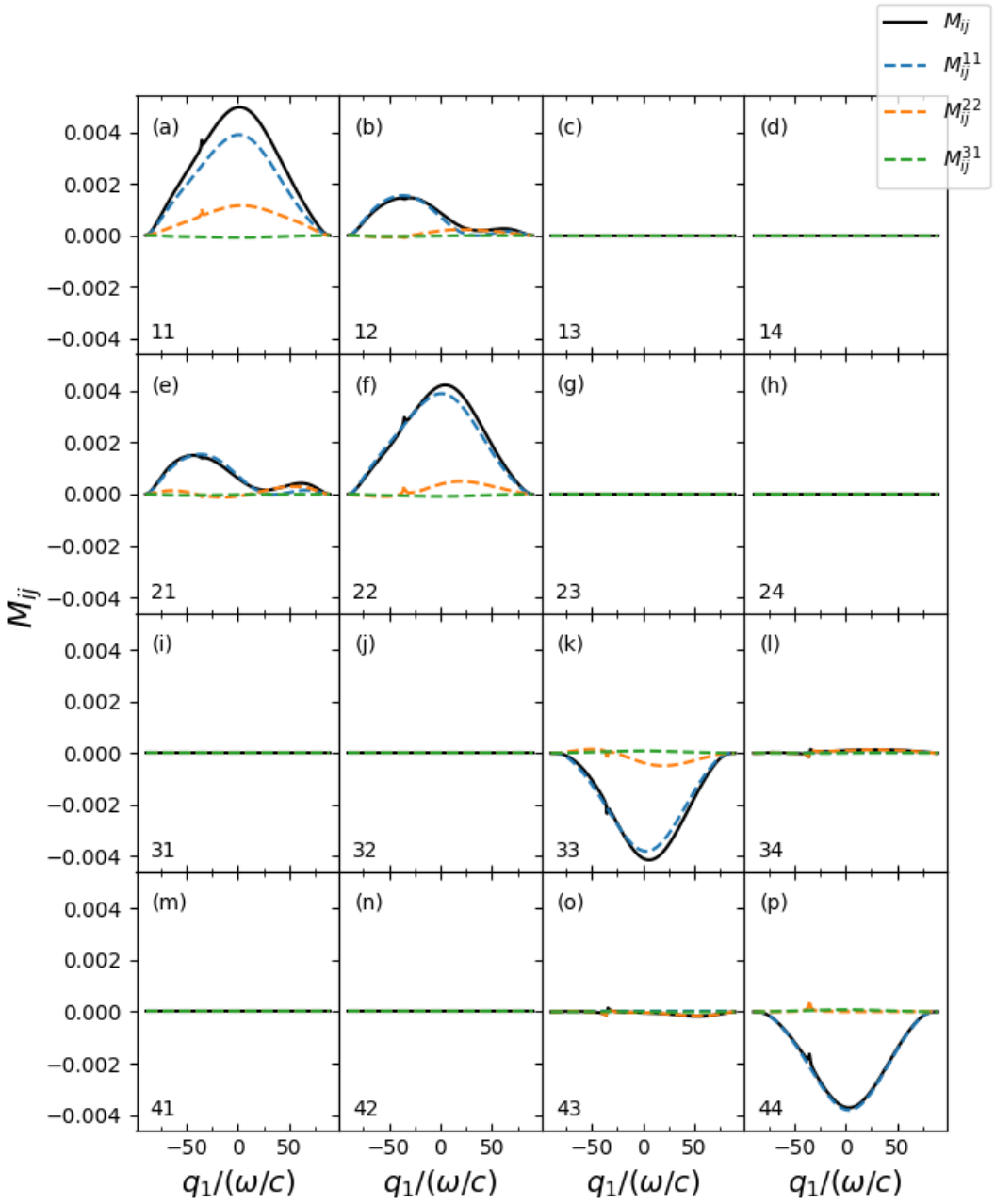

Figure 28: Cross section of the incoherent component of the Mueller Matrix in the plane of incidence for coherent light $\lambda = 457.9$nm incident on a randomly rough surface separating vacuum and glass with angle of incidence $\theta_0 = 35^\circ$. The surface was characterized by the RMS height $\delta = \lambda/80$ and a Gaussian correlation function with correlation lengths $a_1 = a_2 = \lambda/4$. The dielectric function for silver at this wavelength is $\varepsilon_{silver} = -7.5 + 0.24i$. The Mueller Matrix is resolved for 101 scattering angles.

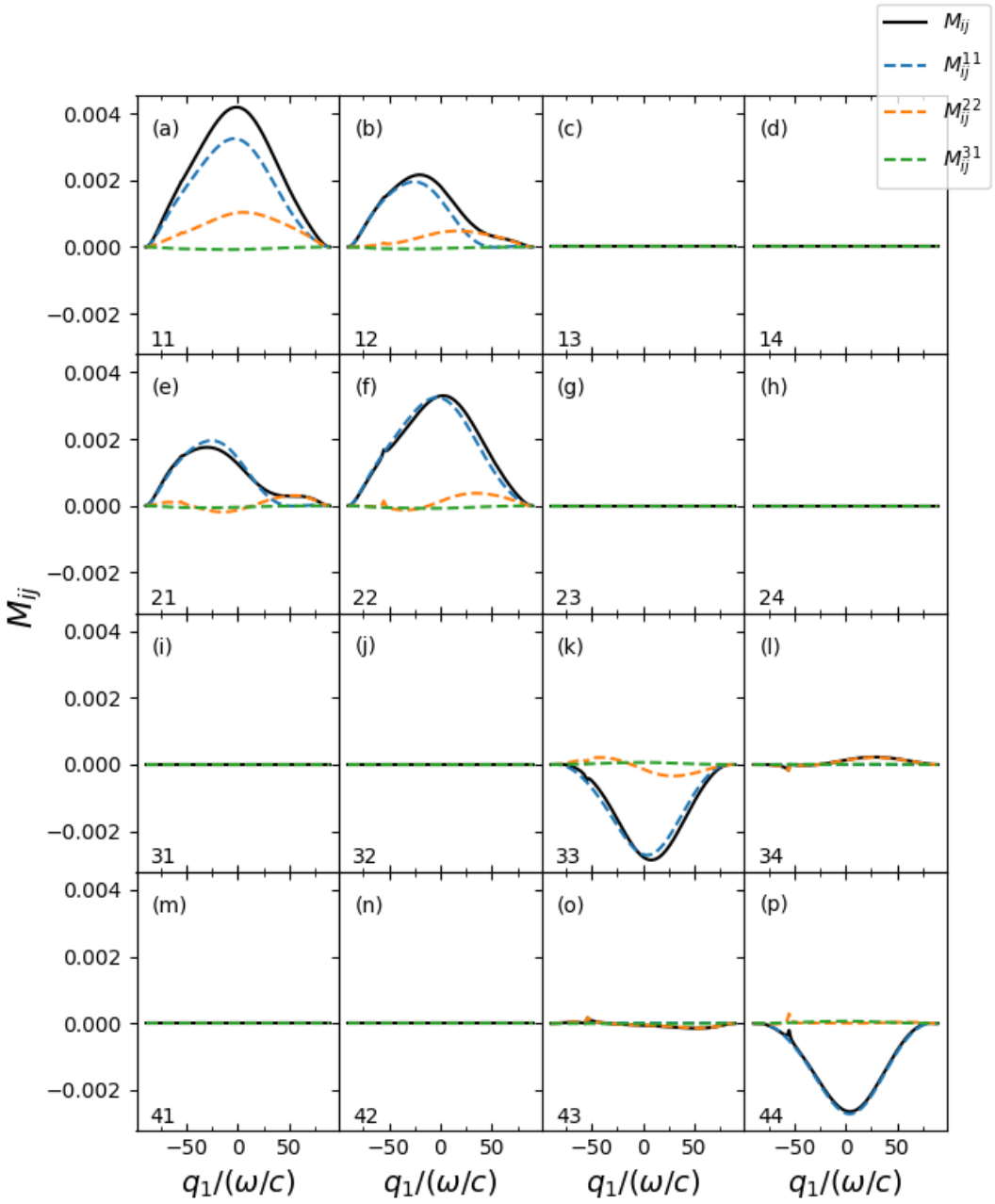

Figure 29: Cross section of the incoherent component of the Mueller Matrix in the plane of incidence for coherent light $\lambda = 457.9$nm incident on a randomly rough surface separating vacuum and glass with angle of incidence $\theta_0 = 55^\circ$. The surface was characterized by the RMS height $\delta = \lambda/80$ and a Gaussian correlation function with correlation lengths $a_1 = a_2 = \lambda/4$. The dielectric function for silver at this wavelength is $\varepsilon_{silver} = -7.5 + 0.24i$. The Mueller Matrix is resolved for 101 scattering angles.

5 Conclusion

The incoherent component of the MDRC and the Mueller Matrix of two dimensional weakly rough glass and silver surfaces defined by Gaussian surface statistics with Gaussian and West & O'Donnel correlation functions were computed using a numerical program based on fourth order Small Amplitude Perturbation Theory. The implemented method was found to agree with previous implementations based on Small Amplitude Perturbation Theory and to have expected level of agreement with DNS. For silver surfaces the incoherent MDRC was found to present with significant in-plane cross-polarization and an enhanced back-scattering peak. The three contributing terms to the incoherent MDRC were depicted for normally incident light, revealing a pronounced increase in double scattering contributions for silver surfaces from the Two-two contribution (81), which was also shown to be the origin of the enhanced back-scattering phenomenon and the significant increase in in-plane cross polarization. The behaviour of the cross-polarized back-scattering was found to depend heavily on the angle of incidence. For small angles of incidence the cross-polarized contributions presented with similar back-scattering peaks as for co-polarized light, but as the angle of incidence increased a destructive phenomenon was observed, resulting in a dip in the back-scattering direction for the cross-polarized scattering contributions for large angles of incidence. Unlike the enhanced back-scattering peak, in-plane cross polarization is not completely extinguished for glass surfaces, only severely diminished. The presence of in-plane cross polarization but lack of enhanced back-scattering peak for the glass surface was explained by considering the Rayleigh Hypothesis which neglects one of the geometrical scattering paths that would interfere constructively in the back-scattering direction to form the enhanced back-scattering peak. Furthermore, when considering scattering from incident unpolarized light a preference for diffuse scattering of s-polarized light was found for the glass surface similar as for specular reflection from dielectrics, while a preference for diffuse scattering of p-polarized light was found for the silver surface. The latter phenomenon was found not to originate from the excitation of SPPs on the silver surface, as it is clearly present for all terms in the incoherent expansion of the MDRC, meaning that it also occurs for One-one scattering contributions that don't involve SPPs.

The incoherent component of the Mueller Matrix was presented and discussed for glass and silver surfaces. The enhanced back-scattering effect was observed for many of the Mueller Matrix elements describing the silver surfaces, and it was concluded that these effects have the same origin as the enhanced back-scattering phenomenon in the incoherent MDRC. The depolarization index was computed from the Mueller Matrix elements, revealing a significant drop from the value one in the depolarization index for silver surfaces for all scattering angles. In addition to this the enhanced back-scattering phenomenon observed in the Mueller Matrix elements of silver surfaces were shown to produce a back-scattering phenomenon in the depolarization index with strong dependence on the angle of incidence. This back-scattering phenomenon presents as a dip for angles of incidence smaller than a critical angle, which evaluates to around $\theta_0 \approx 40^\circ$ for the chosen configuration, and increases in magnitude as the angles of incidence approaches zero. For angles of incidence larger than the critical angle the back-scattering phenomenon presents as a peak in the depolarization. This behaviour can be observed to originate from the varying dependence on the angle of incidence for the different Mueller Matrix elements, most notably that the peak in the M_{11} element vanishes for large angles of incidence, which is not the case for the other Mueller Matrix Elements.

Appendices

A1: Useful identities

In order to derive the expressions for the incoherent MDRC and Mueller Matrix it is necessary to average over the contributions from the Fourier transforms of various powers of the surface roughness function. Starting out with Eq. (27), the explicit expression for the Fourier transform of the surface roughness function is inserted into the left hand side

$$\langle\hat{\zeta}(\boldsymbol{k}_\parallel)\hat{\zeta}(\boldsymbol{k'}_\parallel)\rangle = \langle\int dx_\parallel \int dx'_\parallel \zeta(\boldsymbol{x}_\parallel)\zeta(\boldsymbol{x'}_\parallel)\exp(-i\boldsymbol{k}_\parallel\cdot\boldsymbol{x})\exp(i\boldsymbol{k'}_\parallel\cdot\boldsymbol{x'}_\parallel)\rangle. \tag{110}$$

Moving the average inside the integral and inserting for Eq. (21) yields

$$\langle\hat{\zeta}(\boldsymbol{k}_\parallel)\hat{\zeta}(\boldsymbol{k'}_\parallel)\rangle = \int dx_\parallel \int dx'_\parallel \delta^2 W(\boldsymbol{x}_\parallel - \boldsymbol{x'}_\parallel)\exp(-i\boldsymbol{k}_\parallel\cdot\boldsymbol{x}_\parallel)\exp(-i\boldsymbol{k'}_\parallel\cdot\boldsymbol{x'}_\parallel). \tag{111}$$

Performing the change of variables $\boldsymbol{u}_\parallel = \boldsymbol{x}_\parallel - \boldsymbol{x'}_\parallel$ the integral becomes

$$\langle\hat{\zeta}(\boldsymbol{k}_\parallel)\hat{\zeta}(\boldsymbol{k'}_\parallel)\rangle = \int du_\parallel \int dx'_\parallel \delta^2 W(\boldsymbol{u}_\parallel)\exp(-i\boldsymbol{k}_\parallel\cdot\boldsymbol{u}_\parallel)\exp(-i(\boldsymbol{k'}_\parallel+\boldsymbol{k}_\parallel)\cdot\boldsymbol{x'}_\parallel). \tag{112}$$

After inserting for the Fourier transform of the correlation function, i.e the effect spectrum (24), leaves the Fourier transform of a constant

$$\langle\hat{\zeta}(\boldsymbol{k}_\parallel)\hat{\zeta}(\boldsymbol{k'}_\parallel)\rangle = g(\boldsymbol{k}_\parallel)\delta^2 \int dx'_\parallel \exp(-i(\boldsymbol{k'}_\parallel+\boldsymbol{k}_\parallel)\cdot\boldsymbol{x'}_\parallel), \tag{113}$$

which evaluates to the delta function

$$\langle\hat{\zeta}(\boldsymbol{k}_\parallel)\hat{\zeta}(\boldsymbol{k'}_\parallel)\rangle = (2\pi)^2\delta^2 g(\boldsymbol{k}_\parallel)\delta(\boldsymbol{k}_\parallel+\boldsymbol{k'}_\parallel), \tag{114}$$

The factor of $(2\pi)^2$ out front follows from the chosen Fourier convention. The derivation of Eq. (115) can be performed following steps akin to the derivation of Eq. (110). It is straightforward, if slightly more tedious, though involving a higher order moment of the multivariate normal distribution, which can either be calculated from the statistical distribution or by using Isserlis' theorem [20].

$$\begin{aligned}\left\langle\hat{\zeta}^{(1)}(\boldsymbol{k_1}_\parallel)\hat{\zeta}^{(1)}(\boldsymbol{k_2}_\parallel)\hat{\zeta}^{(1)}(\boldsymbol{k_3}_\parallel)\hat{\zeta}^{(1)}(\boldsymbol{k_4}_\parallel)\right\rangle &= (2\pi)^2\delta^4 s \\ &\times \big[g(\boldsymbol{k_1}_\parallel)g(\boldsymbol{k_3}_\parallel)\delta(\boldsymbol{k_1}_\parallel+\boldsymbol{k_2}_\parallel) \\ &+\ g(\boldsymbol{k_1}_\parallel)g(\boldsymbol{k_2}_\parallel)\delta(\boldsymbol{k_1}_\parallel+\boldsymbol{k_3}_\parallel) \\ &+\ g(\boldsymbol{k_1}_\parallel)g(\boldsymbol{k_2}_\parallel)\delta(\boldsymbol{k_1}_\parallel+\boldsymbol{k_4}_\parallel)\big].\end{aligned} \tag{115}$$

The following relation for the absolute square of the dirac delta function is essential in the calculation of the expansion elements

$$(2\pi)^4\delta(\boldsymbol{q}_\parallel-\boldsymbol{k}_\parallel)\delta(\boldsymbol{k}_\parallel-\boldsymbol{q}_\parallel) = (2\pi)^2 S\delta(\boldsymbol{q}_\parallel-\boldsymbol{k}_\parallel). \tag{116}$$

It is derived by inserting for the Fourier representation of the delta function

$$\delta(\boldsymbol{q}_\parallel-\boldsymbol{k}_\parallel)\delta(\boldsymbol{k}_\parallel-\boldsymbol{q}_\parallel) = \int_{-\infty}^{\infty} dx_\parallel^2 \int_{-\infty}^{\infty} dx_\parallel'^2 \exp[-i(\boldsymbol{q}_\parallel-\boldsymbol{k}_\parallel)\cdot\boldsymbol{x}_\parallel]\exp[-i(\boldsymbol{k}_\parallel-\boldsymbol{q}_\parallel)\cdot\boldsymbol{x'}_\parallel]. \tag{117}$$

Combining the exponentials, performing the change of variables $\boldsymbol{u}_\parallel = \boldsymbol{x}_\parallel - \boldsymbol{x'}_\parallel$ and integrating over $\boldsymbol{u}_\parallel$, leaves the following expression

$$\delta(\boldsymbol{q}_\parallel-\boldsymbol{k}_\parallel)\delta(\boldsymbol{k}_\parallel-\boldsymbol{q}_\parallel) = (2\pi)^2 S\delta(\boldsymbol{q}_\parallel-\boldsymbol{k}_\parallel)\int_{-\infty}^{\infty} dx_\parallel'^2. \tag{118}$$

Finally, changing the limits of the remaining integral such that the limits correspond to the edge of a non-infinite surface and performing the integration we arrive at Eq. (116)

$$(2\pi)^4\delta(\boldsymbol{q}_\parallel - \boldsymbol{k}_\parallel)\delta(\boldsymbol{k}_\parallel - \boldsymbol{q}_\parallel) = (2\pi)^2 S\delta(\boldsymbol{q}_\parallel - \boldsymbol{k}_\parallel). \tag{119}$$

The surface factor also appears in the derivation of Eq. (75), where the fourier expansion of the delta-function with argument zero is inserted

$$\delta(0) = \int d^2x_\parallel \exp(-i\mathbf{0}_\parallel \cdot \boldsymbol{x}_\parallel). \tag{120}$$

Bounding the integral to a finite surface then yields

$$\delta(0) = \int_{s/2}^{s/2} d^2x_\parallel \exp(-i\mathbf{0}_\parallel \cdot \boldsymbol{x}_\parallel) = S. \tag{121}$$

By insertion of Eq. (116) or Eq. (121) it turns out that the MDRC and Mueller matrix are in fact independent of surface size. Though it is still necessary to demand a suitably large surface, since any geometric deviance from a plane has been assumed to be negligble. It is also imperative that the surface is sufficently large for the assumption that the average over surface realizations can be replaced by an ergodic average.

The following identity [21][Eq. B.5] is necessary in order to rewrite Fourier transforms of higher orders of the surface roughness function into products of the Fourier transform of the first order of the surface roughness function.

$$\hat{\zeta}^{(l+j)}(\boldsymbol{q}_\parallel - \boldsymbol{k}_\parallel) = \int \frac{d^2p_\parallel}{(2\pi)^2}\hat{\zeta}^{(l)}(\boldsymbol{q}_\parallel - \boldsymbol{p}_\parallel)\hat{\zeta}^{(j)}(\boldsymbol{p}_\parallel - \boldsymbol{k}_\parallel), \tag{122}$$

A2: Additional Plots That Might Be of Interest

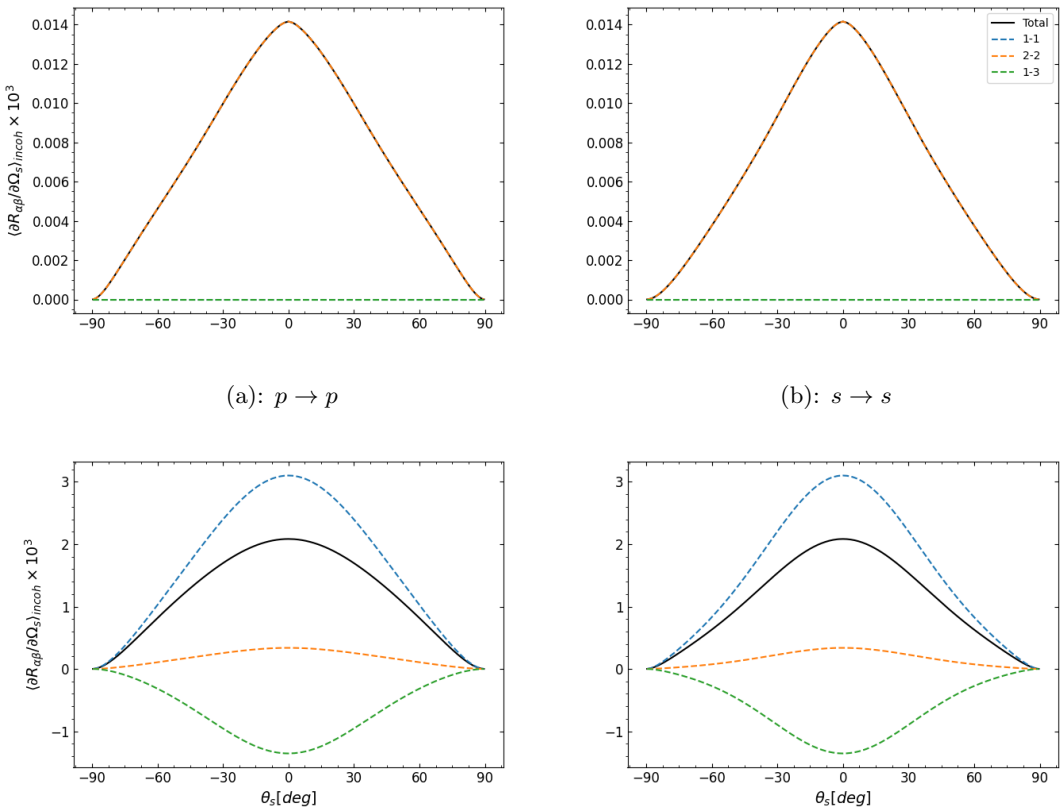

(a): $p \to p$ (b): $s \to s$

(c): $p \to s$ (d): $s \to p$

Figure 30: The contributions to out of plane scattering from the three terms in the incoherent expansion of the MDRC to the co- and cross-polarized scattering modes for coherent light with wavelength $\lambda = 632.8$nm incident on a glass surface described by a Gaussian effect spectrum as a function of the scattering angle θ_s. The numerical and scattering parameters are identical to Fig. 4. It is important to note the difference in the scale for the co-polarized and cross-polarized components, as the co-polarized is in general two orders of magnitude larger than the cross-polarized terms.

Fig. 30 depicts the incoherent component of the MDRC in the plane orthogonal to the plane of incidence for light normally incident on a weakly rough glass surface. It is observed that the cross-polarized scattering are exactly equal to the co-polarized scattering modes in the plane of incidence presented in Fig. 7.

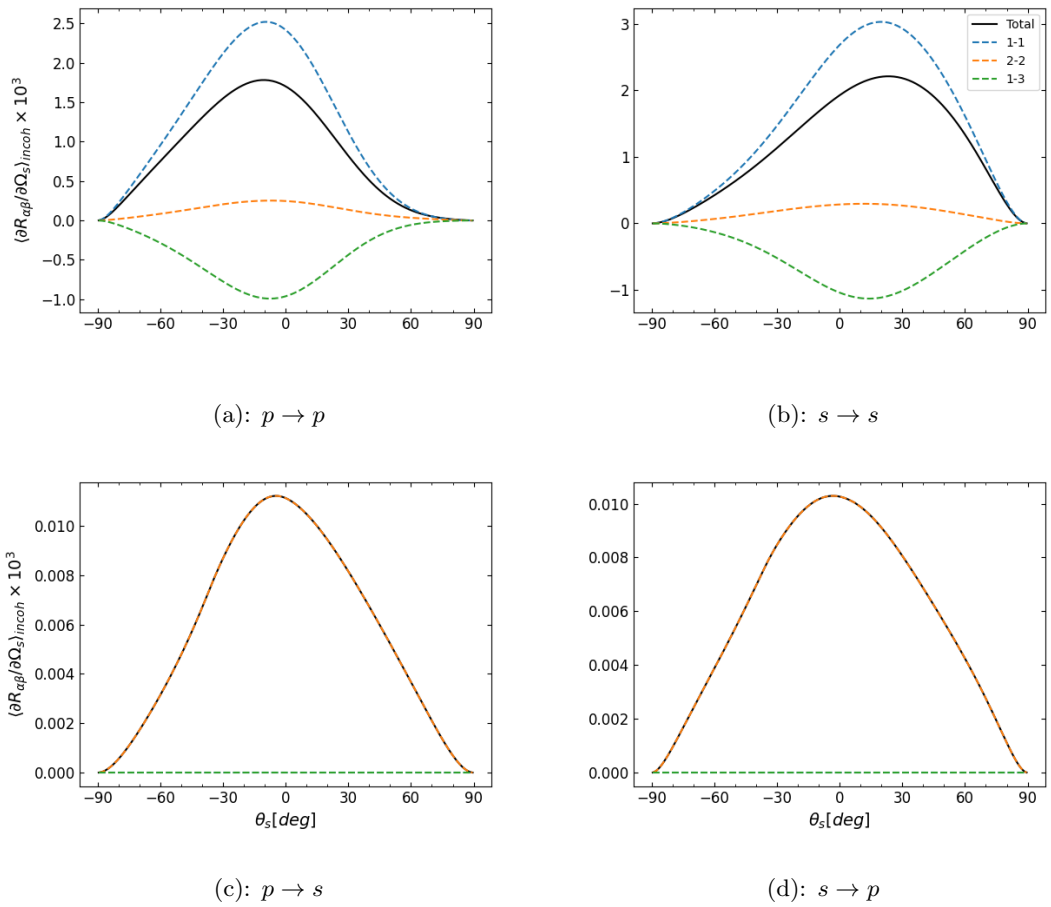

(a): $p \to p$

(b): $s \to s$

(c): $p \to s$

(d): $s \to p$

Figure 31: The contributions to the MDRC in the plane of incidence from the three terms in the incoherent expansion of the MDRC to the co- and cross-polarized scattering modes for coherent light with wavelength $\lambda = 632.8$nm incident on a glass surface described by a Gaussian effect spectrum as a function of the scattering angle θ_s. The numerical and scattering parameters are identical to Fig. 4(b). It is important to note the difference in the scale for the co-polarized and cross-polarized components, as the co-polarized is in general two orders of magnitude larger than the cross-polarized terms.

References

[1] J. J. Gil and E. Bernabeu. "A Depolarization Criterion in Mueller Matrices". In: *Optica Acta* 32:3 (1985), pp. 259–261.

[2] A. R. Mcgurn and A. A. Maradudin. "Perturbation theory results for the diffuse scattering of light from two-dimensional randomly rough metal surfaces". In: *Waves Random Media* 6:3 (1996), pp. 251–267.

[3] M. Haller G.C. Brown V. Celli and A. Marvin. "Vector Theory of Light Scattering from a Rough Surface: Unitary and Reciprocal Expansions". In: *Surface Science* 136 (1984), pp. 381–397.

[4] A. Maradudin. *Light Scattering and Nano Scale Surfaces*. First. US: Springer, 2007.

[5] A.A Maradudin A. R. McGurn and V. Celli. "Localization effects in the scattering of light from a randomly rough grating". In: *Phys. Rev. B* 31 (1984), p. 4866.

[6] K. A. O'Donnell and E. R. Mendez. "Experimental study of scattering from characterized random surfaces". In: *J. Opt. Soc. Am. A* 4 (1987), pp. 1194–1205.

[7] C. S. West and K. A. O'Donnell. "Observations of backscattering enhancement from polaritons on a rough metal surface". In: *J. Opt. Soc. Am. A* 12.2 (Feb. 1995), pp. 390–397.

[8] I. Simonsen. "Optics of surface disordered systems". In: *The European Physical Journal* 181 (2010), pp. 1–103.

[9] P Letnes et al. "Calculation of the Mueller matrix for scattering of light from two-dimensional rough surfaces". In: *Phys. Rev. A* 86 (Aug. 2011).

[10] D. Griffiths. *Introduction to electrodynamics*. Second. Essex, England: Pearson Education Limited, 2017.

[11] N. P. Jørstad. *Reflection of diffuse light from two-dimensional rough surfaces and The light scattering properties of Gaussian-cosine correlated surfaces [Master's Thesis NTNU]*. 2020.

[12] Sheldon M. Ross. *Introduction to Probability Models*. Twelfth. 125 London Wall, London, United Kingdom: Academic Press, 2019.

[13] R.F. Millar. "On the Rayleigh assumption in scattering by a periodic surface". In: *PTOC. Gamb. Phil. Soc* 65 (1969), p. 773.

[14] PA Letnes T Nordam and I Simonsen. "Validity of the Rayleigh hypothesis for two-dimensional randomly rough metal surfaces". In: *Journal of Physics: Conference Series* 454 (2013), p. 012033.

[15] N. C. Bruce. "Calculations of the Mueller matrix for scattering of light from two-dimensional surfaces". In: *Waves in Random Media* 8:1 (1998), pp. 15–28.

[16] J. A. Sánchez-Gil, A. A. Maradudin, and E. R. Méndez. "Limits of validity of three perturbation theories of the specular scattering of light from one-dimensional, randomly rough, dielectric surfaces". In: *J. Opt. Soc. Am. A* 12.7 (1995), pp. 1547–1558.

[17] C. Ueberhuber R. Piessens E. deDoncker-Kapenga and D. Kahaner. *QUADPACK: A Subroutine Package for Automatic Integration*. 1983. URL: https://people.math.sc.edu/Burkardt/f_src/quadpack_double/quadpack_double.html.

[18] Michael Hirsch. *h5fortran*. DOI: 10.5281/zenodo.3562521.

[19] P. B. Johnson and R. W. Christy. "Optical Constants of the Noble Metals". In: *Phys. Rev. B* 6 (1972), p. 4370.

[20] L. Isserlis. "On a Formula for the Product-Moment Coefficient of any Order of a Normal Frequency Distribution in any Number of Variables". In: *Biometrika* 12 (Nov. 1918), pp. 134–139.

[21] R. M. Fitzgerald and A. A. Maradudin. "A reciprocal phase-perturbation theory for rough surface scattering". In: *Waves Random Media* 4:3 (2006), pp. 275–296.

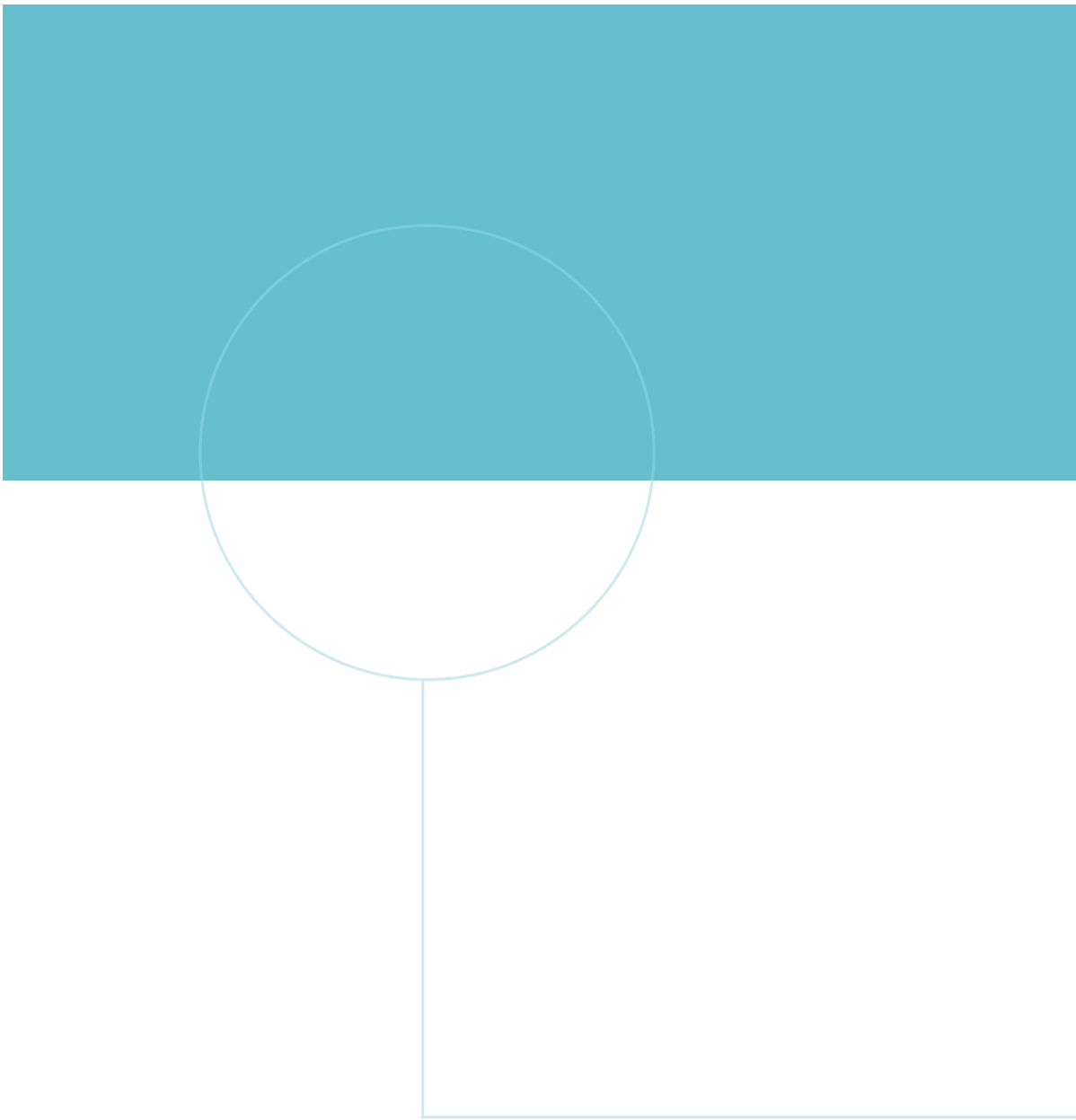

NTNU

Norwegian University of
Science and Technology